NASA Technical Memorandum 107730

REYNOLDS NUMBER INFLUENCES IN AERONAUTICS

Dennis M. Bushnell, Long P. Yip, Chung-Sheng Yao,
John C. Lin, Pierce L. Lawing, John T. Batina,
Jay C. Hardin, Thomas J. Horvath, James W. Fenbert,
and Christopher S. Domack

NASA

National Aeronautics and
Space Administration

Langley Research Center
Hampton. Virginia 23681-0001

Reynolds Number Influences in Aeronautics

By: The 1991-1992 Aerodynamics Technical Committee of the NASA Langley Research Center

Reynolds Number Influences in Aeronautics

Table of Contents

Reynolds Number Influences In Aeronautics

Introduction and Executive Summary

D. M. Bushnell
Fluid Mechanics Division

Reynolds number, a measure of the ratio of inertia to viscous forces, is a fundamental similarity parameter for fluid flows and, therefore, would be expected to have a major influence in Aerodynamics and Aeronautics. Reynolds number influences are generally large, but monatomic, for attached laminar (continuum) flows; however, laminar flows are easily separated, inducing even stronger, non-monatomic, Reynolds number sensitivities. Probably the strongest Reynolds number influences occur in connection with transitional flow behavior. Transition can take place over a tremendous Reynolds number range, from the order of 20×10^3 for 2-D free shear layers up to the order of 100×10^6 for hypersonic boundary layers. This variability in transition behavior is especially important for complex configurations where various vehicle and flow field elements can undergo transition at various Reynolds numbers, causing often surprising changes in Aerodynamic characteristics over wide ranges in Reynolds number. This is further compounded by the vast parameterization associated with transition, in that any parameter which influences mean viscous flow development (e.g. pressure gradient, flow curvature, wall temperature, Mach number, sweep, roughness, flow chemistry, shock interactions, etc. and incident disturbance fields (acoustics, vorticity, particulates, temperature spottiness, even electro static discharges) can alter transition location to first order. The usual method of dealing with the transition problem is to trip the flow in the, generally lower Reynolds number, wind tunnel to simulate the flight turbulent behavior. However, this is not wholly satisfactory as it results in incorrectly scaled viscous region thicknesses and cannot be utilized at all for applications such as turbine blades, and helicopter rotors, nacelles, leading edge and nose regions and High Altitude Long Endurance and hypersonic air-breathers where the transitional flow behavior is an innately critical portion of the problem.

Variations in transition behavior typically produce Reynolds number variation in lift, drag, stability and control, propulsive performance integration, heat transfer, and dynamic loading. Even if the flow is turbulent, Reynolds number effects are still non-negligible. The order of 100 viscous layer thicknesses are usually required downstream of the nominal end of transition before the transitional flow dynamic "artifacts" relax and a "fully turbulent" behavior is reached.

The relative importance/magnitude of Reynolds number effects due to viscous interactions also varies with speed range, being, in general, strongest in the transonic and hypersonic flight regimes due to the extraordinary area ratio sensitively in the former and thick viscous regions in the latter. Compounding the problem is that, in some cases, reported "Reynolds number effects" are in

fact spurious and due to "test technique" problems such as roughness, stream distortions or disturbances ("flow quality"), tunnel wall interference, sting interference, model wall temperature changes (esp. for cryo tunnel testing and hypersonic speeds), aeroelastic effects and 3-Dimensional effects (in "2-D" tests).

Key recommendations regarding Reynolds number related research problems and issues include the following:

1. Increased and continuing efforts in physical modeling of transition and turbulence for 3-D flows (including chemistry and radiation effects for Hypersonics) and in reduction of spurious Reynolds number effects via improved test techniques.

2. Correct the tremendous (order of magnitude) shortfall in Reynolds number ground test capability for the high-lift problem via development of a reasonable dynamic pressure facility including consideration of a "heavy gas" option and utilization of model wall temperative tailoring to aid in viscous layer simulation (for the heavy gas case).

3. Investigate circulation control for CTOL high-lift which, among many other benefits, should severely reduce the Reynolds number sensitivity of the high-lift system operation.

4. Investigate, in detail, the physics associated with the surprising configuration Reynolds number effects which are being measured in NTF at relatively high Reynolds numbers. This should involve considerable CFD and experimentation in the .3M or both unit and combinational problems which are suspected to be responsible for the observed variations in configuration performance.

5. Conduct investigations of the Reynolds number variability/sensitivity of 3-D separated and longitudinal vortical flows. Such sensitivities are largely unknown and usually large where known and are required for many applications including HSCT, high alpha and wake vortex hazard.

6. Develop wind tunnel simulation techniques to allow evaluation of CTOL performance with HLFC in conventional (non-low disturbance) ground facilities. Candidate approaches include "over suction" through fine holes to maintain laminar flow in the presence of strong background disturbances and suction of turbulent boundary layer upstream of the wing shock to simulate the correct (HLFC) boundary layer momentum deficit entering the shocked region.

7. Improve CFD (speed, geometry, physical modeling) to the point where meaningful system analyses can be made of advanced configuration concepts which offer large (factors of 2+) increases in lift to drag ratio for both CTOL and HSCT.

Reynolds Number Sensitivities In Longitudinal Vortex Flows

by D. M. Bushnell
Fluid Mechanics Division

Obvious sources of Reynolds number effects on vortex initiation include alteration of the thickness and structure of the initial viscous regions which "feed" the vortex, as well as the overall issue of whether the incident viscous flow is laminar, transitional or turbulent. The streamline skewing which occurs during vortex formation would be expected to induce, via crossflow destabilization, transition in the incoming boundary layers are initially laminar. Unfortunately, this problem of transition during vortex formation, as well as transition processes within developed or developing vortices has been little studied thus far, although isolated vortex stability has received considerable attention. Reynolds number effects on vortex behavior subsequent to formation can result from vortex instabilities, transition processes, transitional flow regimes, and turbulence structure variations within a developing and developed/decaying vortex. If the vortex is subjected to the influence of bounding or free-stream turbulence fields then there may be other Reynolds number effects associated with the dynamics of such imposed fields, or other boundary conditions.

Early conventional wisdom, gleaned primarily from sharp edged delta wing experiments, indicated that initial vortex formation, subsequent vortex interactions, and pressure gradient-induced vortex busting are not qualitatively influenced, to first order, by Reynolds number (e. g., ref. 1, 2). For example, the trailing edge vortex breakdown condition for a delta wing indicates similar behavior over a factor of 10^3 in Reynolds numbers (from low-speed water tunnel conditions to flight, ref. 2). See ref. 3 for a similar result on the F-18 Fighter. However, in the absence of appreciable imposed pressure gradients, the vortex core Reynolds number dominates vortex core behavior. In fact, "Core dynamics, almost completely ignored in previous research, is very important in Vortex Dynamics" (ref. 4). Also, Reynolds number effects are important for blunt leading-edge wings (see ref. 5), and bodies at angle-of-attack where the separation process is more gradual, compared to the sharp leading edge/salient edge case, especially for lower angle-of-attack (see ref. 6). For these latter condition low Reynolds number information is viewed as of qualitative interest only (e. g., ref. 2) due to the direct influence of the initial and subsequent body boundary layer growth. In fact, relatively strong Reynolds number effects on vortex position have been noted in flight experiments for the rounded leading edge/cambered delta wing case (ref. 7, 8).

Relatively strong Reynolds number effects have also been observed even for relatively sharp leading-edge single and double delta configurations wherein the number, positions and interactions of the vortex systems produced altered significantly between Reynolds numbers of $O(10^4)$ to $O(10^6)$ (ref. 9). These latter results along with those of ref. 10 and 11 tend to confirm the

remarks of ref. 12 made after study of the available quantitative data over slender wings including data for such quantities as vortex trajectories, vortex axial velocity, vortex burst location, and transverse forces, "flows over low aspect ration swept leading-edge wings with vortices over them are very strongly influenced by viscous effects; and are therefore, strong functions of the Reynolds numbers of the flows." The argument being that even with separation fixed the extent of the vortex is still a viscous-dominated problem. In addition, reference 13 concludes that "the form of these (separated) 3-D flow patterns are much more sensitive to Reynolds number than two-dimensional ones." Both computations and experiments indicate that the details of the secondary vortex systems induced on the wing by the primary vortices are also Reynolds-number sensitive to a moderate degree, which in turn alters the location of the primary vortex (e. g., ref. 14).

There is also considerable evidence that the nature and behavior of the wing tip trailing vortex system for high-aspect-ratio wings is Reynolds number dependent, with large differences in vortex Reynolds-number, and hence, turbulence stress level and decay rate between ground facilities and flight (e. g., refs. 15-22). The turbulence structure for wing-tip vortices in particular, and longitudinal vortices in general, is influenced to first order by streamline curvature effects. The overall effect is a stabilization of the corean annular ring of turbulence between the outer, "superlayer" boundary of the vortex turbulence field and this inner core of relatively quiescent fluid (ref. 23, 24 and 25-27). However, increased vortex core regime mean shear in the longitudinal velocity component can evidently increase production in the core regime sufficiently to overcome the stabilizing effects of curvature and provide increased vortex dissipation. The presence of large streamline curvature effects in longitudinal vortices precludes use of simplex eddy viscosity turbulence closures/models. The Reynolds stress equation ("second order closure") approaches are the lowest order closure which includes such effects (e. g., refs. 23, 24 and 28, 29).

Probably the largest, or certainly one of the most dramatic, vortex Reynolds number effects occur in the asymmetric nose vortex problem, where asymmetric differences in transition and their Reynolds number influenced behavior can alter the resultant side forces to first order, refs. 30 and 31-34. In junction flows, both experiment and horseshoe vortices produced in the nose region (ref. 35, 39), changes the interference heating rate (ref. 40) and alters the vortex shape and position (ref. 37 and 41).

Overall, to put it charitably, the Reynolds number sensitivities of vortex flows have not yet been well mapped. Zeroth order, longitudinal vortices have been easy to induce and many of their qualitative features could be deduced from inviscid theory. However, detailed quantitative prediction and design, optimization and control of longitudinal vortices requires a level of understanding and knowledge regarding vortex viscous flow behaviors which we are just beginning to understand the nature of. As an example, details of the vortex initiation process can alter the vortex 3-D mean velocity field, which will subsequently influence the vortex turbulence field and interaction

4

with surfaces, shocks, other vortices, etc., as well as stability. As stated previously, systematic information is lacking regarding non-linear transition and transitional regimes underneath (during surface interaction/formation) and within (see ref. 42) longitudinal vortices, as well as the turbulence structure and modeling for such flows. We are just beginning to seriously develop the requisite Reynolds stress equation closures. Vortex formation is often observed to occur as an amalgamation process (e. g., refs. 43-46) or in a distributed fashion (e. g., ref. 7, 8) and can be a sensitive function of geometric details which typically differ between the research laboratory and industrial practice/application (ref. 42). Also, the Reynolds numbers of many applications are considerably greater than those available in most laboratory flows, particularly for the facilities typically utilized for flow visualization. This sizable difference in Reynolds number may be at least partially responsible (along with differences in detailed geometry) for discrepancies between the laboratory and application (e. g., ref. 48).

1. McMillin, S. N.; Thomas, J. L.; and Murman, E. M.: Navier-Stokes and Euler Solutions for Lee-Side Flows Over Supersonic Delta Wings. NASA TP-3035, December 1990.
2. Erickson, G. E.: Vortex Flow Correlation. AFWAL-TR-80-3143, 1981.
3. Fisher, D. F.; DelFrate, J. H.; and Zuniga, F. A.: Summary of In-Flight Flow Visualization obtained from the NASA High ALPHA Research Vehicle. NASA TM-101734.
4. Hussain, F. and Melander, M. V.: New Aspects of Vortex Dynamics: Helical Waves, Core Dynamics, Viscous Helicity Generation, and Interaction with Turbulence. In "Topological Aspects of the Dynamics of Fluids and Plasmas, Ed. H. K. Moffatt et al (Kluwer Pub.), 1992.
5. Poll, D. I. A.: Spiral Vortex Flow Over a Swept Back Wing. Aeron. J, pp. 185-199, May 1986.
6. Narayan, K. Y.; and Seshadri, S. N.: Vortical Flows on the Lee Surface of Delta Wings. NAL Tech. Mem. AE8802, 1988.
7. Lamar, J. E.: In-Flight and Wind Tunnel Leading Edge Vortex Study on the F-106B Airplane. NASA CP-2416, pp. 187-201, 1986.
8. Green, G. C.; Lamar, J. E.; and Kubendran, L. R.: Aircraft Vortices: Juncture, Wing and Wake. AIAA Paper 88-3743, 1988.
9. Thompson, D. H.: A Visualization Study of the Vortex Flow About Double Delta Wings. Australian Aeron. Res. Lab. Rpt. AR-004-047, 1985.
10. Lowson, M. V.: Visualization Measurements of Vortex Flows. AIAA Paper 89-0191, 1989.
11. Payne, F. M.: The Structure of Leading-Edge Vortex Flows Including Vortex Breakdown. Ph.D Diss. (1987), Univ. of Notre Dame.
12. Wortman, A.: On Reynolds Number Effects in Vortex Flow Over Aircraft Wings. AIAA Paper 84-0137, 1984.
13. Hunt, J. C. R.: Recent Developments and Trends: Physical and Mathematical Modeling. Wind Engineering, J. E. Cormak Ed. Pergamon Press, v. 2, pp. 957-964, 1980.

14. Schrader, K. F.; Reynolds, G. A.; and Novak, C. J.: Effects of Mach Number and Reynolds Number on Leading-Edge Vortices at High-Angle - of-Attack. AIAA Paper 88-0122, 1988.

15. Iversen, J. D.: Correlation of Turbulent Trailing Vortex Decay Data. J. Aircraft, v. 13, No. 5, pp. 338-342, May 1976.

16. Govindaraju, S. P.; and Saffman, P. G.: Flow in a Turbulent Trailing Vortex. Phys. of Fluids, v. 14, No. 10, pp. 2074-2080, Oct. 1971.

17. Lee, H.: Computational and Experimental Study of Trailing Vortices. Ph.D. Diss, VPI and SU, 1983.

18. Saffman, P. G.: The Structure of Turbulent Line Vortices. AFOSR-TR-72-2283 (AD 753131), 1972.

19. Bippes, H.: Experimente Zur Entwicklung der Freien Wirbel Hinter Einem Rechteck Flugel. Acta Mechanica, v. 26, pp. 223-245, 1977.

20. Freymuth, P.; Finaish, F.; and Bank, W.: Parametric Exploration of Unsteady Wing Tip Vortices. pp. 419-424 of Flow Visualization IV, C. Veret Ed., Hemisphere Pub. Co. Washington, 1987.

21. Lee, H.; and Schetz, J. A.: Experimental Results for Reynolds Number Effects on Trailing Vortices. J. Aircraft, v. 22, No. 2, pp. 158-160, Feb. 1985.

22. Baldwin, B. S.; Sheaffer, Y. S.; and Chigier, N. A.: Prediction of Far Flow Field in Trailing Vortices. AIAA Paper 72-989, 1972.

23. Donaldson, C. duP; and Bilanin, A. J.: Vortex Wakes of Conventional Aircraft, AGAR-Dograph, No. 204, May 1975.

24. Bushnell, D. M.: Turbulence Modeling in Aerodynamic Shear Flow-Status and Problems. AIAA Paper 91-0214, 1991.

25. Vladimorov, V. A.; Lugovtsov, B. A.; and Tarasov, V. F.: Suppression of Turbulence in the Cores of Concentrated Vortices. J. Applied Mechanics and Technical Physics, v. 21, No. 5, pp. 632-637, March 1981.

26. Vladimorov, V. A. and Turasor, V. F.: Structure of Turbulence Near the Core of a Vortex Ring. Sov. Phys. Dokl., v. 24, No. 4, pp. 254-256, April 1979.

27. Baldwin, B. S.; Chigier, N. A.; and Sheaffer, Y. S.: Decay of Far Flow Field in Trailing Vortices. NASA TN D-7568, Feb. 1974.

28. Cutler, A.; and Bradshaw, P.: Vortex/Boundary Layer Interactions. AIAA Paper 89-0083, 1989.

29. Liandlat, J.; Cousteix, J.; and AuPoix, B.: Vortices-Boundary Layer Interaction Flows; Analysis of Some Turbulent Closures. J. Theoretical and Applied Mech., v. 7, No. 6, pp. 799-818, 1988.

30. Ericsson, L. E. and Reding, J. P.: Asymmetric Vortex Shedding From Bodies of Revolution. pp. 243-296 in Tactical Missile Aerodynamics, Edited by M. J. Hemsch and J. N. Nielsen, v. 104 of Progress in Astronautics and Aeronautics Series, AIAA, 1986.

31. Lamont, P. J.: Pressures Around an Inclined Ogive Cylinder with Laminar, Transitional or Turbulent Separation. AIAA J., v. 20, No. 11, pp. 1492-1499, Nov. 1980.

32. Champigny, P.: Effect of the Reynolds Number on the Aerodynamic Characteristics of an Ogive-Cylinder at High-Angle-Of-Attack. Rech. Aerosp. 1984, No. 6, pp. 33-41, 1984.

33. Golovatyuk, G. I.; and Tetryukov, Ya. I.: The Effect of Superstructures on the Vortex System of a Body of Revolution with a Conical Nose Section at High Angles of Attack and Different Reynolds Number. Uchenye Zapiski Tsagi, v. 12, No. 4, 1981, pp. 110-117.

34. Ericsson, L. E.; and Reding, J. P.: Vortex-Induced Asymmetric Loads, in 2-D and 3-D Flow. AIAA Paper 80-0181, 1980.

35. Norman, R. S.: On Obstacle Generated Secondary Flows in Laminar Boundary Layers and Transition to Turbulence. Ph.D. Thesis, Ill. Inst. of Tech., Chicago, 1972.

36. Visbal, M. R.: Numerical Investigation of Laminar Juncture Flows. AIAA Paper 89-1873, 1989.

37. Lakshmanan, B.; Twiari, S. N.; and Hussaini, M. Y.: A Parametric Study of 3-Dimensional Separation at a Wing/Body Juncture for Supersonic Free-Stream Conditions. AIAA Applied Aerodynamics Conference, Seattle, WA., June, 1989.

38. Baker, C. J.: The Laminar Horseshoe Vortex. J. Fluid Mech., v. 95, Pt. 2, pp. 347-367, 1979.

39. Chen, C-L and Hung, C-M: Numerical Study of Juncture Flows. AIAA Paper 91-1660, 1991.

40. Fisher, E. M. and Eibeck, P-A: The Influence of a Horseshoe Vortex on Local Convective Heat Transfer. J. Heat Transfer, v. 112, pp. 329-335, May 1990.

41. Sung, C-H; Griffin, M. J.; and Coleman, R. M.: Numerical Evolution of Vortex Flow Control Devices. AIAA Paper 91-1825, 1991.

42. Leibovich, S.: Vortex Breakdown: A Coherent Transition Trigger in Concentrated Vortices. "In Turbulent and Coherent Structures," Kluwer Publishers,: 1991, O. Metais and M. Lesieur Eds., pp. 285-302.

43. Gad-EL-Hak G. and Blackwelder, R. F.: The Discrete Vortices from a Delta Wing. AIAA J., v. 23, No. 6, pp. 961-926, June 1985.

44. Winkelmasson, A.: Flow Visualization Studies of the Tip Vortex System of a Semi-Infinite Wing. AIAA 89-1807, 1989.

45. Francis, T. B. and Katz, J.: Observation on the Development of a Tip Vortex on a Rectangular Hydrofoil. J. Fluids Engineering, v. 110, pp. 208-215, June 1988.

46. Ward, K. C. and Katz, J.: Topology of the Flow Structures Behind an Inclined Projectile, Part A. J. Aircraft, v. 26, No. 11, pp. 1016-1021, Nov. 1989.

47. Hartwich, P. M.; Hall, R. M.; and Hemseh, M. J.: Navier-Stokes Computations of Vortex Asymmetries Controlled by Small Surface Imperfections. AIAA Paper 90-0385.

48. Ericsson, L. E.: Critical Issues in High Alpha Vehicle Dynamics. AIAA Paper 91-3221, 1991.

7

Reynolds-Number Effects in High-Lift / High-Angle-of-Attack Aerodynamics

Long P. Yip
Flight Research Branch
Flight Applications Division

Chung-Sheng Yao and John C. Lin
Experimental Flow Physics Branch
Fluid Mechanics Division

OUTLINE

ABSTRACT

INTRODUCTION

CURRENT UNDERSTANDING OF THE PROBLEM

Reynolds-Numbers Effect on High-Lift Aerodynamics

Reynolds-Number Effects on Wake Vortices

Reynolds-Number Effects on High-Angle-of-Attack Aerodynamics

Smooth-Sided Forebodies

Highly-Swept Wings

Spin Damping

RECOMMENDATIONS FOR FUTURE RESEARCH

REFERENCES

Reynolds-Number Effects in High-Lift / High-Angle-of-Attack Aerodynamics

Long P. Yip, Chung-Sheng Yao, and John C. Lin

ABSTRACT

In this chapter, the state of technology of Reynolds-number effects on high-lift and high-angle-of-attack aerodynamics is assessed, and recommendations for future research are made. The following areas of high-lift or high-angle-of-attack aerodynamics are surveyed: 1) aerodynamic problem areas that are dependent on Reynolds number to the first order, 2) flow physics for the Reynolds number dependence, if known, and 3) future research required to address Reynolds number issues and challenges. A limited technology assessment is presented on Reynolds-number effect in the area of high-lift and high-angle-of-attack aerodynamics, and recommendations for further research to advance the state-of-the-art are also presented herein.

INTRODUCTION

Accurate predictions of aerodynamic characteristics for flight at high-lift and high-angle-of-attack conditions continues to be a problem for the aircraft designer because of the limited understanding of the complex flow physics and associated scale effects at these conditions. For advanced subsonic transport design, predictions of surface-pressure distributions, boundary-layers, separated-flow regions, and wake vortex characteristics are critical in the design of efficient high-lift systems. Likewise, for fighter configurations, predictions of vortical flow and massive separation characteristics are critical in the design of aircraft stability and control characteristics at high angles of attack. These critical flow parameters (i.e., boundary-layer transition, turbulence, merging wakes, separation, and vortical flows) are highly sensitive to Reynolds number.

The purpose of this chapter is to address scale-effects issues in the areas of high-lift and high angle-of-attack aerodynamics. The following areas of high-lift or high-angle-of-attack

9

aerodynamics are surveyed: 1) aerodynamic problem areas that are dependent on Reynolds number to the 1st order, 2) flow physics for the Reynolds number dependence, if known, and 3) future research required to address Reynolds number issues and challenges. In this chapter, a limited technology assessment is presented on Reynolds-number effect in the area of high-lift and high-angle-of-attack aerodynamics, and recommendations for further research to advance the state-of-the-art are presented herein.

CURRENT UNDERSTANDING OF THE PROBLEM

Currently, the effects of Reynolds numbers on flows at high-lift and high-angle-of-attack conditions are not fully understood due to limitations in experimental and computational capabilities which have hindered the modeling of the fundamental viscous flow physics for accurate flow predictions. Experimentally, wind tunnels are generally limited in their capability to test over the broad range of Reynolds numbers while holding Mach number constant. Notable exceptions to this limited capability at Langley are the National Transonic Facility (NTF) and the Low-Turbulence Pressure Tunnel (LTPT), however, most tests in these facilities are directed towards configuration studies and not necessarily studies on flow physics to investigate Reynolds-number effects. Flight experiments provide full-scale conditions, however, availability of detailed data for code validation and for scaling wind-tunnel results to flight has been very limited perhaps because of the perceived difficulty and costs in obtaining flight data. Computationally, advanced codes have been limited in their prediction capabilities by the lack of transition and turbulence modeling for accurate attached and separated flow calculations. In order to better understand the flow phenomena, more detailed data over a larger range of Reynolds numbers are needed for correlation and validation of the design methods. The availability of detailed measurements of pressure distributions and viscous flow parameters at flight Reynolds numbers is critical to the evaluation of computational methods and to the modeling of turbulence structures for closure of the flow equations. Most of the available

10

wind-tunnel investigations for detailed flow measurements of the turbulent Reynolds-stress components have been conducted at sub-scale Reynolds numbers although this data is very useful for code calibration and validation. In addition, availability of detailed flight data for code validation and wind-tunnel correlation has been very limited, and further understanding of scale effects on 2-D and 3-D sub-scale wind-tunnel results is required to accurately extrapolate to 3-D full-scale flight conditions.

Reynolds-Numbers Effect on High-Lift Aerodynamics

The flow field around a multi-element wing with sweep is characterized by several aerodynamic properties which are highly complex in nature and presently not well understood. The complexity of the multi-element flow field has generally limited the measurements and analyses to two-dimensional studies. Although two-dimensional studies address most of the dominant multi-element flow issues, many three-dimensional issues remain unaddressed by these studies. Some of the dominant two-dimensional, multi-element flow features include the following (see Fig. 1):

- compressibility effects including shock/boundary-layer interaction near the slat leading edge;
- laminar separation-induced transition on the upper surfaces;
- confluent boundary layer(s) - the merging and interacting of wakes from upstream elements with the boundary layers of downstream elements;
- cove separation and reattachment; and,
- massive flow separation on the upper surfaces of the wing/flap elements

Three-dimensional multi-element flow issues include the following:

- leading-edge attachment-line transition;
- relaminarization of the flow in the leading-edge region;
- crossflow transition downstream of the attachment line;

11

- sweep effects on confluent boundary layer development, turbulent boundary layer separation, and separated cove flows; and

- highly three-dimensional, local flow modifications, e.g., vortex generators on engine-nacelle and wing surfaces, finite-flap span edge, flap-track fairings, engine pylons, and landing gear strut.

Scale effects associated with high-lift flows were classified by Woodward, Hardy, and Ashill[1] into five categories - 1) conventional, 2) bubble-dominated, 3) slot-flow dominated, 4) 3-D transition dominated, and 5) vortex dominated. These flow issues are closely interrelated and are highly dependent on Reynolds numbers. For example, viscous flow separation depend on Reynolds number to the 1st order and consequently determines the lift curve shape and attainable maximum lift. Generally, maximum lift of a single-element airfoil increases with Reynolds number due to conventional scale effects where separation is determined by the behavior of the turbulent boundary layer near the trailing-edge. On the contrary, maximum lift of multi-element airfoils does not follow such a predictable trend where maximum lift increases with increasing Reynolds number (for example, see data of Valarezo et al.[2], shown in figure 2).

The laminar separation bubble that typically occurs in low Reynolds numbers can lead to erroneous extrapolation of maximum lift as illustrated in Figure 3.[1] The rapid change in $C_{L_{max}}$ near a Reynolds number of 3.2 million results from a bubble-dominated scale effect that was replaced by a conventional scale effect; i.e - the stall pattern changing from a short-bubble leading-edge flow separation to a turbulent boundary-layer separation of the trailing edge. Interestingly, even when the transition was fixed (at Reynolds number of about 2.1 million) in an attempt to produce more representative stall patterns at higher Reynolds number by suppressing the bubble burst, the resulting change in $C_{L_{max}}$ was small. An apparent, but incorrect, conclusion would be that this geometry is not scale sensitive. The

12

data clearly points out the dangers of relying on low Reynolds number data to design wings for maximum lift.

Another high-lift flow phenomena, called the slot-flow dominated scale effect by Woodward et al.[1] or the inverse Reynolds-number effect by Morgan et al.[3], is highly dependent on Reynolds number and causes difficulty for the designer to optimize slot gaps for maximum performance. The data of figure 4 illustrates this effect. At lower angles of attack, C_L decreases as Reynolds number is increased. This reduction in lift is a result of the thinning of the boundary-layer thickness as Reynolds number is increased and thereby increasing the effective slot gap. The effect of increasing the effective slot gap is to reduce the wake/flap interaction, thereby increasing the flap suction peak, and consequently leads to premature flap boundary-layer separation at lower angles of attack. However, at angle of attack near maximum lift, the increasing boundary-layer thickness with increasing Reynolds number suppresses the trailing-edge separation, thereby delaying stall of the flow and generating higher maximum lift. Again, the data point out the dangers of relying on data taken at sub-scale Reynolds numbers without a more complete understanding of the flow physics and the Reynolds-number effects.

The confluent boundary layer that forms when upstream wakes merge with downstream boundary layers also significantly influences the aerodynamic performance of high-lift systems. The formation of confluent boundary layers, which is dependent on Reynolds number, gap size, angle of attack, and Mach number, is always turbulent in the Reynolds number range of interest. Depending on the placement of the elements relative to each other, the wake/boundary-layer interaction can behave inviscidly and not closely coupled, or the interactions can be highly viscous such as in a confluent boundary layer. Strong interaction between the wake of the upstream element with the boundary layers on the downstream elements can significantly influence the separation phenomena of a lifting

system. The confluent boundary layer has been studied in a limited number of experiments and only at sub-scale Reynolds numbers and in two-dimensional flow conditions.[4,5,6,7]

In three-dimensional flows, transition can occur at higher Reynolds numbers at the attachment line near the leading edge, thereby, significantly influencing the downstream flow field, i.e. - confluent boundary layers and separated flows. Swept-wing, wind-tunnel experiments[8,9] and flight measurements[10] on the state of the boundary layer over the swept leading edges of high-lift configurations reveal the presence of laminar, transitional, and turbulent flows along the attachment-line of the slat and fixed leading edge at certain conditions. An illustration of the transition mechanisms for swept wings as a function of Reynolds number was discussed by M.G. Hall et al.[11] and is illustrated by figure 5 as presented in A. Elsenaar's paper.[12] Depending on the pressure-distribution shape, leading-edge sweep angle and Reynolds number, the attachment line can be laminar, transitional, or turbulent.[13,14] A possibility exists for relaminarization of the chordwise flow downstream of a turbulent attachment line if the streamwise flow acceleration is sufficiently strong.[15,16] Boundary-layer crossflow is the primary cause of laminar instability and transition for swept wings without boundary-layer suction at cruise conditions,[17,18] however, the presence and significance of crossflow instability and crossflow-induced transition along the leading edges of a swept high-lift system had not been studied with boundary-layer stability theory until recently by Vijgen et al.[19] Previous experience suggests that crossflow growth does not necessarily limit the amount of laminar flow achievable for these conditions.[20,21] If the flow ahead of the sharp adverse pressure gradient along the upper surface of the elements is laminar, significant Reynolds-number effects can occur due to the presence or absence of a laminar-separation bubble in this region. High-Reynolds-number wind-tunnel tests on swept wings indicated that maximum-lift losses of the order of 10 percent occurred when transition occurred in the leading-edge region.[9] In the recent analysis of the relaminarization issue by Vijgen et al.[19] using linear three-

dimensional stability methods on a multi-element transport wing with 25° sweep, relaminarization of the upper-surface leading-edge flow was predicted along the upper surface of each element, including the fixed leading edge behind the slat element. Based on these results, laminar-separation bubbles may also occur in flight on the upper surface of the elements. This issue is of significant importance in the extrapolation of sub-scale three-dimensional wind-tunnel results to flight Reynolds numbers, as well as in the analysis of flight experiments using computational methods.

Reynolds-number effects on Wake Vortices

Aircraft wake vortices dictate safe in-trail separation distances for aircraft in the terminal area and impose a limit on airport capacity. During the wake vortex program of the 1970's there were many experimental programs to measure various aspects of wake vortices.[22,23] These programs were conducted in many different wind and water tunnels and in flight. Many different test techniques were used because of the difficulties of making wake measurements and relating them to a hazard on another airplane. These measurements range from detailed velocity measurements in a vortex to integrated measurements such as the rolling moment imposed on a model placed in the wake of another model. Measurements taken with similar techniques in similar facilities tended to agree with each other in most respects. However, there is a fundamental difference in vortex decay trends between ground and flight tests illustrated in data published by Greene et al.[24] and shown herein as figure 6. All of the data are for a comparable pair of models or aircraft. The data points are the measured rolling-moment coefficient on the following aircraft as a function of the real or scaled separation distance between the two aircraft. The low-Reynolds-number data from ground facilities show a steady decrease in rolling moment with increasing distance. This is consistent with the prevailing view that vortices decay from the inside with the core size growing and maximum velocities decreasing. The high Reynolds number flight data show a different trend with the rolling moment constant or even

15

increasing with distance. Some of the mechanisms for this type of decay are now better understood and are published by Greene.[25] One mechanism is illustrated in the Greene's paper and is shown in figure 7 by the equation for the polar moment of vorticity and its rate of change in a vortex. The polar moment is roughly proportional to the core size of a vortex. As the sketch indicates, the flow field is symmetric right to left but not top to bottom. The first term in the rate of change equation is due to this vertical asymmetry and the other is twice the product of the viscosity and vortex strength. At high Reynolds number the asymmetry term can apparently be the dominant term while the viscous term is dominant at low Reynolds numbers. Currently, there is no viscous computational method which can completely predict these effects. Accurate prediction of wakes is especially important for high lift design since subtle changes in span loading can create a wake which emphasizes the asymmetric term during rollup.

Reynolds-number effects on High-Angle-of-Attack Aerodynamics

The most severe limitations to the usefulness of predictive methods for the analysis of stall/spin behavior are the effects of Reynolds number and Mach number.[26] The high-angle-of-attack aerodynamics of modern fighter configurations are dominated by vortex flows emanating from the forebody, wing, and wing-leading-edge extensions. The development, interaction, and breakdown of these vortices can produce highly complex, nonlinear aerodynamics that are hard to predict and design for. Because of the relatively long moment arms of modern fighters between the nose forebody and the aircraft center of gravity, aerodynamic forces produced by vortical flows at high angles of attack or angles of sideslip can significantly impact the stability and control characteristics of the configuration. The current development process for high-angle-of-attack aerodynamic design involves many levels of testing and validation from preliminary design to production. Key elements in providing effective design for high-angle-of-attack aerodynamics include improved understanding of the flow physics and improved aerodynamic design/ prediction/ analysis

techniques which include advanced computational fluid dynamics (CFD) methods.[27] To address these challenges, research efforts involving CFD[28,29,30], wind-tunnel[31], and flight activities[32] are being conducted in a broad and coordinated program.

Reynolds-number effects on Smooth-Sided Forebodies

Current research in high-angle-of-attack aerodynamics have shown large Reynolds-number effects in both experimental and computational results for separated flows over smooth-sided forebodies. The flow physics are driven by whether the cross-flow boundary layer at high angles of attack (1) separates in a fully laminar manner, (2) separates laminar, then reattaches due to the onset of turbulence in the separated shear layer, and then undergoes turbulent separation, or (3) transitions to turbulent flow before any separation has occurred resulting in separation of a turbulent nature. Data illustrating the impact of Reynolds number on side force generated by an ogive-cylinder body were published by Lamont[33] and is shown herein by figure 8. Strong vortex influences on side force were exhibited in the high and low range of Reynolds numbers, however, in the mid-range of Reynolds numbers the vortex influence was minimal. Unfortunately, for typical models in subsonic and transonic tests, the Reynolds number based on the forebody diameter falls into this mid-range Reynolds number region. Consequently, test results obtained in this mid-range Reynolds number region would underpredict the aerodynamic forces and moments at flight Reynolds numbers. Again, caution is needed to interpret sub-scale wind-tunnel results.

Since most wind tunnels do not achieve flight Reynolds number values nor include surface imperfections representative of typical flight vehicles, high-angle-of-attack gritting strategies are needed to simulate the turbulent boundary-layer separation character associated with full-scale flight.[31] Traditionally, a grit ring is applied around the nose for simulation of flows at low angles of attack. However, gritting techniques for forebodies at high angles of attack must account for the cross-flow boundary layer characteristics. In

17

research by R. M. Hall et al.,[31] gritting strategies for high angles of attack flows on a 6-percent scale wind-tunnel model of the F-18 aircraft were successfully demonstrated. These tests demonstrated that gritting patterns were repeatable for different applications and that the trends for force and moment development were consistent with available high Reynolds number data. Comparisons of pressure distributions on the gritted forebody with pressures obtained in flight showed good agreement. High-angle-of-attack gritting strategies show promise for simulating high Reynolds number flows, however, further research is clearly needed to validate this transition fixing technique for other high-angle-of-attack aerodynamic tests. Similarly, simulation of high-Reynolds number conditions for active manipulation of forebody vortices (e.g. - strake, blowing, suction, etc.) also require attention.

Reynolds-number effects on Highly-Swept Wings

Highly-swept wing configurations such as those studied in the High-Speed Civil Transport (HSCT) program[34] or military configurations with wing/strake planforms produce leading-edge separated flows that form into vortices over the lifting surfaces at high angles of attack. Complex vortical flow fields and their interactions with aircraft surfaces can significantly impact the high-angle-of-attack aerodynamics characteristics such as longitudinal and lateral-directional stability and control as well as tail buffeting. Some flow phenomena such as vortical flows breakdown are not dependent on Reynolds number to the first order while other flow phenomena such as vortex structure and trajectory and leading-edge hingeline separation are very dependent on Reynolds number.

Boundary-layer separation in the leading-edge region determines the onset of the formation of the primary vortex.[35] For swept wings, the boundary layer state is highly dependent on leading-edge sweep, Reynolds number, Mach number, and pressure distribution. The boundary-layer state also influences the formation and the effect of the secondary separation underneath the primary vortex. Reynolds-number effects on vortex

initiation include alteration of the thickness and structure of the initial viscous regions which feed the vortex, as well as the overall issue of whether the incident viscous flow is laminar, transitional, or turbulent. In the paper of Woodward et al.[1], large variations in pressure distributions with Reynolds number were observed on a delta wing configuration even though the overall longitudinal forces and moments did not significantly change. The data of Woodward et al.[1] are reproduced herein as figure 9. A turbulent secondary separation at the higher Reynolds number apparently shifted the secondary vortex position to one that is nearer to the leading edge. These results can have significant implications on the high-angle-of-attack lateral-directional stability and control characteristics. In a study of vortical flow on the F-106B configuration by Lamar et al.[36,37], the rounded leading edge of the 60° sweep delta configuration caused interesting effects due to changes in the Reynolds number. The flight results showed multiple co-rotating vortices to exist above the wing at the higher flight Reynolds numbers. Ground-based results did not reveal the multiple vortices that were seen in flight. Photographs of in-flight flow visualization using natural condensation effects collected in a published paper by Campbell, Chambers, and Rumsey[38] provided additional evidence of vortex substructures at flight Reynolds numbers. These vortical substructures and multiple vortices have been generally overlooked in ground-based experiments, however, knowing their existence in flight, more recent wind-tunnel and computational research have been conducted to investigate more closely these vortical-flow phenomena.

Leading-edge flap systems that utilize large deflection angles frequently encounter flow separation at the flap hingeline with resultant adverse changes to the aerodynamic characteristics. The phenomenon has been observed on vortex flap configurations as well as configurations with conventional flap systems designed to promote attached flows, and can have a first order sensitivity to Reynolds number.[39] Extension of the experimental data

19

base is needed for development and validation of computational codes on leading-edge hingeline separation as well as leading-edge vortex flow formation.

Reynolds-number effects on Spin Damping

As aircraft enter into regions of higher angles of attack, spin and spin recovery characteristics become pertinent, and the aerodynamics of the forward and aft fuselage as well as wing sections near the outboard tip become very important because of their influence on spin damping.[26] In spinning motion, the side forces produced by the configuration's cross sections produce either propelling or damping forces to counter the rotary spinning motions. The forces produced by some cross-section shapes are highly dependent on Reynolds number as illustrated by the data of figure 10. The data show that the rectangular nose contributed pro-spin forces at low Reynolds numbers and anti-spin forces at higher Reynolds numbers whereas the circular nose was relatively insensitive to Reynolds number.

Prediction of spin characteristics is an important requirement for high-angle-of-attack design. Currently, there is no design methodology for assessing Reynolds-number effects on spin aerodynamics. Development of an analytical method for determining Reynolds-number effects on rotary flows and methods for simulating high Reynolds number spin damping characteristics at low Reynolds number testing are needed to enhance the effectiveness and efficiency of spin testing and design. Recent advancements in computational methods using Navier-Stokes solutions for separated flow conditions offer an opportunity for developing the capability needed to predict Reynolds-number effects on rotary aerodynamics and to predict spin-damping characteristics of configurations of interest. Spin-damping data at higher Reynolds number with sufficient flow measurement details are needed to develop and validate predictive methods. A systematic study involving wind-tunnel and computational methods is needed to advance the state of the art in the understanding of Reynolds-number effects on rotary flows.

20

RECOMMENDATIONS FOR FUTURE RESEARCH

To advance the technological state of the art in understanding Reynolds-number effects at high-lift and high-angle-of-attack conditions requires intensive research activities. Currently, flows are not accurately modeled in computational codes as a result of the complex flow physics at high-lift and high-angle-of-attack conditions. Much of this shortfall is due to the lack of an experimental data base with sufficient detail and accuracy to provide for code development and validation. A three-pronged technical approach (see Fig. 11) involving computational fluid dynamics, wind-tunnel, and flight research activities is recommended. Each sector of research has its own unique contribution to the analysis and design of aircraft configurations. For instance, flight research experiments can provide full-scale Reynolds number data for three-dimensional flows on "real-world" surfaces in an environment relatively free of small-scale turbulence. Wind-tunnel experiments can allow for a systematic and parametric study of scale effects and their associated flow physics through the use of varying model size or flow conditions in two- or three-dimensional settings. CFD can provide analysis of data from flight and/or wind tunnels to bridge the gap between experimental results obtained at different Reynolds number conditions. CFD methods can also provide simulation of the flows at conditions hard to obtain experimentally to provide insight into the flow physics and the design of experiments in both wind tunnel and flight. Much additional development and validation of the CFD methods are needed before they can be practically applied to a complete complex aircraft configuration; however, promising preliminary results indicate that this approach will ultimately provide a powerful tool for high-lift and high-angle-of-attack aerodynamic design and will complement the traditional wind-tunnel and flight-test methods as well. The need to understand scale effects for application of aerodynamic concepts on advanced aircraft design will require additional wind-tunnel, CFD, and flight research in concert with

21

each other in order to address and advance the state-of-art technology on full-scale Reynolds-number effects.

In order to provide for the required database of detailed measurements for correlation and validation purposes, improvements are needed in facility, flow-visualization and measurement techniques, and instrumentation capabilities. New facility capabilities are required to provide flow phenomena similar to those observed at full-scale flight Reynolds numbers. Currently, the NTF provides full-scale Reynolds number capability but accomplishes this capability at high dynamic pressures and cold temperatures.[40] A problem associated with this type of model testing for high-lift configurations is the strict aeroelastic deformations requirements for model construction. To help alleviate this concern, new approaches in wind-tunnel testing such as using heavy gases like Freon or SF_6 to obtain high Reynolds numbers need to be investigated.[41,42] However, because these heavy gases depart from the perfect gas law criteria used for air, flow similarities issues need to be addressed in order to establish the appropriate scaling laws. Half-span-model testing techniques provide increased Reynolds number testing, but several issues such as wall interference, blockage, and carry-over lift effects will need to be addressed in order to provide a good correlation with the full-span model. This correlation study would require use of experiment and CFD to overcome these issues.

Even with improved facility capability, deficiencies in instrumentation and measurement techniques hinder the progress in obtaining the required database for modeling of the flow fields. Traditionally, measurements of forces and moments and pressure distributions are key measurements in an experiment. More flow parameters such as attachment-line, skin friction, separation, wake, and turbulence characteristics are desired for understanding of complex flows. The required database should include off-body flow measurements as well as surface flow measurements. New and innovative techniques will be required to obtain this information in a qualitative and quantitative manner. Recently, the use of pressure-

22

sensitive paints[43] have been studied at various research laboratories and have shown promise in providing not only qualitative visualization of the flow but also quantitative pressure distributions. This technique will require further development particularly for applications in flight tests where temperature and lighting conditions are not as easily controlled. Other innovative techniques being explored include infrared imaging, laser doppler velocimetry, particle image velocimetry, doppler global velocimetry, laser skin friction, and laser light sheet flow visualization techniques.

In order to determine the boundary-layer state of flows for Reynolds number research, flow measurements will also require dynamic instrumentation capable of handling massive storage of data with the real-time data analysis capability. This requirement will be particularly true for flight research where flight time at high-lift or high-angle-of-attack test conditions are limited. New measurement techniques using miniature sensors for boundary-layer research have proved promising for measuring stagnation/ attachment-line, transition, and separation characteristics in wind tunnel and in flight.[44,45] More sensors for boundary-layer research need to be developed where quantitative details of three-dimensional shear layers and cross-flow transition characteristics are obtained.[46] Since relaminarization and transition issues are significant to maximum lift, measurement of the transition locations in the leading-edge region of the high-lift elements are needed both in wind-tunnel and in flight experiments.

Computationally, advanced CFD methods have provided the designer with greater tools to analyze designs at high-lift and high-angle-of-attack conditions. These CFD tools need to both augment and improve the overall design process for high-lift and high-angle-of-attack aerodynamics. Lack of knowledge in the fundamental flow physics has hindered the progress of CFD for analysis of high-lift and high-angle-of-attack flows. Turbulence modeling is a major limiter of CFD accuracy, hence, analysis of transitional and separated flows is a major challenge for CFD.[47,48] Transition and separation predictions and the

23

modeling of transitional flow require further attention in current Navier-Stokes methods. Much progress has been made in two-dimensional viscous flow calculations (e.g. - Drela[49,50], Mavripilis[51,52], Cebeci[53], and Chow[54]), and there is a need to move into three-dimensional flow calculations (e.g. - Thomas[55], Frink[56], and Balasubramanian et al.[57]) for complete aerodynamic analysis of configurations at high-lift and high-angle-of-attack conditions. The situation for prediction of wake-vortex flows is less clear because calculations for turbulent separated flows are difficult in general, and this area has received little attention compared to wing and body flows.

Overall, a significant effort will be required in computational, wind-tunnel, and flight research to understand scale effects for application of aerodynamic concepts on advanced aircraft design in order to address and advance the state-of-art technology on full-scale Reynolds-number effects. Much additional development and validation of the CFD methods are needed before they can be practically applied to a complete complex aircraft configuration; however, promising preliminary results indicate that this approach will ultimately provide a powerful tool for high-lift and high-angle-of-attack aerodynamic design and will complement the traditional wind-tunnel and flight-test methods as well.

In summary, recommendations for future research in the area of Reynolds-number effects in high-lift and high-angle-of-attack aerodynamics are listed as follows:

1. Conduct computational, wind-tunnel, and flight research in concert with each other in order to understand the flow physics associated with the complex flows in high-lift and high-angle-of-attack aerodynamics and ultimately, to develop better design tools for advanced aircraft configurations.

2 Develop improved and innovative facility, test technique, and instrumentation capabilities in order to provide the required database of detailed flow characteristics for correlation, validation, and development of predictive methods.

24

3. Develop computational tools with improved turbulence modeling for accurate simulation of full-scale aerodynamic characteristics to augment and improve the design process for application to complete complex aircraft configurations.

4. Develop innovative and improved methods for experimentally simulating flight Reynolds number and "real-world" surface conditions in sub-scale test facilities.

5. Investigate scale effects in 3-dimensional flows to augment detailed database in two dimensions to obtain better understanding of the flow physics on high-lift systems for accurate extrapolation to 3-dimensional full-scale flight conditions.

6. For high-lift flows, investigate scale-effects issues of leading-edge attachment-line transition and crossflow contamination, relaminarization, confluent boundary-layer development and wake interaction, sweep effects on confluent boundary-layer development, turbulent boundary-layer separation, and cove-separated flows, and highly three-dimensional local flow development.

7. For high-angle-of-attack separated flows over smooth-sided forebodies, leading-edges, and tail empennages, investigate scale-effects issues of cross-flow transition, separation, laminar and turbulent reattachment; and vortical flow formation, development, interaction with surfaces and with other vortices, re-attachment and hinge-line separation, trajectory, and breakdown.

8. For trailing-wake vortex flows, address the problem of viscous modeling of turbulent, edge-separated vortical flow and vortex decay to correlate experiments in wind tunnels and flight.

Acknowledgements

REFERENCES

[1] Woodward, D.S., Hardy, B.C., and Ashill, P.R., "Some Types of Scale Effect in Low-Speed High-Lift Flows," ICAS Paper 4.9.3, 1988.

[2] Valarezo, W.O., Dominik, C.J., McGhee, R.H., Goodman, W.L., Paschal, K.B., "Multi-Element Airfoil Optimization for Maximum High-Lift Reynolds Number," AIAA Paper 91-3332, September, 1991.

[3] Morgan, H.L., Ferris, J.C., and McGhee, R.J., "A Study of High-Lift Airfoils at High Reynolds Numbers in the Langley Low-Turbulence Pressure Tunnel," NASA TM 89125, July 1987.

[4] Braden, J.A., Whipkey, R.R., Jones, G.S., Lilley, D.E., "Experimental Study of the Separating Confluent Boundary-Layer," NASA CR-3655, June 1983.

[5] Brune, G.W., and Sikavi, D.A., "Experimental Investigation of the Confluent Boundary Layer of a Multielement Low Speed Airfoil," AIAA Paper 83-0566, January 1983.

[6] Nakayama, A., Kreplin, H.P., and Morgan, H.L., "Experimental Investigation of Flowfield About a Multielement Airfoil," *AIAA Journal*, Vol. 28, No. 1, pp. 14-21, January, 1990.

[7] Olson, L.E., and Orloff, K. L., "On the Structure of Turbulent Wakes and Merging Shear Layers of Multi-Element Airfoils," AIAA Paper 81-1238, June 1981.

[8] Kirkpatrick, D., and Woodward, D., "Priorities for High-Lift Testing in the 1990's," AIAA Paper 90-1413, June, 1990.

[9] Garner, P.L., Meredith, P.T., and Stoner, R.C., "Areas for Future CFD Development as Illustrated by Transport Aircraft Applications," AIAA-91-1527-CP, June 1991.

[10] Greff, E., "In-Flight Measurement of Static Pressures and Boundary Layer State with Integrated Sensors," *Journal of Aircraft*, v.28, May 1991, pp. 289-299.

[11] Hall, M.G., Treadgold, D.A., "Difficulties in Predicting Boundary-Layer Transition on Swept Wings," RAE Technical Memorandum Aero 1465, ARC 35160 (1972).

[12] Elsenaar, A., "On Reynolds Number Effects and Simulation," AGARD-CP-429, October, 1988.

[13] Pfenninger, W., "Laminar Flow Control Laminarization, USAF and NAVY Sponsored Northrop LFC Research Between 1949 and 1967," in *Special Course on Concepts for Drag Reduction*, AGARD Report No. 654, March 1977, pp. 3-1 to 3-75.

[14] Poll, D. I. A., "Transition in the Infinite-Swept Attachment-Line Boundary-Layer," *The Aeronautical Quarterly*, Vol. 30, part 4, November 1979, pp. 607 - 629.

[15] Launder, B. E., and Jones, W. P., "On the Prediction of Relaminarization," ARC CP 1036, 1969.

[16] Arnal, D., and Juillen, J. C., "Leading-Edge Contamination and Relaminarization on a Swept Wing at Incidence," *Fourth Symposium on Numerical and Physical aspects of Aerodynamic Flows*, edited by T. Cebeci, Cal. State University, Long Beach, CA, January 1989. 11 p.

[17] Owen, P. R., and Randall, D. J., "Boundary-Layer Transition on a Swept Back Wing," RAE TM Aero 257, 1952.

[18] Saric, W. S., and Reed, H. L., "Stability and Transition of Three-Dimensional Boundary Layers," AGARD Conference Proceedings CP 438, October 1988, pp 1-1 to 1-20.

[19] Vijgen, P.M.H.W., Hardin, J.D., and Yip, L. P., "Flow Prediction over a Transport Multi-Element High-Lift System and Comparison with Flight Measurements," Fifth Symposium on Numerical and Physical Aspects of Aerodynamic Flows, Long Beach, CA, January 13-15, 1992.

[20] Runyan, L. J., Navrasan, B. H., and Rozendaal, R. A., "F-111 Natural Laminar Flow Glove Flight Test Data Analysis and Boundary-Layer Stability Analysis," NASA Cr 166051, October 1983.

[21] Obara, C. J., Vijgen, P.M.H.W., and Lee, C. C., "Analysis of Flight-Measured Boundary-Layer Stability and Transition Data," AIAA Paper 91-3282, 9th AIAA Applied Aerodynamics Conference, Baltimore, MD, September 23-26, 1991.

[22] Donaldson, C. duP., and Bilanin, A.J., "Vortex Wakes of Conventional Aircraft," AGARDograph No. 204, May 1975.

[23] "Wake Vortex Minimization," NASA SP-409, 1977.

[24] Greene, G.C., Lamar, J.E., and Kubendran, L.R., "Aircraft Vortices: Juncture, Wing, and Wake," AIAA Paper 88-3743, July 1988.

[25] Greene, G.C., "An Approximate Model of Vortex Decay in the Atmosphere," *Journal of Aircraft*, v.23, July 1986, pp. 566-573.

[26] Chambers, J.R., "Overview of Stall/Spin Technology," AIAA Paper 80-1580, August 1980.

27

[27]Nguyen, L.T., and Gilbert, W.P., "Impact of Emerging Technologies on Future Combat Aircraft Agility," AIAA Paper 90-1304, May 1990.

[28]Ghaffari, F., Luckring, J.M., Thomas, J.L., and Bates, B.L., "Navier-Stokes Solutions About the F/A-18 Forebody-Leading-Edge Extension Configuration," Journal of Aircraft, v.27, September 1990, pp. 737-748.

[29]Hartwich,P.-M., and Hall, R.M., "Navier-Stokes Solutions for Vortical Flows over a Tangent-Ogive Cylinder," AIAA Journal, v.28, July 199, pp. 1171-1179.

[30]Schiff, L.B., Degani, D., and Cummings, R.M., "Computation of Three-Dimensional Turbulent Vortical Flows on Bodies at High Incidence," Journal of Aircraft, v.28, November 1991, pp. 689-699.

[31]Hall, R.M., Erickson, G.E., Banks, D.W., and Fisher, D.F., "Advances in High-Alpha Experimental Aerodynamics: Ground Test and Flight," NASA High-Angle-of-Attack Technology Conference, October 1991.

[32]Fisher, D.F., Richwine, D.M., and Banks, D.W., "Surface Flow Visualization of Separated Flows on the Forebody of an F-18 Aircraft and Wind-Tunnel Model," NASA TM 100436, May 1988.

[33]Lamont, P.J., "Pressure Measurements on an Ogive-Cylinder at High Angles of Attack with Laminar, Transitional, or Turbulent Separation," AIAA Paper 80-1556, August 1980.

[34]Whitehead, A.H., "Overview of Airframe Technology in the NASA High-Speed Research Program," AIAA 91-3100, September 1991.

[35]Elsenaar, A., "On Reynolds Number Effects and Simulation," AGARD-CP-429, October, 1988.

[36]Lamar, J.E., Hallissy, J.B., Frink, N.T., Smith, R.H., Johnson, T.D., Pao, J.-L., and Ghaffari, F., "Review of Vortex Flow Flight Projects on the F-106B," AIAA Paper 87-2346, August 1987.

[37]Lamar, J.E., and Johnson, T.D., "Sensitivity of F-106B Leading-Edge-Vortex Images to Flight and Vapor-Screen Parameters," NASA TP 2818, June 1988.

[38]Campbell, J.F., Chambers, J.R., and Rumsey, C.L., "Observation of Airplane Flow Fields by Natural Condensation Effects," AIAA Paper 88-0191, January 1988.

[39]Hallissy, J.B., Frink, N.T., and Huffman, J.K., "Aerodynamic Testing and Analysis of Vortex Flap Configurations for the 5-Percent Scale F-106B," NASA CP-2417, October 1986.

[40]Beach, H.L., and Bushnell, D. M., "Aeronautical Facility Requirements into the 2000's," AIAA Paper 90-1375, June, 1990.

[41]McMasters, J.H., Roberts, W.H., and Payne, F.M., "Recent Air-Freon Tests of a Transport Airplane in High-Lift Configurations," AIAA Paper 88-2034, May 1988.

[42]Bengelink, R.L., "The Integration of CFD and Experiment: An Industry Viewpoint (Invited Paper)," AIAA Paper 88-2043, May, 1988.

[43]DeMeis, R., "Paint under Pressure," Aerospace America, March 1992.

[44]Sewall, W.G., Stack, J.P.,McGhee, R.J., and Mangalam, S.M., "A New Multipoint Thin-Film Diagnostic Technique for Fluid Dynamic Studies," SAE Paper 881453, October 1988.

[45]Wusk, M.S., Lee, C.C., Obara, C.J., and Norfolk, D.R., "Instrumentation System for In-Flight Boundary-Layer Instability Measurement," ICAS Paper 90-6.1.4, September 1990.

[46]Nitsche, W., and Szodruch, J., "Concepts and Results for Laminar Flow Research in Wind Tunnel and Flight Experiments," 36th International Instrumentation Symposium, May, 1990.

[47]Bengelink, R.L., and Rubbert, P.E., "Computational Fluid Dynamics," Aerospace Engineering, March 1992.

[48]Haines, A.B., "Turbulence Modelling," Aeronautical Journal, vol. 86, pp. 269-277, August/September 1982.

[49]Drela, M., "Newton Solution of Coupled Viscous/Inviscid Multi-Element Airfoil Flows," AIAA Paper 90-1470, June 1990.

[50]Drela, M., "A User's Guide to MSES V1.2," MIT Computational Fluid Dynamics Laboratory, July 1991.

[51]Mavripilis, D.J., Unstructured and Adaptive Mesh Generation for High Reynolds Number Viscous Flows," NASA CR-187534, June 1991.

[52]Mavripilis, D., "Turbulent Flow Calculations using Unstructured and Adaptive Meshes," ICASE Report 90-61, NASA CR 182102, Sept. 1990.

[53]Cebeci, T., "An Interactive Boundary-Layer Approach to Multielement Airfoils at High Lift," Fifth Symposium on Numerical and Physical Aspects of Aerodynamic Flows, Long Beach, CA, January 13-15, 1992.

[54]Chow, R., and Chu, K., "Navier-Stokes Solution for High-Lift Multielement Airfoil System with Flap Separation," AIAA Paper 91-1623, June 1991.

[55]Thomas, J.L., "Reynolds Number Effects on Supersonic Asymmetrical Flows over a Cone at High Angle of Attack," AIAA Paper 91-3295, September 1991.

[56]Frink, N.T., Parikh, P., and Pirzadeh, S., "Aerodynamic Analysis of Complex Configurations Using Unstructured Grids," AIAA Paper 91-3292, September 1991.

[57]Balasubramanian, R., Jones, K.M., and Waggoner, E.G., "Assessment of Computational Issues Associated with Analysis of High-Lift Systems," Fifth Symposium on Numerical and Physical Aspects of Aerodynamic Flows, Long Beach, CA, January 13-15, 1992.

Multi-Element High-Lift Flow Issues

Possible shock/
B.L. interaction

Thick wakes

Flow
separation

Confluent boundary layers

Transition

Turbulent attachment
line and possible
relaminarization
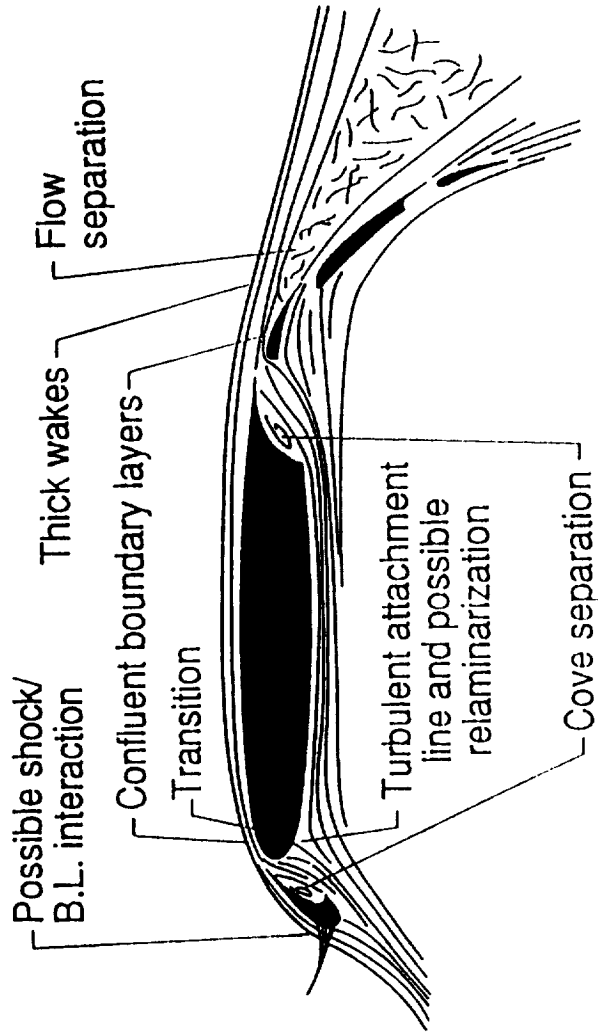
Cove separation

Two-Dimensional Airfoil Issues

- Compressibility effects
- Laminar separation bubbles
- Relaminarization and transition
- Massive flow separation in coves
- Merging of wakes and boundary layers
- Separation of confluent boundary layers

Three-Dimensional Swept-Wing Issues

- Attachment-line transition
- Relaminarization
- Crossflow transition
- Sweep effects on confluent boundary layers
- Sweep effects on boundary-layer separation
- Local, highly 3-D flow modifications; e.g., flap
  cut outs, pylons, track fairings, v.g.'s, etc.

Figure 1.- Multi-element airfoil flow issues.
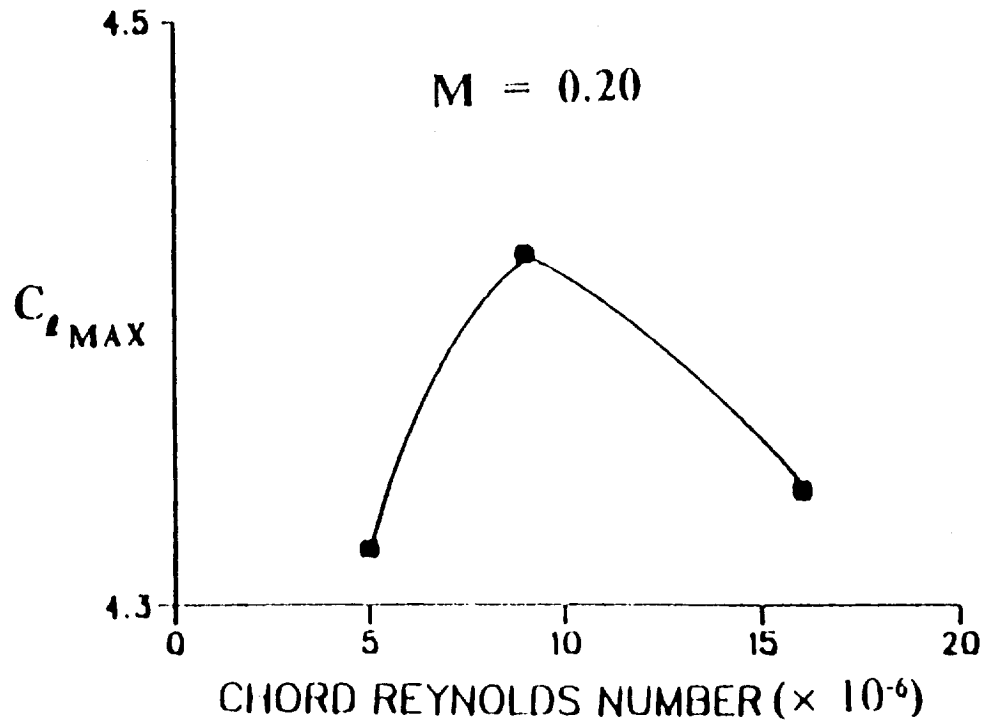
Figure 2. -   Reynolds number effect on configuration optimized at Re = 9 million (data from Valarezo et al.[2]).
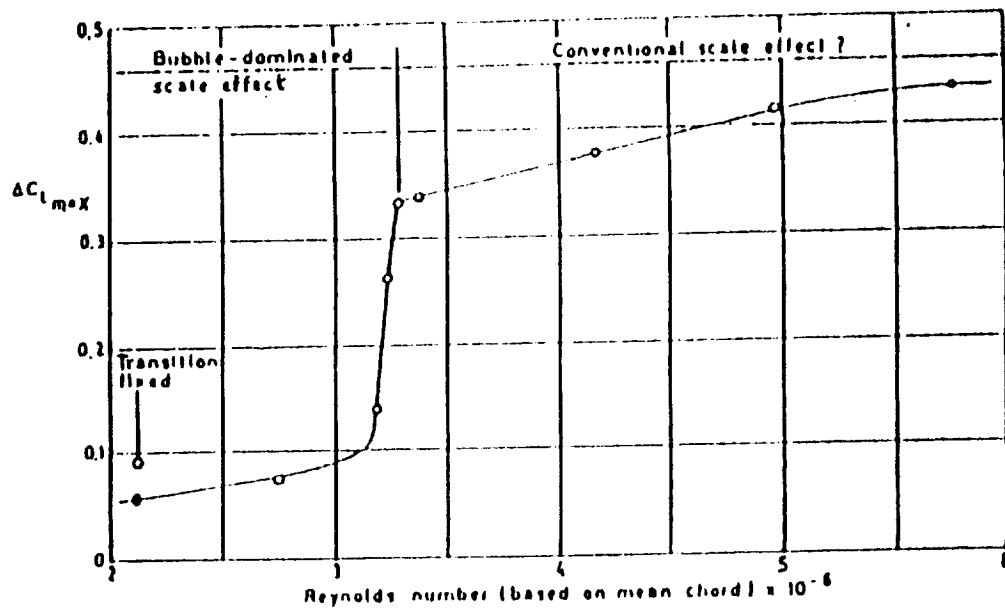
Figure 3. -   Bubble-dominated Reynolds-number effect (data from Woodward et al.[1]).
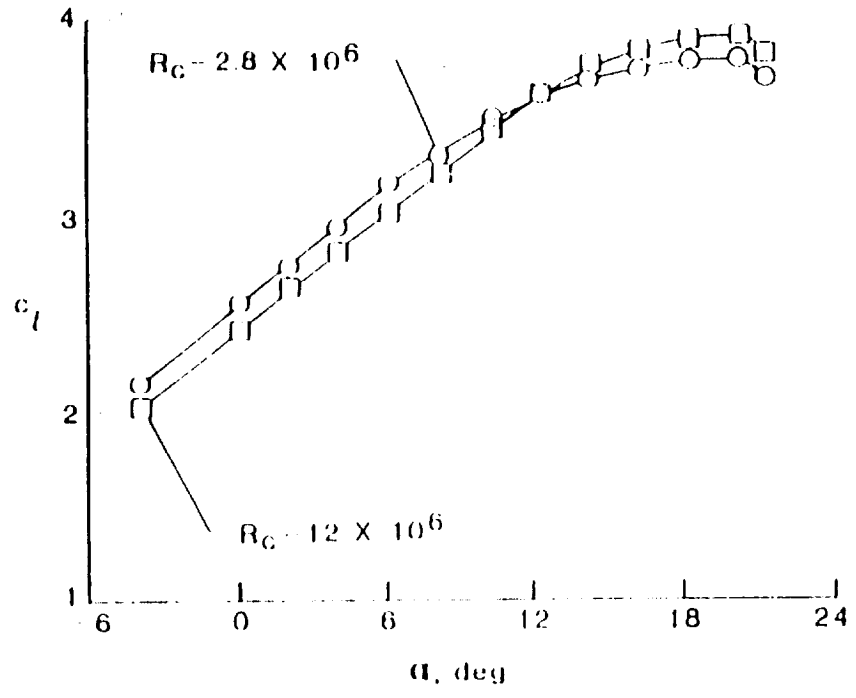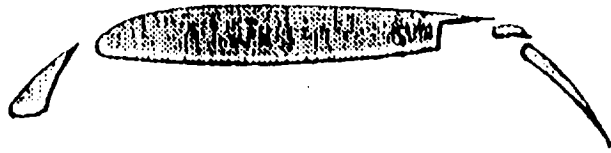
Figure 4.- Inverse Reynolds number effect (data from Morgan et al.[3]).

TRANSITION FOLLOWING
TOLLMIEN-SCHLICHTING
INSTABILITY

GRANVILLES CURVE

$\frac{s}{c}$

CROSS-FLOW
INSTABILITY

Re-LAMINARISATION ?

K

LEADING-EDGE CONTAMINATION

X

R_1 R_2 R_3 R_4 R_c
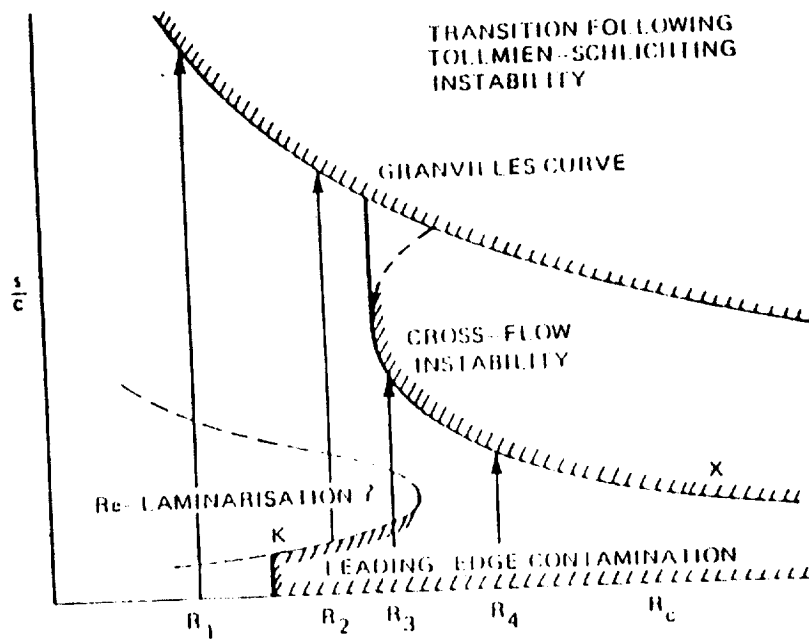
AT R_1 TRANSITION FOLLOWS FROM TOLLMIEN-SCHLICHTING
INSTABILITY

AT R_2 LEADING-EDGE CONTAMINATION, FOLLOWED
POSSIBLY BY RE-LAMINARISATION AND THEN
TRANSITION THROUGH TOLLMIEN-SCHLICHTING
INSTABILITY

AT R_3 LEADING-EDGE CONTAMINATION, FOLLOWED
POSSIBLY BY RE-LAMINARISATION AND THEN
TRANSITION THROUGH CROSS-FLOW INSTABILITY

AT R_4 TRANSITION FOLLOWS FROM CROSS-FLOW
INSTABILITY IF LEADING-EDGE CONTAMINATION
WERE ABSENT

Figure 5.- Illustration of transition types for swept wings (figure from M. G. Hall et al.[11] and A. Elsenaar[12]).

34
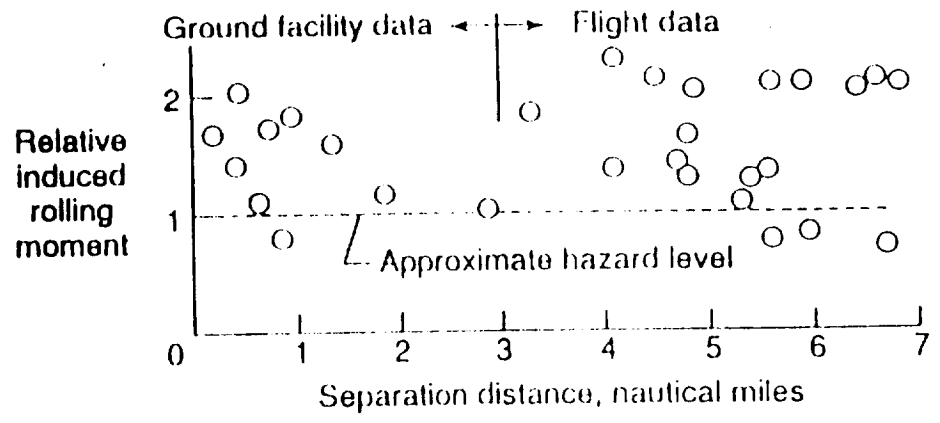
Figure 6.- Aircraft wake hazard measurements (data from Greene et al.[25]).

VORTEX DECAY
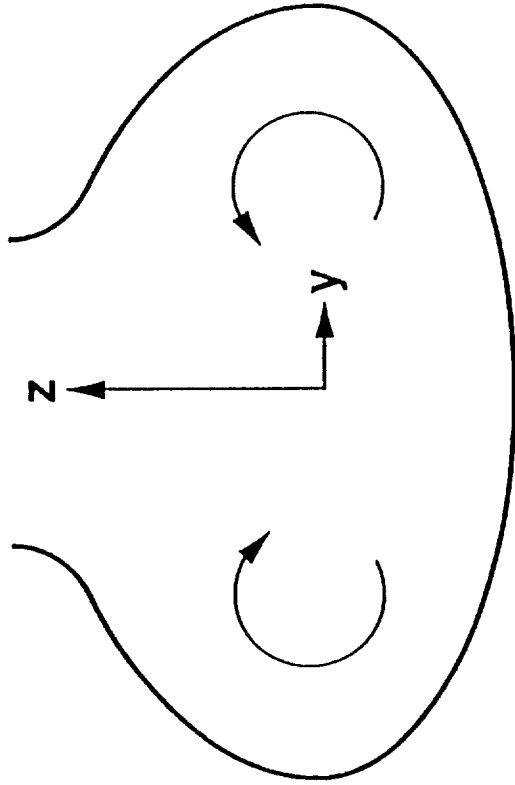
$$\Gamma_r = \int \int (y^2 + z^2)\omega \, dA$$

$$\frac{d\Gamma_r}{dt} = -\int_{-\infty}^{\infty} (z-\bar{z})\frac{w^2}{2}\Big|_{y=0} dz + 2\nu\Gamma$$

$$\Gamma = \int_{-\infty}^{\infty} \int_{0}^{\infty} \omega \, dydz$$

ω = vorticity
w = z velocity component
ν = kinematic viscosity
$\bar{z}$ = z position of vorticity centroid (core)

Figure 7.- Illustration of vortex decay mechanism.

MAXIMUM SIDE FORCE VARIATION WITH REYNOLDS NUMBER

Reference: P.J. Lamont, AIAA 80-1556

$\alpha = 55°$
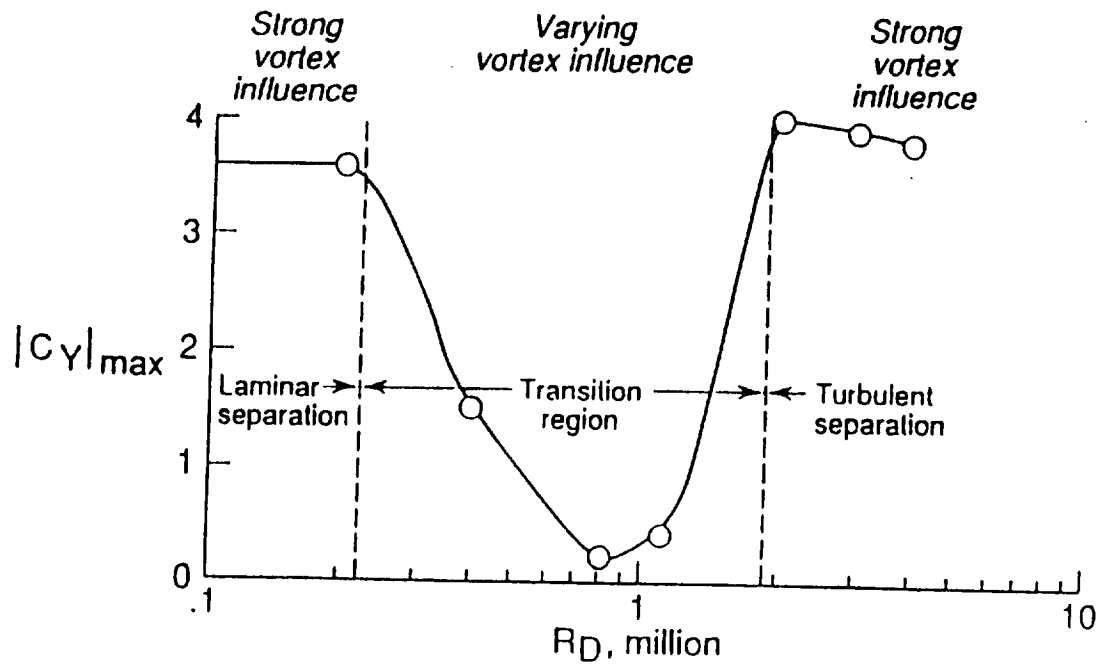
Figure 8.- Maximum side-force variation of ogive/cylinder body with Reynolds number (data from Lamont[33])
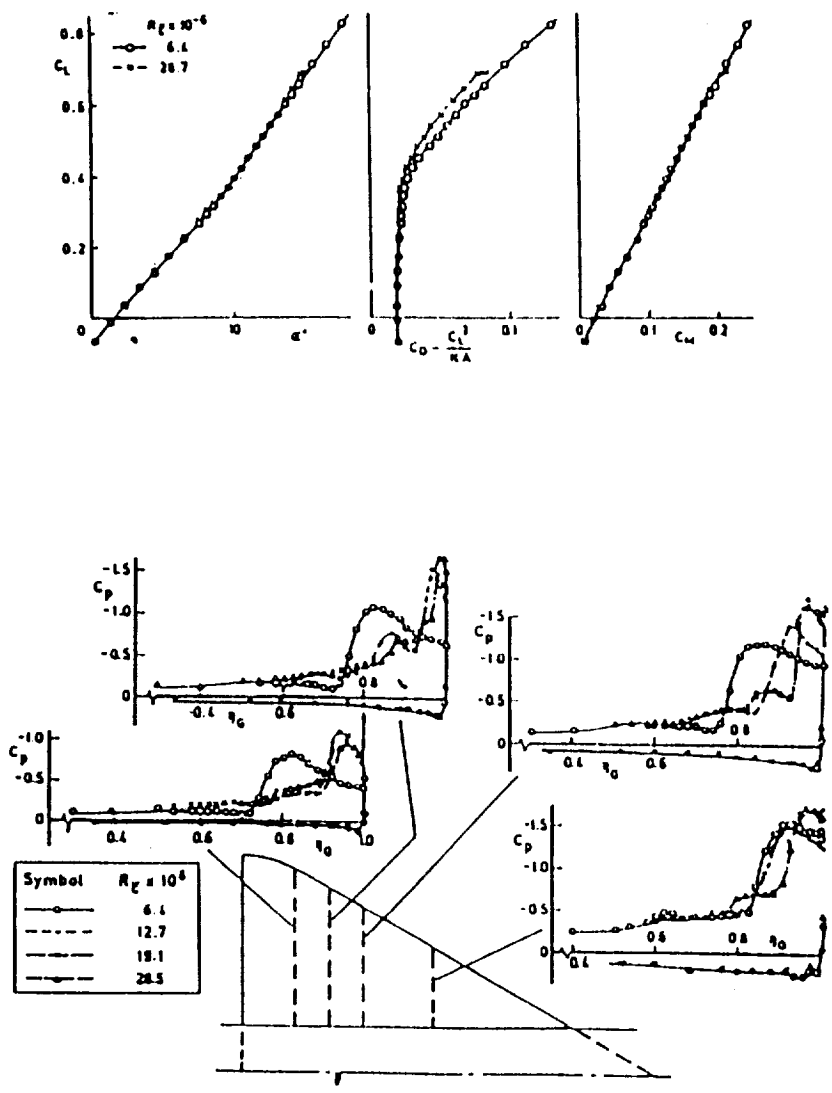
Figure 9.- Scale effect on near-delta wing with round leading-edges (figure from Woodward et al.[1]).
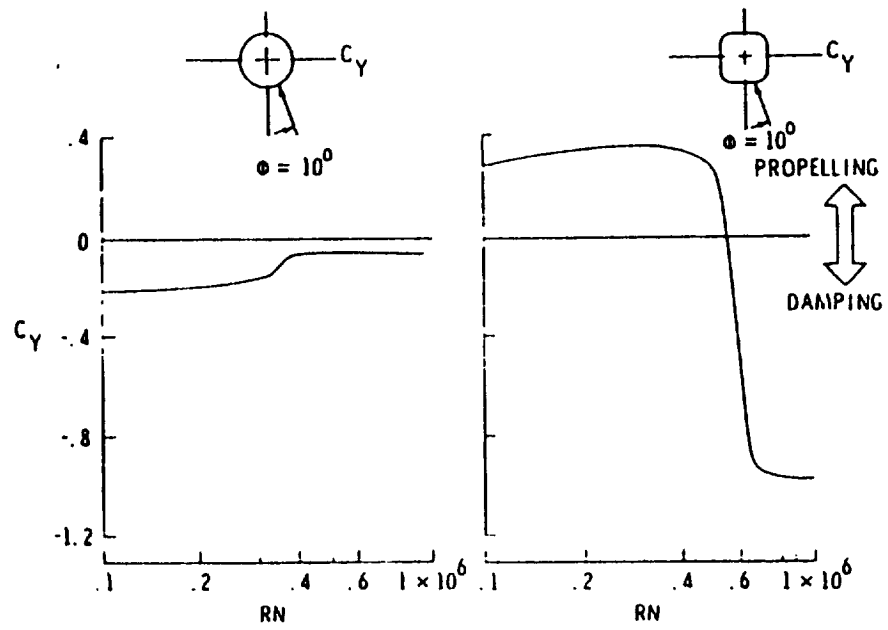
Figure 10.- Effect of Reynolds number on side force produced by two cross-section shapes (figure from Chambers[26]).

Aerodynamics Analysis of Reynolds Number Effects
Technical Approach

- "Real World" environment
- Full Reynolds no.
- 3-D flows

Flight

Wind Tunnel to Flight

CFD to Flight

CFD

- Analysis
- Design
- Flow simulation

CFD to Wind Tunnel

Wind Tunnel

- Scale effects
- 2-D & 3-D flows
- Flow physics
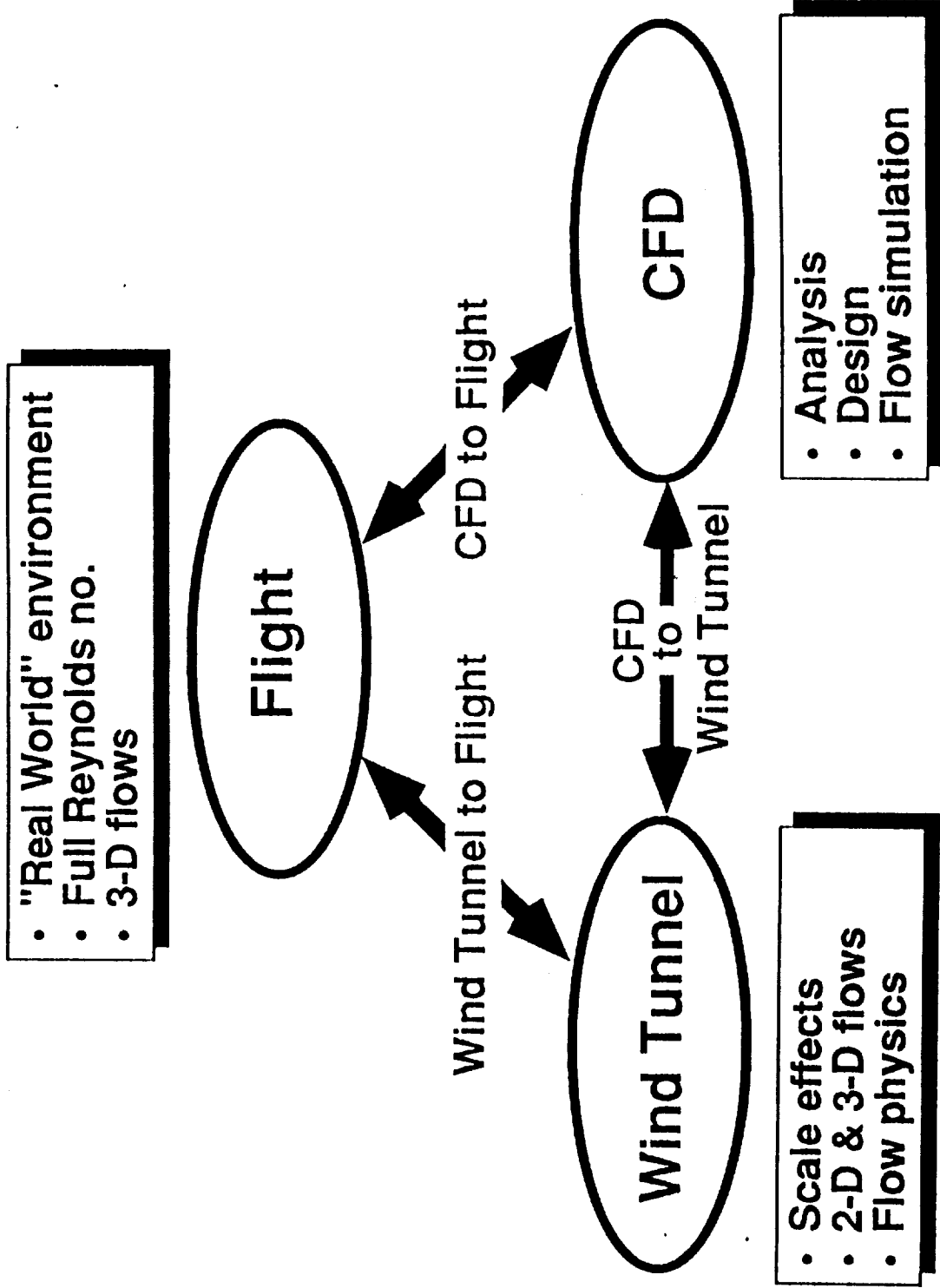
Figure 11. - Three-prong technical approach for Reynolds number research in high-lift and high-angle-of-attack aerodynamics.

REYNOLDS NUMBER EFFECTS: TRANSONIC FLOW REGIME

by

Pierce L. Lawing

INTRODUCTION

It is not the intent of this section to summarize all that is known about Reynolds number effects in transonic flow; the reader is recommended to the extensive body of literature for this purpose (references 1 - 4). It is the intent of this section to highlight the relatively new knowledge gained in recent years through the use of transonic cryogenic wind tunnels for high Reynolds number research. (Please be aware that a good portion of the information is not yet available for general publication and cannot appear here.) Information about cryogenic wind tunnels and the associated technology may be found in references 5 - 7.

The principal reasons for studying Reynolds number effects in transonic flow is that this regime is characterized by flow velocities near the speed of sound. At this speed, normal shock waves can occur which strongly influence momentum loss, mass flow rate and aerodynamic parameters. To further complicate matters, these interactions are usually Reynolds number dependent, making simulation of flight in ground facilities very difficult. Transonic effects are not limited to high Mach number flight, but may appear over a wide range of velocities, depending on the local geometry involved. For instance a cylinder, placed transverse to an airstream, will have local transonic flow in its flow field at airstream Mach numbers as low as Mach 0.5; well designed high lift systems may have local transonic flow at free stream Mach numbers of 0.3, and a commercial transport will have supersonic flow on the wing upper surfaces at a Mach number of about 0.8. Rotating machinery also frequently develops transonic Mach numbers, for instance the blade tips on propellers and helicopters and the turbine blades in an engine.

MODEL TESTING

Reynolds number effects in 2-D airfoil testing.

One of the earliest published results on 2-D airfoil testing in the 0.3-m Transonic Cryogenic Tunnel is shown in figure 1 from reference 8. The drag coefficient as a function of Reynolds number are shown for three airfoils at transonic Mach numbers. The subsonic drag of the NACA 0012 airfoil is seen to decrease steadily with increasing Reynolds number. As Mach number increases, drag divergence occurs at just over 0.7 Mach number and at a lift coefficient of only 0.4. This poor performance highlights the fact that the NACA 0012 was designed for subsonic flight and cannot be expected to perform well at transonic Mach numbers. The other two airfoils are supercritical airfoils and were designed for transonic conditions. They exhibit lower drag and much higher drag divergence Mach numbers, all at a more useful lift coefficient of 0.6. The lowest drag and the highest drag-rise Mach number of the two is achieved by the BAC 1 airfoil. These comparisons are for uncorrected data, however figure 2 shows a pressure distribution for the NASA designed airfoil to illustrate the typical supercritical pressure distribution and the magnitude and direction of correction to be expected.

The model cited above as BAC 1 is a 10% thick supercritical airfoil designed and built by the Boeing company for test in the 0.3-m TCT. Figure 3, taken from reference 9, presents an airfoil performance analysis in terms of Reynolds number by the use of a maximum lift-to-drag performance parameter as a function of Mach number. From this analyses comes the very significant result that there is no "plateau" Reynolds number; at least for this airfoil, the improvement in performance steadily increases with increasing Reynolds number. This is in contrast to the conventional wisdom, which has believed that after a Reynolds number high

41

enough to include natural transition to turbulent flow had been reached, no more significant effects would occur.

The NASA designed supercritical airfoil, designated SC(3)-0712, also exhibits continuous improvement in performance with Reynolds number by a monotonically decreasing drag coefficient. Figure 4, taken from reference 3, shows a decrease in drag roughly predicted by the slope of the Karman-Schoenher relationship for turbulent flat plate flow. This figure also shows the effect of fixing transition at 5% chord. The slope of the Karman-Schoenher curve is of significance here; the level has been matched to the magnitude of the transition fixed, or mostly turbulent, curve. The feature of interest is that the decrease in drag as a function of increasing Reynolds number is approximately predicted by the (flat-plate, or zero pressure gradient) Karman-Schoenher theory, particularly at the higher value of lift coefficient.

A Reynolds Number Scaling Law For Transonic Duct Flow.

Figure 5 presents the fan pressure ratio for the 0.3-m TCT as a function of test section Reynolds number for a range of Mach numbers. This Reynolds number is based on test section hydraulic diameter, which for this particular test section geometry, just happens to be one foot, and the scale may also be read as unit Reynolds number. In reference 10, it is shown that the drag coefficient is proportional to the fan pressure ratio minus 1; therefore figure 5 tells us that the drag coefficient for the tunnel circuit rises rapidly with Mach number, but decreases slowly with Reynolds number. If the data is replotted in terms of Mach number squared, the result is shown in figure 6. A further collapse of the data can be obtained by including the Reynolds number raised to the negative 0.096 power, as shown in figure 7. Since all of the losses in this closed tunnel circuit are viscous, then it is reasonable to think of the dependence of the loss coefficient on Reynolds number in terms analogous to the classic skin friction law, $C_f = A (Re)^{-1/n}$. It is common to see values of n of 7 used to describe high Reynolds number skin friction losses. This coefficient of of 0.096, however is closer to a value of n of 10.4, and describes losses from the turning vanes, the diffusers and contractions, the test section slotted walls and plenum, the tunnel flow conditioning screens, as well as the pipe flow losses of the pipe itself. This remarkable result can be paralleled by the data for airships at length Reynolds numbers of 10^8 where the value of n is as high as 12 (reference 11, page 14-2). If the 0.3-m TCT could be turned inside out, it would have the characteristics of a non-lifting body, such as an airship. Thus the calibration of the tunnel itself has been used as a very high Reynolds number test model.

3-D Airfoil Testing At Flight Reynolds Number

Our modern fighter and fighter-bomber aircraft fly with wings designed by diverse requirements; typical of these are maneuver, supersonic flight, high loading, and weapons carriage. The mix of requirements and the resultant wings may be different depending on the mission, but it is always desirable to maximize the cruise efficiency of these wings. Even though they may be designed to perform at other speeds, these aircraft spend a large percentage of their lifetime at transonic cruise conditions. Good transonic design is made especially difficult by the low aspect ratio of these wings and the associated three dimensional flow field. Another difficulty is the lack of a high Reynolds number data base. Availability of transonic wind tunnel data over the Reynolds number range will aid in the development of computational techniques. Gathering the necessary data has been hampered by the thinness of these wings, typically 5 percent of chord at the maximum thickness. In the past, it has not been possible to heavily instrument these small, thin models. The laminated thin sheet method of building pressure instrumented models, reference 12, allows the construction of wings small enough to test in the 0.3-Meter Transonic Cryogenic Tunnel (0.3-m TCT). Use of this facility and the model building technique provides transonic data at high Reynolds number.

The task is made easier by component, testing on the tunnel side wall. This allows the

size, and thus the Reynolds number, to be doubled. However, the juncture flow between the tunnel sidewall and the model must be understood and compensated for in the test results. In the present example, a model of the canard of the NASA X-29 Research Aircraft has been tested on the sidewall of the Langley 0.3-m Transonic Cryogenic Tunnel. Boundary layer transition was allowed to occur naturally, using no boundary layer trips. It then became important to quell disturbances from the wall boundary layer. An abrupt junction between the wing and the wall would generate a "noisy" horseshoe vortex which could cause a premature boundary layer transition. Also, since this is a wing to be tested at angle of attack, it is important to energize the wall boundary layer so that, as the angle of attack increases, the flow in the juncture does not separate and prematurely stall the wing. This wing/wind-tunnel-wall interaction is therefore a juncture flow problem. In the present case the boundary layer flow was diverted and energized by gradually accelerating it by means of a juncture fillet.

The Mach 0.9 data is shown in figure 8. The occurrence of shock waves complicate the shape of the pressure distributions. At the lowest angle of attack and at the inboard station, a shock occurs at roughly midchord. As the angle of attack increases, a complex shock pattern appears near the leading edge. The flow patterns become more complex at the outboard stations, but have the same general character. The pressures near the leading edge are above the sonic value and there may be a shock very near the leading edge that is not shown by the available pressure taps. Also, the vortex present at the lower Mach numbers and higher angle of attack may be present. There was no flow visualization available for this test (such as shadowgraph). Some additional information is available in the form of momentum deficit surveys in the model wake. These data have not been analyzed, and are presented here to illustrate features of the flow.

Figure 9 presents data for one of the angles of attack shown in figure 8, plus momentum deficit surveys at 6 spanwise stations in the wake of the model. These data were generated by a spanwise rake with 6 pitot probes. It was stepped vertically behind the model at 100 steps per scan to produce the traces shown. The momentum deficit can be integrated to produce the sectional drag coefficient at each pitot probe location. Accurate determination of the drag requires knowledge of the cross-flow at the probes, as well as the blockage of the rake. The drag has not been determined for this paper. However, the shape of the momentum deficit traces indicate qualitative features of the section drag.

The bottom portion of the inboard momentum deficit trace indicates separated flow on the lower surface, and moving up, a peak caused by the viscous drag, and finally a tailing off representing the losses due to shocks. The next trace, at 43 percent span, shows no lower surface separated flow, similar viscous losses, and slightly higher losses due to shocks and other phenomena. The trace at 68 percent has a large peak thought to be part of the tip vortex system. Finally, at 93 percent of span, the drag is dominated by the tip vortex signature. The pressure distributions on the airfoil show multiple shocks but indicate only small areas of separation.

Figure 10 shows a comparison of momentum deficit traces for three angles of attack. The surface pressure traces for all three are contained in figure 8, and the highest angle of attack is the same as in figure 8. As the angle of attack decreases, the losses due to shocks and tip vortices quickly diminish. However, the losses due primarily to skin friction remain about the same.

Flight Data

Figure 11 shows flight data for a nominal Mach number of 0.6 and a range of angle of attack. The two rows of pressure taps are at the same spanwise stations as for the inboard and midspan stations of the wind tunnel model. The angles of attack shown are local angles of attack and are determined by multiplying the aircraft angle of attack by 1.6, and then adding the deflection angle of the canard. This correction is to compensate for the effect of the local

upwash angle of the forward-swept wing. (The method of calculating angle of attack was provided by Grumman Aerospace Corporation, and the flight data set is courtesy of Lisa Bjarke of NASA Ames-Dryden Flight Research Facility). At the inboard station, the data traces show attached flow as high as 16 degrees in angle of attack. The midspan station shows flow separation at the highest angle of attack. A vortex roughly parallel to the leading edge can be seen in the lower angle-of-attack traces at the third orifice for the inboard trace, and at the fifth orifice in the midspan trace. This vortex is probably also present at the higher angle of attack and perhaps explains the attached flow at the higher angles.

The 0.7 Mach number data is shown in figure 12 and provides even stronger evidence of a vortex, at about 1/4 chord, than the 0.6 Mach number case. The data show attached flow near the trailing edge for all angles of attack available. Figure 13 presents data for the 0.9 Mach number case which indicates a flow dominated by shocks and vortex flow. The flow remains attached near the trailing edge at angles of attack up to 6 degrees.

Comparison Of Wind Tunnel And Flight Data

The mounting of the canard in flight is on the side of the inlet, rather than the more usual mount on the fuselage. It was impossible to mount the wind tunnel model in such a fashion due to the large number of pressure tubes at the model root, or wall juncture. In addition, the wind tunnel model would be immersed in the thick, side-wall boundary layer. In this situation, the side wall boundary layer, at the canard root, tends to separate at lower angles of attack than the freestream flow on the outboard portions of the canard, tending to spoil the data. To alleviate this condition, the canard was joined to the side wall by a fillet, as discussed earlier. This appears to have been successful, since in all cases the flow separates at the tip earlier in angle of attack than at the root. Details of the fillet may be found in reference 13.

The data at Mach 0.7 for the wind tunnel and flight are compared in figure 14. The agreement at the midspan station is very good. The mismatch in angle of attack indicates that a more sophisticated correlation may be needed for the flight local upwash angle. The agreement at the inboard station is not as good. However, increasing the flight angle of attack as shown in figure 15 improves the agreement, in character if not in level. At the same time, the midspan station agreement has deteriorated. This may indicate that a spanwise term is needed in the correlation for upwash angle.

It is difficult to compare the bulk data plots for the Mach 0.9 case, partially because much of the flow phenomena occurs close to the leading edge and the flight experiment has no data points in this region. Favorable comparison is available however, as shown in figure 16. Now the flow is dominated by shocks, and the angle of attack, or upwash, correlation works very well at both span stations. The filled symbols are the flight data and show a vortex at the inboard row where the tunnel does not. The shock location is matched very well and the overall agreement is considered good. The midspan row is more dominated by shocks than vortex flow and the agreement is excellent. Viscous-inviscid interactions (e.g. Reynolds number effects) are of first order importance for the transonic airfoil case, due primarily to the hypersensitivity of transonic flows to area ratio. Reynolds number effects on the wind tunnel data, including values well beyond the flight range, may be found in reference 13.

UNSTEADY AERODYNAMICS

Reynolds Number Effects in Flutter Model Testing

A flutter test has been conducted in the 0.3-m Transonic Cryogenic Tunnel to explore problems, develop testing techniques, and determine the potential of a cryogenic tunnel to advance the state of the art in flutter testing. A simple "text book" rectangular planform wing model supported by a beam flexure was used for the test. Model and support were machined

from a single piece of 18 Nickel grade 200 maraging steel (trade name Vascomax 200). This material is characterized by its good dimensional stability with temperature change and its high fracture toughness at cryogenic temperatures. Although no "hard" flutter points were included in the test, the model oscillations were large enough to be easily visible on a video monitor at conditions near flutter onset. Figure 17 presents a comparison of analytical and experimental flutter results in terms of the flutter dynamic pressure as a function of Mach number. It is presented here only to illustrate flutter data taken at cryogenic temperatures, and was taken from reference 14. The conclusion is that Reynolds number effects are small. Further details including the effect of Reynolds number on transonic flutter are also contained in this reference.

Buffet Testing.

Buffet testing has been conducted in the 0.3-m TCT using semi-span models mounted on one turntable. Instrumentation included a root bending gage to indicate buffet onset. Models included both delta and straight wing planforms. The ability to hold Mach number and Reynolds number constant while varying the velocity demonstrated the strong dependence of buffet onset on the reduced frequency. This research is ongoing and recent tests have used carbon composite models to increase the resonant frequency of the model; the reader is referred to the research documented in reference 15.

In the NTF, buffet boundaries have been established for a modern transport wing, figure 18. The boundaries were established at transonic conditions over a range of Reynolds number. These results are particularly interesting because, with the wing clean (no vortex generators), buffet was not encountered at Reynolds numbers of 7 and 35 million per foot, but was encountered at higher Reynolds numbers. This result is best understood in light of the model dynamic response characteristics. A detailed discussion of this data and the associated dynamics and other variables is contained in reference 16. See reference 17 for the oscillating airfoil case.

MEASUREMENT PROBLEMS IN HIGH REYNOLDS NUMBER CRYOGENIC FLOW

The term non-intrusive implies optical access through the wind tunnel wall, usually a window. For cryogenic facilities operating at high pressures and cryogenic temperatures, such windows pose major problems. For instance, in the 0.3-m TCT, a quartz window shrinks much slower with decreasing temperature than the aluminum structure. At room temperature, the quartz piece must fit loosely, and provide room for the aluminum to shrink around the quartz as the temperature is lowered to cryogenic operation conditions. At the same time, the window and frame must support the pressure drop when operating at room temperatures.

A window at cryogenic temperatures exposed to room temperature air and its attendant humidity must be kept clear of fog and/or frost. One method of maintaining a clear window is to position a thin piece of glass about 10% of the window diameter away from the quartz and purge the resulting gap with dry, heated, Nitrogen gas. Since this is a transonic tunnel with a plenum chamber, there must be a window in the test section wall as well. Thus an optical beam must traverse a thin, unloaded, piece of glass with a small thermal gradient, the purge gas region, the heavily loaded, up to 6 atmospheres, pressure shell window, the nitrogen in the plenum, the lightly loaded, essentially isothermal, test section window, the tunnel wall boundary layer, and finally the test flow. In the case of some techniques, such as a shadowgraph, the process is repeated in reverse on the other side of the test section. In the case of backscatter laser measurements, the low intensity signals must travel back through the same set of conditions.

There are several additional difficulties to recognize in the application of optical techniques to the 0.3-m TCT: Since all of the structural parts must contract with decreasing temperature, and it is not possible to insure isothermal structures, provision must be made for

referencing measurements in space to the model locations. For example, this required a special alignment laser for laser velocimeter measurements, reference 18. Other sources of error that must be considered are deflection of structural parts due to differential pressures or model support loads and effects such as lensing of the windows under distortion from pressure or thermal loading. Most of these difficulties are inherent in a facility designed to provide aerodynamic coefficients at flight conditions as opposed to a facility designed for pure fluid mechanics studies or for validation of analytical methods.

Optical Methods

Various flow diagnostic and visualization techniques have been tried in the 0.3-m TCT both to enhance the research utility of the tunnel and to explore the problems and opportunities offered by cryogenic testing. The use of the Laser Transit Anemometer to survey velocity distributions in flow fields and boundary layers is described elsewhere in this paper and in reference 18. Other methods reference (19-24), include laser holographic inteferometry, schlieren, shadowgraph, image quality studies, and moire deflectometry measurements. All have been successful to some extent. One major problem that was encountered was a swamping of the flow features by an optical disturbance that strengthened as the tunnel temperature was lowered. This problem was isolated and identified as thermal inhomogeneities external to the test section, primarily due to convective currents in the plenum chamber. The optical degradation becomes more severe with decreasing temperature and increasing pressure, and exhibits a $(p/T)^2$ dependence. This problem is discussed in detail in reference 20.

Seeding a Cryogenic Tunnel

Several of the more promising laser diagnostic techniques require the flow to be seeded with reflective particles a few microns in diameter. At this time there is no clearly satisfactory method of seeding a cryogenic tunnel. Measurements have been made using "natural" seeding generated by running the tunnel cold enough to preserve condensed nitrogen droplets, or by pulsing the liquid nitrogen control to generate a temporary cloud of liquid nitrogen droplets. A chance oil leak past the fan shaft seal provided very satisfactory data rates when the flow was cold enough to promote condensation of the oil into droplets. However, these schemes have serious drawbacks in that the errors introduced by testing in condensed flow are not defined and no correction method exists, the flow conditions are not known during injection pulsing, and at the extreme cold necessary for high Reynolds number operation, it is suspected that the oil freezes into solid particles and is responsible for eroding the model leading edges. Seeding has also been accomplished by bleeding service air into the tunnel and reducing the temperature to form condensed water, or ice, depending on the temperature. Once again, the larger condensates are expected of causing model erosion at the lower temperatures. To offset the fan heat, the tunnel must be continually injected with liquid nitrogen and the resulting gas vented. Thus the facility continually purges itself, and seeding material must be constantly replenished. Also, since the material is continually vented, it must be environmentally acceptable.

High Reynolds number testing requires good model surface finish, particularly on the leading edges, and small pressure orifices. Great care must be exercised to preserve the finish and keep the orifices unblocked even before the model is installed into the tunnel; introduction of solid particles is advisable only if they do not aggregate and form clumps that have sufficient ballistic coefficient to impact the model, and if they cannot accumulate in the model orifices or other sensitive mechanisms such as actuators. Liquid particles must not form ice clumps at low temperatures and must evaporate at room temperatures to allow cleanup. Thus far the only solid particles that have been tried are kaolin powders. The liquids are water and lubricating oil. Both the kaolin and the oil required extensive cleaning of the tunnel after use and are considered unsuitable materials.

Two-spot Laser Boundary Layer Survey

The two-spot laser, or more properly the Laser Transit Anemometer, LTA, focuses two laser beams into spots 9 microns in diameter with a spot-to-spot separation of about 20 spot diameters. When the spots are aligned with the flow in a wind tunnel, that is with one spot upstream of the other, any reflective particle in the flow that happens to pass through the upstream spot will reflect back a pulse of light. As the particle passes through the second spot it will reflect back a second pulse of light. Since the distance between the spots is known, a measurement of the time between the two pulses yields velocity. This process may be greatly enhanced by seeding the flow with appropriate particles. The data in figure 19 was generated by such a process where the LTA was used to survey the flow field of a 1.2 inch diameter cylinder along the line indicated in the "scan location" inset. This data is unique in that it was taken in a cryogenic environment and is one of the first successful attempts at measuring points in the boundary layer with this type of device. The two decreasing velocity points nearest the cylinder surface are in the boundary layer. Further details are available in reference 18.

FLUID MECHANICS

Skin Friction Measurements

Figure 20 serves to illustrate the principal of operation of the UTSI (University of Tennessee Space Institute) moving belt skin friction balances. The balance is mounted such that the belt part is flush with the surface to be investigated. The two drums that support the belt are in turn supported by flexures. When the belt experiences force due to the shear of a passing fluid, it rotates the drums against the restoring force of the flexures. The stiffness of the flexures is selected to allow a maximum of 3 degrees of rotation for the expected forces. Strain gages are attached to the flexures to produce a voltage proportional to, and linear with, the torque produced by the belt rotating the drums. Since the small gaps that are open to the flow do not change with this rotation, there is no need for a closed-loop nulling device to center the measuring element, as there is in the floating element type balances. Further details are available in reference 25.

Figure 21 summarizes the experience at LaRC with UTSI (University of Tennessee Space Institute) skin friction balances. The results shown were measured on the test section sidewalls of the 0.3-meter Transonic Cryogenic Tunnel, or 0.3-m TCT, and the Unitary Wind Tunnel. The comparison is presented in the incompressible plane since the Mach number ranges from low subsonic to transonic in the 0.3-m TCT, and though the supersonic range in the Unitary tunnel. The Karman-Schoenher flat plate skin friction formula is included for comparison. The shaded area represents data taken over the history of the Unitary tunnel with floating element skin friction balances.

The present results of testing on tunnel sidewalls should not be used to judge the accuracy of the skin friction balances. Rather, the data shown here should simply be taken as evidence of operational experience. Unless extraordinary precautions are taken, tunnel sidewall boundary layers are not classical flat-plate turbulent boundary layers. At a minimum, they are non-adiabatic and affected by wall roughness. Figure 22 shows that the 0.3-m TCT data level shown here can be represented by an equivalent wall roughness of only .02 mm. Since the ratio of boundary layer length to roughness height is the scaling parameter, and the boundary layer length increases with tunnel size, the larger Unitary tunnel would be only only one-forth as sensitive for the same absolute roughness height.

The appropriate conclusion to be drawn here is that the balance is capable of operation in environments as diverse as the cryogenic, transonic, high-shear rate of the 0.3-m TCT, and the high temperature supersonic environment of the Unitary tunnel.

The data shown in figure 22 for the 0.3-m TCT is the same as shown on figure 21, but has not been transformed to incompressible coordinates. Curves are shown for constant values of distributed roughness. The actual roughness was not measured. The approximate formula for rough flat plate flow used to generate the curves was

$$C_f = (2.87 + 1.58\log(x/e))^{-2.5}$$

where e is the roughness height and x is distance form the leading edge, reference 28. References 26 and 27 discuss the details of applying this formula to a test section wall boundary layer, by calculating an equivalent flat plate length. The curve labeled smooth in figure 22 was calculated from the relation,

$$C_f = 0.027 / (Re_x)^{1/7}$$

also from reference 28.

The intent of this figure is not to promote a rough wall prediction method or fully explain the data trends. It does serve to demonstrate the severe effects of small roughness heights in a turbulent boundary layer, and that an equivalent roughness height of only .02mm is sufficient to match the data. Further discussion may be found in references 26 and 27.

Current plans call for further testing of UTSI balances on a large flat plate in the NTF. Floating element balances as well as other types of skin friction measuring devices will also be tested for comparison. The surface finish will be carefully controlled and extensive boundary layer profile surveys will be conducted. The result will be a boundary layer much better understood than the test section sidewall cases.

The basic feasibility of the UTSI balance to operate in cryogenic conditions has been demonstrated. Carefully controlled testing will be required to establish limits on accuracy.

Transition Detection With Specialized Hot Films

An investigation to determine the location of boundary-layer transition was carried out using a cooled model. The photograph in figure 23 shows the model mounted in the 0.3-m TCT with the chordwise rows of hot-film gages mounted on the upper surface. The model is a 9 inch chord, 12 percent supercritical 2-D airfoil and was instrumented with 48 hot-films. The extremely thin hot-films were applied to the surface of the model by the Douglas Aircraft Company (DAC), using a newly developed method, as part of a NASA/DAC cooperative program to develop a specialized system for detecting boundary-layer transition in cryogenic wind tunnels. The tests, conducted in the Langley 0.3-m TCT, were done both at an adiabatic wall condition and at a non-adiabatic wall condition with liquid nitrogen circulation through the model to cool the surface below the adiabatic recovery temperature. The surface cooling was done to determine the effect of wall temperature on the location of boundary-layer transition at wall to total temperature ratios as low as 0.47. The test results indicated, that with the proper electronic data acquisition equipment, an "on-line" location of boundary-layer transition could be obtained both at ambient and cryogenic conditions. The on-line signal from the hot-films clearly indicated either a laminar, transitional or turbulent boundary layer. Preliminary results indicated that model cooling actually decreased the transition Reynolds number due to the apparent dominance of surface roughness on transition at this condition.

Transition Location by Fluctuating Pressure Measurements

Figure 24 shows the outline of a 14 percent thick airfoil recently tested in the 0.3-m TCT. This two-dimensional model was largely hollow and contained 43 transducers capable of measuring fluctuating pressures. The three traces shown above the airfoil are typical of the output data from these transducers. The trace at the left is near the nose of the model, has a low length Reynolds number, and exhibits a low amplitude fluctuating pressure trace typical of laminar flow. The center trace is from a transducer measuring pressures further back on the airfoil and produces a trace typical of transitional flow with a higher fluctuating amplitude as background and with superimposed turbulent precursor bursts of much higher amplitude. The

48

trace at the right is well into fully developed turbulent flow characterized by high amplitude, high frequency fluctuations in pressure. High amplitude fluctuations in the turbulent regime are perhaps expected for pressure measurements, as opposed to the decreased amplitudes recorded by the heat transfer devices, since the thickening boundary does little to attenuate pressure waves, but generally lowers heat transfer rates. Reference 17 presents greater detail on this work.

New Techniques For High Reynolds Number Testing

Two-dimensional airfoil testing is a standard test technique used to examine the characteristics of an airfoil section in more detail than would be possible in a full aircraft configuration. One problem peculiar to this type of testing is error introduced by the penetration of the model through the thick, tunnel-side-wall, boundary layer. Since this boundary layer does not have as much momentum as the external stream, it will separate much easier than the free stream flow. At low lift conditions, separation may not occur. As the lift increases, the side wall boundary layer will separate. At high lift, this separated region becomes large enough to influence measurements at the center of the airfoil, thus spoiling the data. This problem can occur at even low lift conditions when there is a transonic shock present. Other errors are introduced by the presence of the floor and ceiling of the test section. One serious error is caused by the blockage of the model, especially at transonic conditions. This is commonly alleviated by slots in the walls, or in the current 0.3-m TCT test section, by adaptive walls. Methods of dealing with these error sources are described in the next sections.

Adaptive Wall Test Section. To reduce or eliminate wall interference we need to use adaptive wall test sections. Although we include adaptive walls under advanced techniques, British researchers first used them 50 years ago, reference 29. Modern digital controls and powerful computers have made the application of adaptive wall technology an easier process. Adaptive walls address the problem of wall interference at its source, the test section walls. We can use analytical techniques to correct any wall induced errors left after wall streamlining. For the 0.3-m TCT we have chosen an adaptive wall test section with solid but flexible top and bottom walls. We have had success with both 2-D and 3-D models through the transonic speed range. We and other researchers have demonstrated the practicality of adaptive wall test sections for transonic testing.

COMMENTARY

Many of the things that we call Reynolds number effects may actually be the effect of some other variable that we are unable to change independently of the Reynolds number. For example, in many of our facilities to change Reynolds number means also changing Mach number, dynamic pressure, and the unsteadiness of the flow. Also, in configuration flow, we describe any change in boundary thickness in terms of a Reynolds number, usually invented specifically for the particular case, when the change may not be a function of Reynolds number at all. An example is the change in boundary thickness due to cross flow. This is primarily a function of the transverse pressure gradient, but this author dutifully found a way to represent this effect as a function of Reynolds number. Other variables are flow disturbances, flow angularity, flow divergence, non-symmetrical flow, etc. Great care needs to be taken in high Reynolds number facility design, otherwise, we could spend years trying to understand phenomena generated by poor facilities that have no bearing on the problems of flight.

Test Technique

The advantages of the cryogenic concept for wind tunnel testing are, by now, well documented and understood, references 6 & 7. However, the development of cryogenic testing tools is an ongoing process. Also, in order to properly take advantage of all of the

research opportunities offered by cryogenic operation of a wind tunnel, it is necessary to develop some new techniques unique to cryogenic operation. In addition, the fact that the cryogenic facility can produce realistic flight boundary layers requires a quantum improvement in model construction techniques, involving surface finish, fidelity of model contours, and dimensional stability. A similar effort is required in instrumentation technique, particularly instrumentation techniques for transition detection and the study of unsteady aerodynamics. Summaries of test technique, model construction methods, and energy management for cryogenic high Reynolds number tunnels are found in references 30, 31, and 32.

Transition

Transition as referred to here is the transition from laminar to turbulent flow. It is of primary aerodynamic importance because laminar boundary layers have much lower drag than turbulent ones. It is important computationally because knowledge of transition location is necessary in linking a code with an experiment. It is important in controls and airfoil performance because laminar boundary layers separate much more easily than those that are turbulent. Many other phenomena require a knowledge of transition in order to understand their physics. It is of particular interest here because transition location can be a strong function of Reynolds number. The next paragraphs describe, in basic language, the physics of the transition process.

A laminar boundary layer on a surface of interest, an aircraft wing for example, must move along the wing surface. As it moves along, it exerts a force due to the friction between the wing and the air. This force is called skin friction, and as the boundary moves a set distance, this force times the distance moved is, by definition, energy expended. For the hypothetical case of a flat-plate wing, or zero pressure gradient, the boundary layer must replenish this energy by entraining higher energy from the freestream. This is accomplished by slowing down the adjacent freestream air by the shear between the boundary layer air and the freestream air. As soon as air is slowed, it becomes part of the boundary layer, and the boundary layer thickens due to the added mass. The shear at the wall and the shear at the free stream introduce flow instabilities. The viscosity of the gas tends to damp these micro-instabilities, but as the boundary layer progesses along the surface, more work is done, more mass is entrained by a ever thickening boundary layer, and the instabilities will become more severe until they can no longer be damped and we have the beginning of transition to turbulent flow.

In aerodynamic practice, we seldom work with bodies of zero pressure gradient since they have no volume, and cannot carry any cargo or fuel. Normally, when a flow first encounters a body, the pressure gradient is positive, tending to accelerate the flow. Initially, this acceleration equals or exceeds the work done by skin friction, and the boundary layer need not thicken, and it can be very stable and remain laminar (at least for the case of zero sweep). If the pressure gradient is not of sufficient strength, then some freestream air will still have to be entrained. In most cases, the wing or body cross-section area must continually increase to maintain a positive pressure gradient. The body will soon become large and the cross-section area must become constant and then diminish toward the aft end of the body. This will produce first zero pressure gradients, and then negative pressure gradients. For a lifting subsonic wing, the positive gradient will last only about 10 percent of chord. After this the boundary layer must thicken rapidly, its stability (damping) rapidly diminishes, and it becomes susceptible to a variety of disturbances, not just the flow instability described above. These disturbances may originate from velocity perturbations in the free stream, surface roughness, cross-flow, acoustic input, and so forth. All of these may affect the boundary layer differently as a function of Reynolds number. Whatever the reason, unless extreme care is taken, transition to turbulent flow will occur.

The above paragraphs serve as a simplistic physical-world introduction to a very complex subject. There are hundreds of papers in the literature regarding amplification and

damping, and no reliable predictor of transition location has emerged. This is a serious impediment the for computationalist, since accurate code development depends on the knowledge of transition location. The experimentalist also needs knowledge of transition location to understand changes in aerodynamics with Reynolds number. One way to "know" transition location is to "trip" the flow at a known location by artificial obstacles placed in the boundary layer. This method has been the traditional means of emulating high Reynolds number flow in a low Reynolds number facility. Unfortunately, using this method of fixing transition at a known location in a high Reynolds number tunnel introduces unacceptable errors. This is because the boundary layer becomes very thin at high Reynolds numbers and there is no trip method small enough in size. In fact, it is difficult to produce model surfaces smooth enough to prevent premature transition.

Although trips are used in transonic cryogenic tunnels, and they provide some valuable information, a means of non-intrusively measuring transition location is required. A promising method is detection of the adiabatic wall temperature change that occurs during transition from laminar to turbulent flow. The Stanton number, or potential to transfer heat, also increases during transition from laminar to turbulent flow. Thus transition location can be determined using thermocouples or other temperature measurement devices. Since the shape of the transition location can be very complex, a large number of thermocouples is required. A more satisfactory method would be to measure the temperature difference in terms of its radiated energy. At cryogenic temperatures, the wavelength of this radiation is in the far infrared and is very weak. However, there are instruments capable of taking an infrared "picture" of the model at cryogenic conditions.

Computation

One of the principal lessons learned in our cryogenic tunnels is that there is no "plateau" Reynolds number; aerodynamic phenomena frequently change even as flight Reynolds number is being approached. For those vehicles having flight Reynolds numbers so high that they exceed our experimental capabilities, extrapolation is necessary. Computation using Navier-Stokes codes appears to be our only source of information in this case. Flight testing will provide answers but it is expensive and is performed at risk to the flight crew, the vehicle, and the social and political support necessary for new programs. Matching the wind tunnel results through the available Reynolds number range and then extrapolating to flight with the computer is the preferable option.

Even for those vehicles and components having their flight Reynolds numbers within the range of our test facilities, computational answers are still necessary. In order to test a model, it must be loaded aerodynamically. All structures flex under loading and change shape. This shape change in turn results in change in the vehicle aerodynamics. One of the great advantages of the cryogenic tunnels is the ability to independently change dynamic pressure and Reynolds number, and thus isolate Reynolds number effects from aeroelastic effects. Experience has shown these effects to be of the same order. Even if it is possible to test at flight Reynolds number and dynamic pressure levels, the answer will only be correct if the model is aeroelasticly tailored to deform the same as the flight vehicle. In practice, this is very difficult and very few of these models have been built for wind tunnel use with small scale models.

The burden of integrating the effects of structural deformation fall to the computationalist. He must be able to subtract the model deformations from his solution and add back in the deformations appropriate to the flight vehicle structure. Efforts are underway to develop the necessary computational techniques. Thus far we have discussed static aeroelastics; the full solution requires treatment of the time varying flows and the extrapolation to these to flight condition. There is only one known set of high Reynolds number transonic data with sufficient detail to allow code calibration. Early development of such a code is in progress.

One of the long-standing goals of the aerodynamic community is to measure aerodynamic coefficients to an accuracy the order of one "count". (To illustrate the concept of a count, consider the definition of drag coefficient which essentially ratios the actual drag to the maximum value likely. This concept results in a coefficient of 1 when all of the momentum of the air processed by the vehicle is removed. A typical aircraft might operate at a value of 0.03. If we assign a value of 10000 counts to a coefficient of 1, then the aircraft flies at a value of 300 counts, and the accuracy implied in one drag count capability is 1/300 or 0.3 percent). The economic viability of a new transport aircraft might depend on a few counts of drag. In our new facilities, we have demonstrated our capability to operate within one count of drag. This is a very significant accomplishment but, due to support effects, model distortions, etc., this is really only the measure of a drag increment. Being able to accurately measure drag increment is important in effecting vehicle improvements, but it cannot forecast final flight performance. Once again, we must depend on computation. Unfortunately, prediction of high Reynolds number performance for flight vehicles is at best a fledgling capability.

Finally there is the question of optimization. At present there is no clear algorithm for optimization of an aircraft. The best efforts to date have come from the intuition and innovation of the researcher's brain. There is a belief, however, that we are no closer than 70 percent of optimum for even our most well understood aircraft. The remaining 30 percent is a very enticing area for further research. This is carried out at present in a painfully slow trial and error process of small perturbations on wind tunnel model geometry. Not only would this process proceed much faster computationally, but the opportunity for real optimization exists. This process has begun with the application of design codes that can create a geometry that produces a predescribed ideal pressure distribution and external flow parameters. Once again, computation seems to be the only hope for real aerodynamic optimization in transonic, high Reynolds number flow.

RECOMMENDATIONS

The 0.3-m TCT and the NTF have proven the worth of the cryogenic test technique to provide high Reynolds number transonic data for aircraft models and components. It is now time to apply this technology to other problems. For example, reference 33 presents a collection of papers that describe the testing of a submarine model in the NTF. Although this was a successful test, it was very expensive and used a large and cumbersome model and still did not provide full scale Reynolds numbers. In reference 33, a superfluid helium cryogenic facility is proposed to better accomplish the submarine test at the desired Reynolds number. In this same vein, it is time to consider other applications. For instance, the NTF is currently involved in high lift testing at low Mach numbers for very large airplanes. Even the cryogenic, 9 atms. capability of the NTF is strained to produce the desired Reynolds number; even at the proper Reynolds number, the dynamic pressure is so high that aeroelastic distortions are a problem. Also, the loads are so high that multi-element airfoils are very difficult to construct, and impossible to operate at the flight level of aeroelastic deformation. A possible solution to this is to construct a very large, low speed, cryogenic tunnel. This solution should be seriously examined, since it will not only allow the proper Reynolds number, but also allow for excursions in dynamic pressure to examine the effects of loading on the critical gap dimensions between elements.

Consideration should also be given to using cryogenic techniques to provide data on rotating systems such as propellers, and helicopters blades, and coupled with magnetic suspension techniques, spin tunnels, dynamic departure, and other neutrally stable or unstable operating modes.

None of these facilities will be useful without models. Model building technique should be the subject of continual development. If a large tunnel requires 20 models per year at an average cost of one million dollars, then in a tunnel life cycle of 50 years, one billion dollars will have been expended on models. The model building efficiency, size and cost

should be considered in the tunnel initial design.

In past facilities, circuit losses were tolerated in the design if they resulted in lowered capital investment. Typically a watt lost in the circuit just cost a watt increase in the drive motor usage. In a liquid nitrogen tunnel a one watt loss will cost on the order of 10 watts in liquid nitrogen cooling, and 1000 watts in superfluid helium (see references 32 and 33). In addition, circuit losses usually create some sort of tunnel disturbance, which in turn requires more losses in the form of flow screens to correct, which in turn requires more input to the fan power, which in turn generates more disturbance. Obviously time would be well spent in designing more efficient circuits, particularly for our high Reynolds number tunnels.

A final recommendation is for teams of researchers that are dedicated to one facility and/or discipline. It requires about 10 years of experience in a facility before the average researcher begins to generate the best results. Continual changing in program focus and the resulting oscillations in the testing staff result in less than the best research results.

Recognize that test technique, model building, computation and staffing all deserve consideration on equal footing as a package for the optimum facility utilization and performance.

REFERENCES

1. Jones, Lloyd J.: The Transonic Reynolds Number Problem, published in High Reynolds Number Research, NASA CP-2009, 1976.

2. Reynolds Number Effects in Transonic Flow, AGARDograph No. 303, Dec. 1988.

3. Johnson, C. B.; Johnson, W. G. Jr.; and Stainback, P. C.: A Summary of Reynolds Number Effects on Some Recent Tests in the Langley 0.3-Meter Transonic Cryogenic Tunnel. SAE 861765, Oct. 1986.

4. Ray, E. J.: A Review of Reynolds Number Studies Conducted in the Langley 0.3-m Transonic Cryogenic Tunnel. AIAA/ASME 3rd Joint Thermophysics, Fluids, Plasma and Heat Transfer Conference, St. Louis Missouri. AIAA-82-0941, June 1982.

5. Tuttle, Marie H.; Kilgore, Robert A.; and McGuire, Peggy D.: Cryogenic Wind Tunnels - A Selected, Annotated Bibliography. NASA TM-86346, April 1985.

6. Kilgore, R. A.; and Dress, D. A.: The Application of Cryogenics to High Reynolds Number Testing in Wind Tunnels. Part 1: Evolution, Theory, and Advantages. Cryogenics, Vol. 24, August 1984, pp. 395-402.

7. Kilgore, R. A.; and Dress, D. A.: The Application of Cryogenics to High Reynolds Number Testing in Wind Tunnels. Part 2: Development and Application of the Cryogenic Wind Tunnel Concept. Cryogenics, Vol. 24, September 1984, pp. 484-493.

8. Ladson, C. L., and Ray, E. J.: Status of Advanced Airfoil Tests in the Langley 0.3-m Transonic Cryogenic Tunnel. Advanced Aerodynamics, NASA CP-2208, September 1981, pp. 37-53.

9. Johnson, William G., Jr.; Hill, Acquilla S.; and Ray Edward J.; Rozendaal, Rodger A.; and Butler, Thomas W.: High Reynolds Number Tests of a Boeing BAC I Airfoil in the Langley 0.3-Meter Transonic Cryogenic Tunnel. NASA TM-81922, April, 1985.

10. Lawing, P. L.; Adcock, J. B.; and Ladson, C. L.: A Fan Pressure Ratio Correlation in Terms of Mach Number and Reynolds Number for the Langley 0.3-Meter Transonic Cryogenic Tunnel. NASA Technical Paper 1752, November 1980.

11. Hoerner, Sighard F.: Fluid-Dynamic Drag. Published by the Arthor, 148 Busteed Drive, Nidland Park, New Jersey, 1958.

12. Lawing, Pierce L.; Wigley, David A.; and Glaab, Louis J.: Construction of Airfoil Pressure Models Using the Multiple Plate Method. Presented at the SAE AEROTECH 88, Anaheim California, October 3-6, 1988. SAE paper no. 881450.

13. Chu, Julio; and Lawing, Pierce L.: High-Reynolds-Number Test of a 5%-Thick Low-Aspect-Ratio Wing Model in the Langley 0.3-Meter Transonic Cryogenic Tunnel. NASA TM-4227, December 1991.

14. Cole, Stanley R.: Exploratory Flutter Test In A Cryogenic Wind Tunnel. NASA TM-86380, February 1985.

15. Mabey, D. G.; Boyden, R. P., and Johnson, W. G., Jr.: Further Buffeting Tests in a Cryogenic Wind Tunnel. Defense Research Agency TM Aero 2231, RAE Bedford, 1991.

16. Young, Clarence P., Jr.; Hergert, Dennis W.; Butler, Thomas, W.; and Herring, Fred M.: Buffet Test in the National Transonic Facility. AIAA 17th Aerospace Ground Testing Conference, July 6-8, 1992. AIAA Paper No. 92-4032.

17. Hess, R. W.; Seidel, D. A.; Igoe, W. B.; and Lawing, P. L.: Transonic Unsteady Pressure Measurements on a Supercritical Airfoil at High Reynolds Numbers. Journal of Aircraft, Vol. 26, No. 7, pp 605-614, July 1989.

18. Honaker, William C., and Lawing, Pierce L.: Measurements In The Flow Field Of A Cylinder With A Laser Transit Anemometer And A Drag Rake In The Langley 0.3-m Transonic Cryogenic Tunnel. NASA TM-86399, April 1985.

19. Gartrell, L. R.; Gooderum, P. B.; Hunter, W. H. Jr.; and Meyers, J. F. Laser Velocimetry Technique Applied to the Langley 0.3-Meter Transonic Cryogenic Tunnel. NASA TM-81913, April, 1981.

20. Snow, W. L.; Burner, A. W.; and Goad, W. K.: "Seeing" Through Flows in Langley's 0.3-Meter Transonic Cryogenic Tunnel. NASA CP-2243, pp. 133-147, March 25-26, 1982.

21. Rhodes, D. B., and Jones, S. B.: Flow Visualization in the Langley 0.3-Meter Transonic Cryogenic Tunnel and Preliminary Plans for the National Transonic Facility. NASA CP-2243, pp. 117-132, March 25-26, 1982.

22. Burner, A. W., and Goad, W. K.: Flow Visualization in a Cryogenic Wind Tunnel Using Holography. NASA TM-84556, November 1982.

23. Snow, W. L., and Burner, A. W., and Goad, W. K.: Image Degradation in Langley 0.3-m Transonic Cryogenic Tunnel. NASA TM-84550, November, 1982.

24. Snow, W. L.; Burner, A. W.; and Goad, W. K.: Improvement in the Quality of Flow Visualization at the Langley 0.3-m Transonic Cryogenic Tunnel. NASA TM-87730.

25. Vakili, A. D., and Wu, J. M.: Direct Measurement of Skin Friction With A New Instrument. International Symposium on Fluid Control and Measurement, Volume 2, pp 875-880. Tokyo, Japan, 1985.

26. Vakili, A. D.; Wu, J. M.; and Lawing, Pierce L.: Wall Shear Stress Measurements Using a New Transducer. Presented at the AIAA/ASME 4th Joint Fluid Mechanics and Plasma Dynamics and Laser Conference, Atlanta, Georgia, May 12-14, 1986. AIAA Paper No. 86-1092.

27. Lawing, Pierce L.; Vakili, A. D.; and Wu, J. M.: Experience at LaRC With a UTSI Skin Friction Balance. Symposium on Natural Laminar Flow and Laminar Flow Control Research. Langley Research Center, Hampton Virginia. NASA CP-2487 Part 2, pp. 407-411, March 16-19, 1987.

28. White, Frank M.: Viscous Fluid Flow. McGraw Hill Book Company. New York, 1974.

29. Wolf, S.W.D.; and Ray, E.J.: Highlights of Experience with Flexible Walled Test Section in the NASA Langley 0.3-meter Transonic Cryogenic Tunnel. AIAA Paper 88-2036, May 1988.

30. Lawing, Pierce L.: Test Techniques for Cryogenic Wind Tunnels. Presented at the AGARD-FDP/VKI Special Course "Advances in Cryogenic Wind Tunnel Technology" at the von Karman Institute for Fluid Dynamics, June 5-9, 1989. AGARD Report R-774, November 1989.

31. Lawing, Pierce L.: Models for Cryogenic Wind Tunnels. Presented at the AGARD-FDP/VKI Special Course "Advances in Cryogenic Wind Tunnel Technology" at the von Karman Institute for Fluid Dynamics, June 5-9, 1989. AGARD Report R-774, November 1989.

32. Lawing, Pierce L.: Energy Management and Recovery. Presented at the AGARD-FDP/VKI Special Course "Advances in Cryogenic Wind Tunnel Technology" at the von Karman Institute for Fluid Dynamics, June 5-9, 1989. AGARD Report R-774, November 1989.

33. Donnelly, Russell J., editor : High Reynolds Number Flows Using Liquid and Gaseous Helium. Springer-Verlag, 1991.

NACA 0012

$C_n = .4$

NASA SC(3)0712A

$C_n = .6$

BAC 1

$C_n = .6$
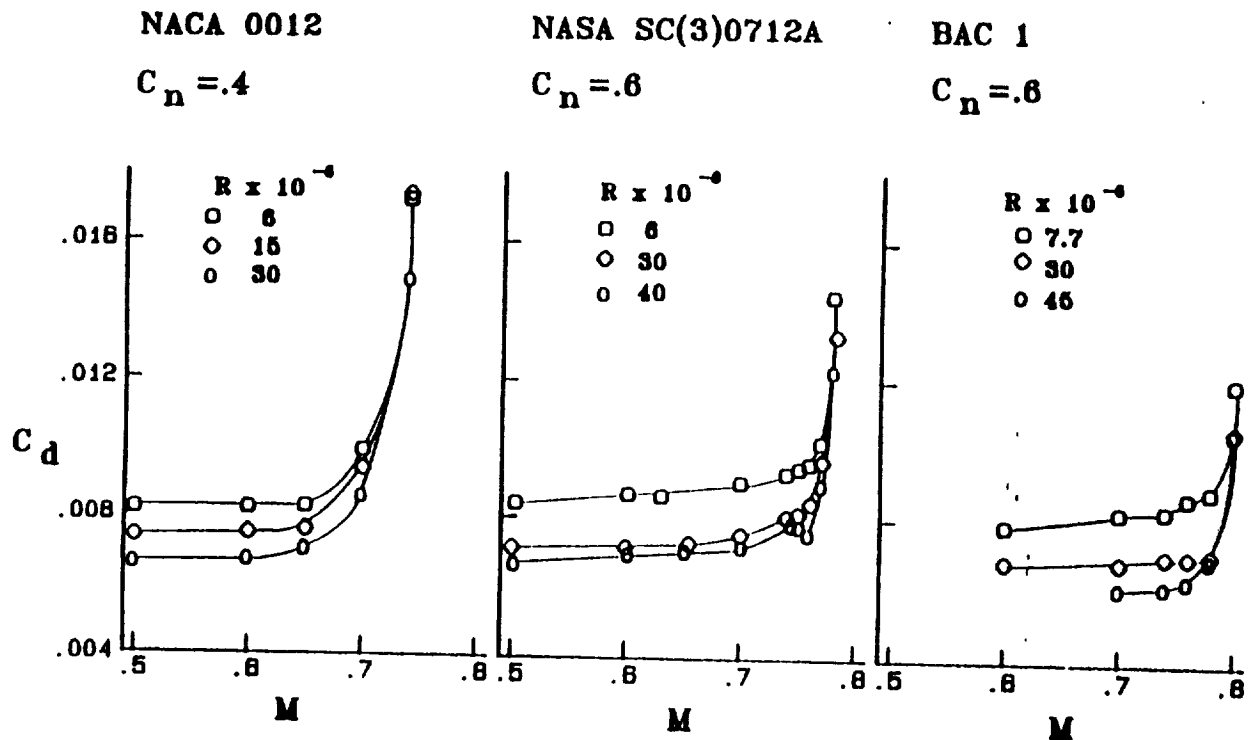
Figure 1. Effects of Reynolds number on drag coefficient.

NASA SC(3)0712A, R=30 x 10^{6}

M=.784

$C_n = .601$

M=.775

$C_n = .609$
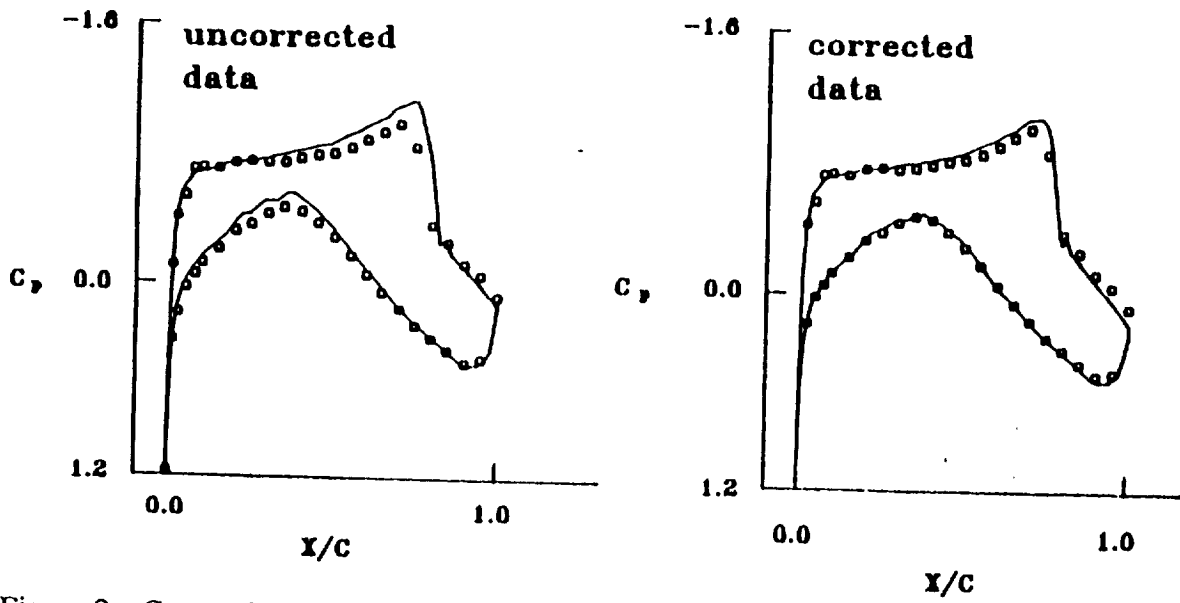
Figure 2. Comparison of experimental data with theory.
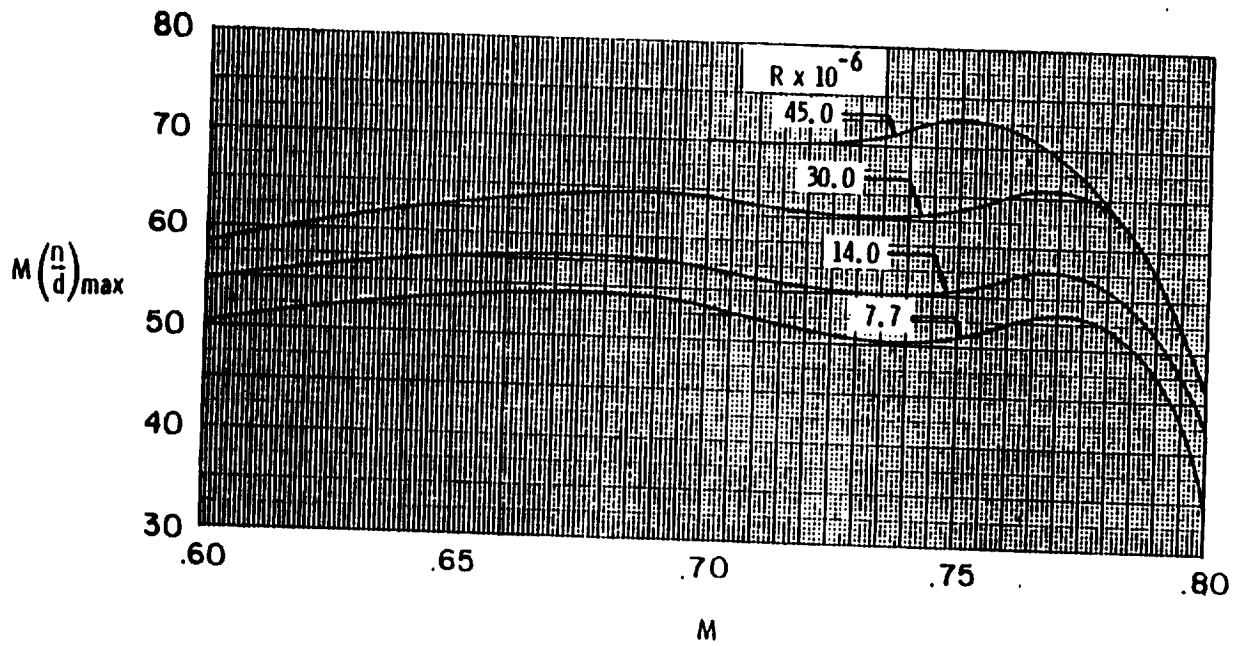
Figure 3. Effect of Reynolds number on variation of range performance factor M (n/d)$_{max}$ with Mach number.
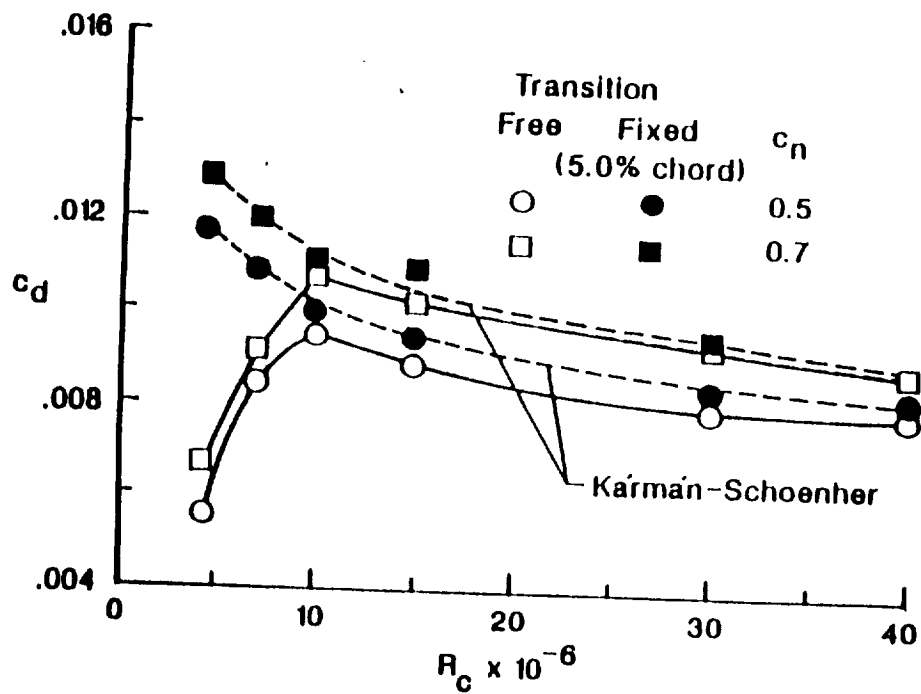
Figure 4. Variation of drag coefficient with Reynolds number for fixed and free transition on the NASA SC(3)-0712 airfoil at M = 0.76.
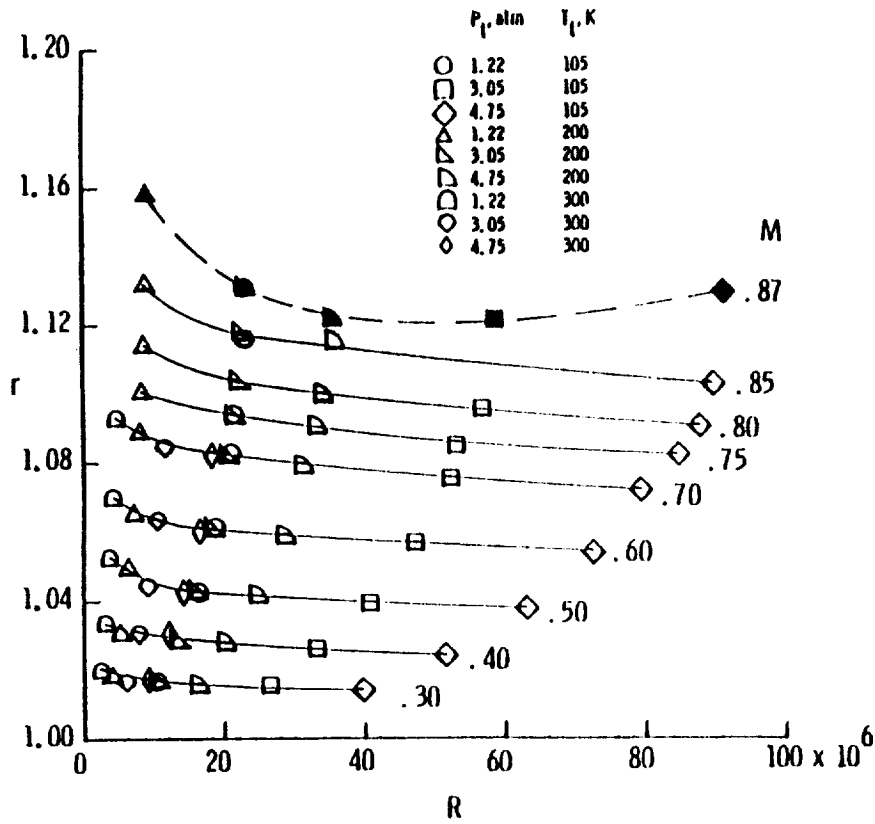
Figure 5. Fan pressure ratio as a function of Reynolds number for a range of Mach numbers. (Solid symbols denote tunnel choked condition.)
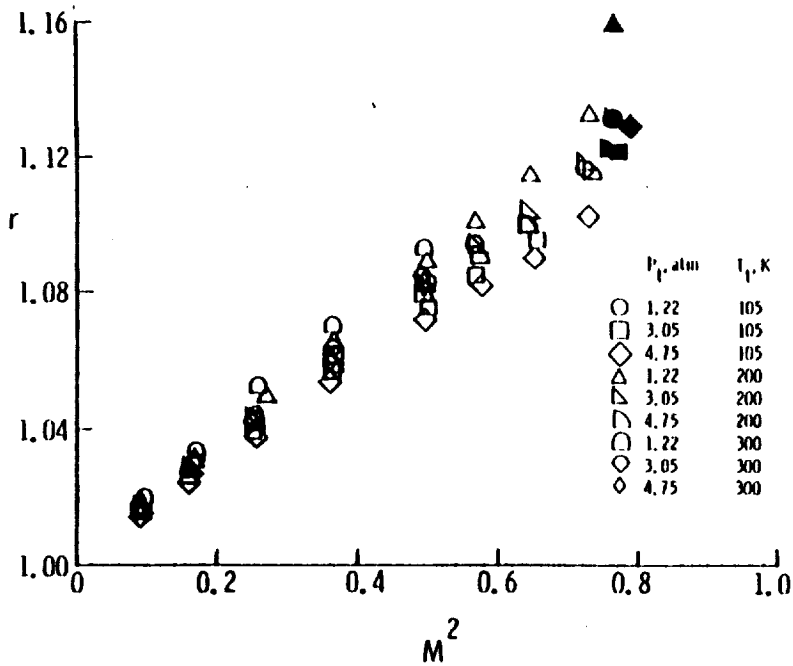
Figure 6. Fan pressure ratio as a function of Mach number squared.

$$r = 0.8205 \, M^2 \, R^{-0.096} + 1.001$$
for $0.3 \leq M < 0.86$
and $2 \times 10^6 < R < 92 \times 10^6$
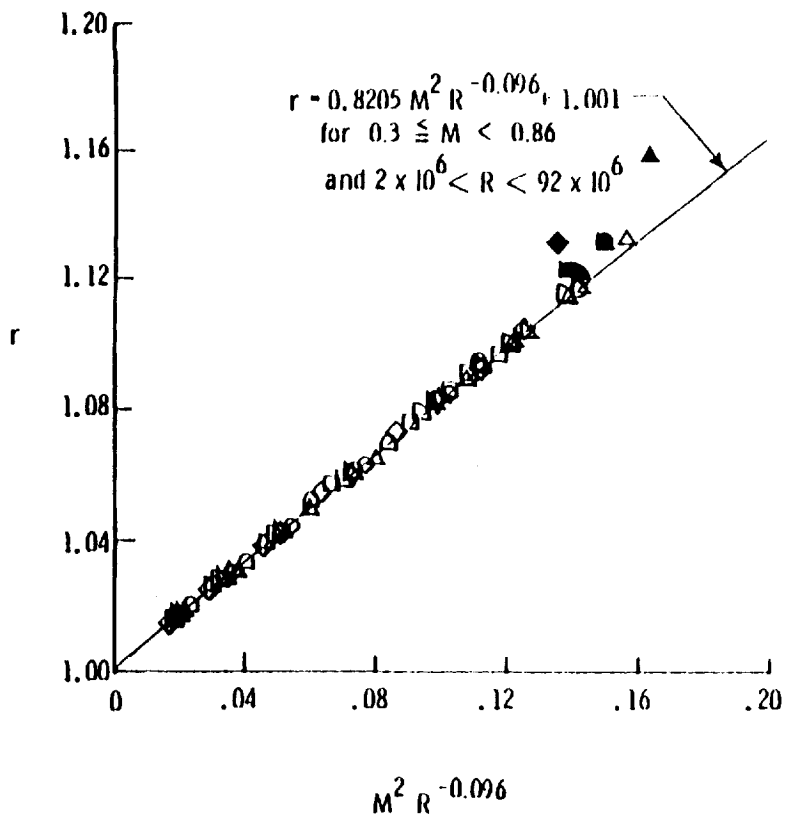
Figure 7. Fan pressure ratio correlated in terms of Mach number and Reynolds number.

Symbol	o	□	◇	△	◊
α	2.3	4.9	5.7	8.4	10.6
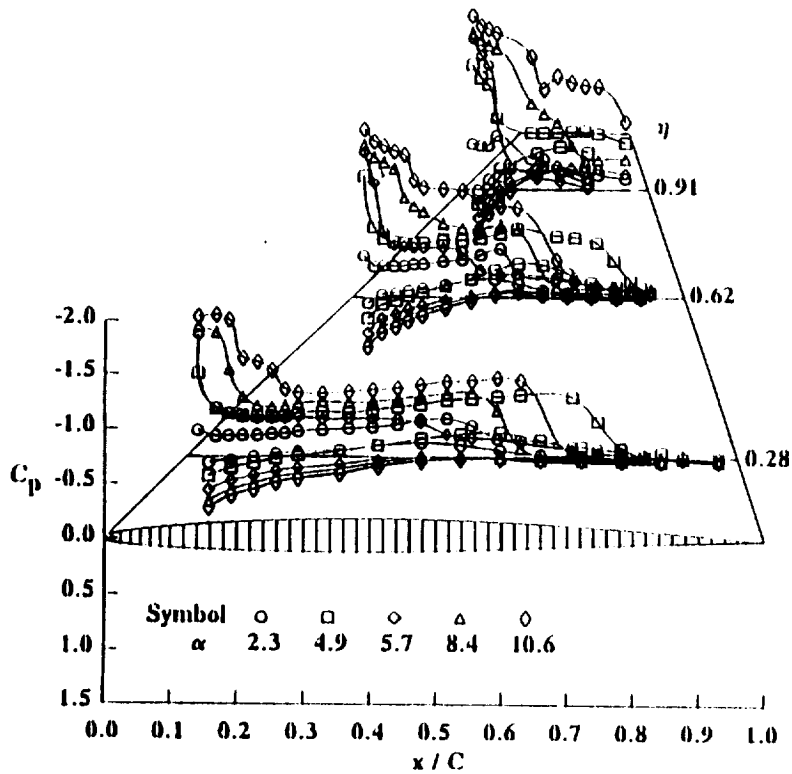
Figure 8. X-29 canard wind tunnel pressure distributions at Mach number = 0.9.

**Sample Pressure Distribution
and Wake Survey**

M = .9, Alpha = 8.4
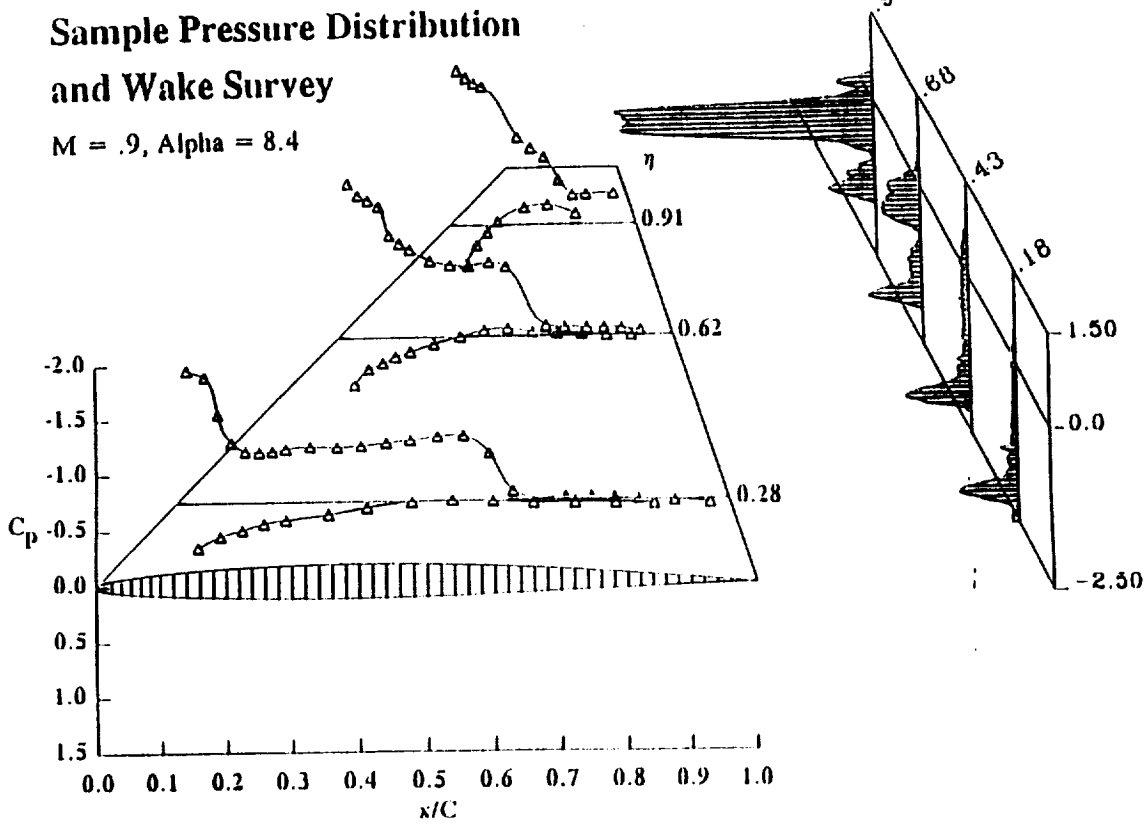
Figure 9. Sample wind tunnel pressure distribution and wake survey for the X-29 canard.
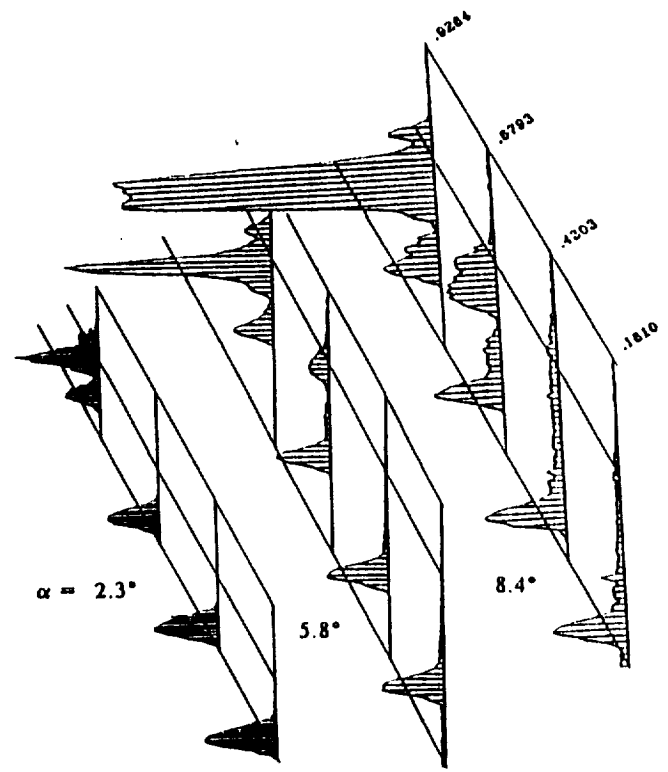
Figure 10. Momentum deficit surveys at three angles-of-attack from the transonic data set for the X-29 canard.
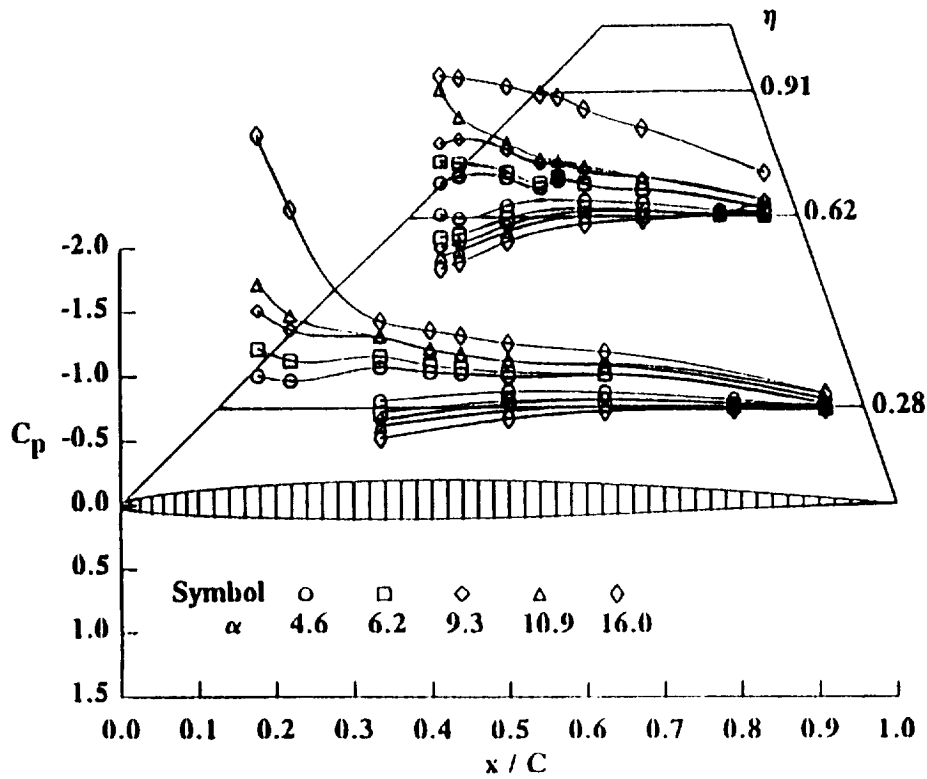
Figure 11. Pressure distributions at Mach 0.6 from X-29 flight data.
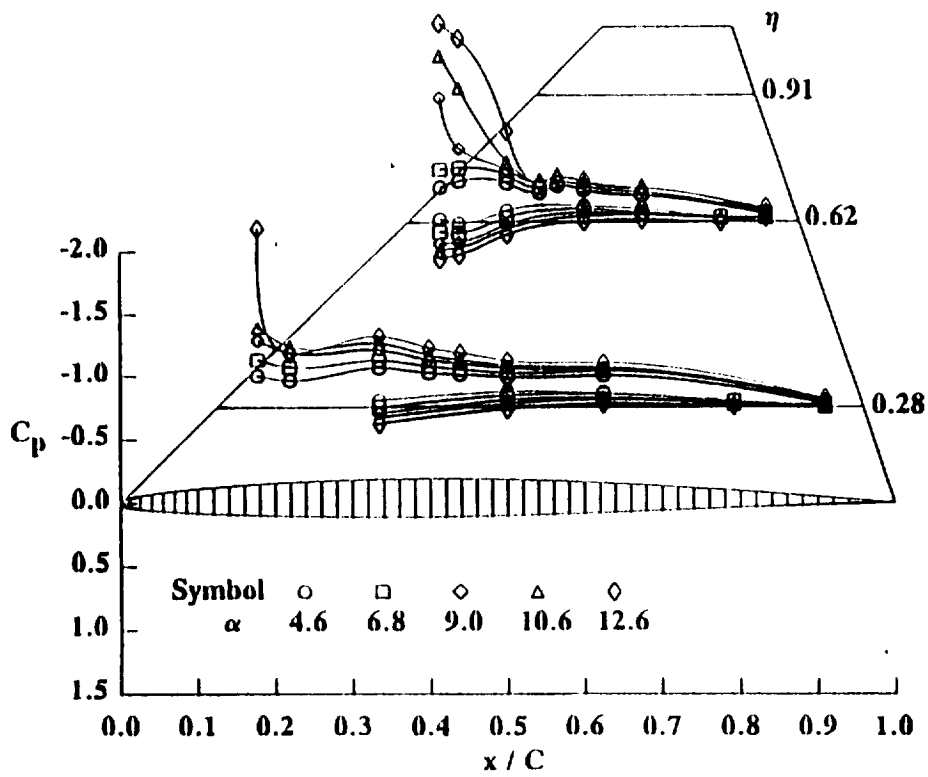
Figure 12. Pressure distributions at Mach 0.7 from X-29 flight data.

61
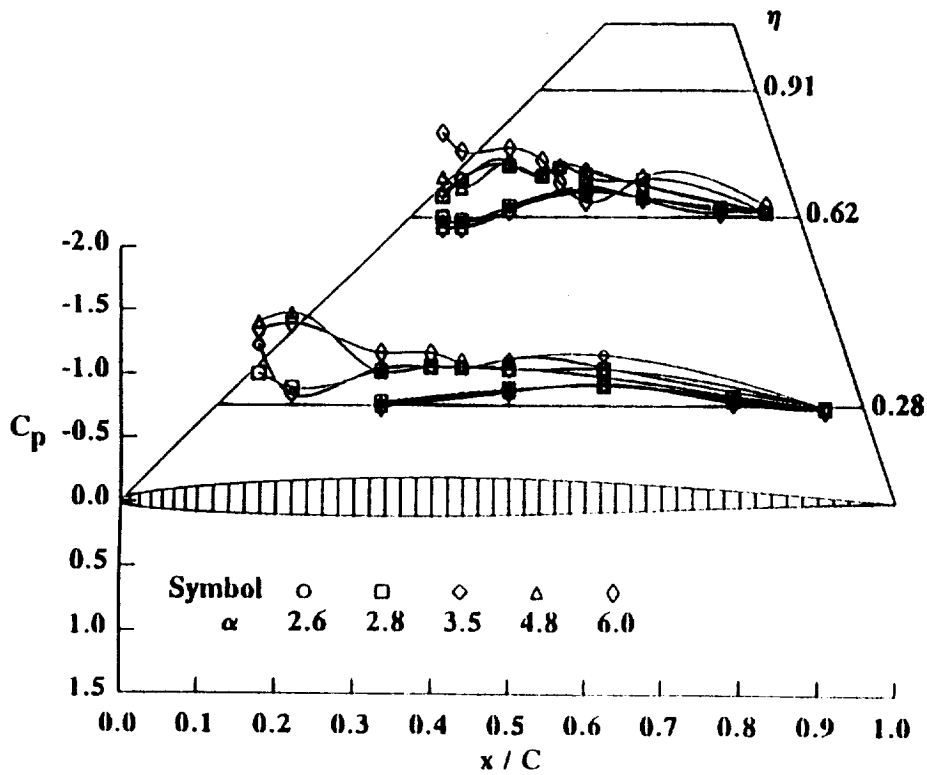
Figure 13. Pressure distributions at Mach 0.9 from X-29 flight data.
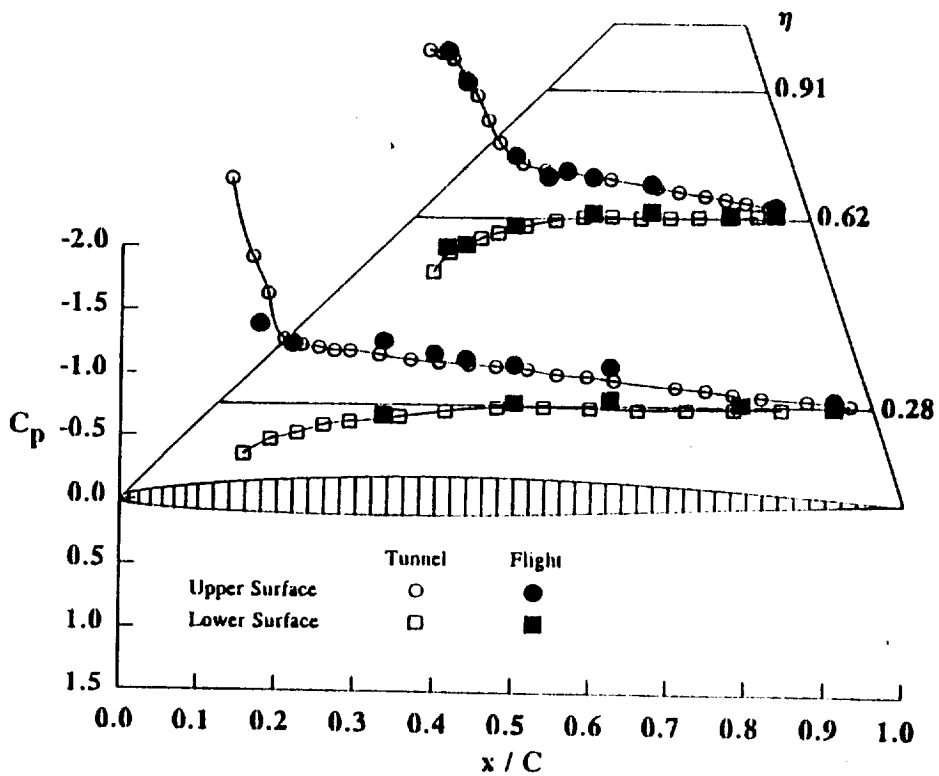
Figure 14. Comparison of flight and 0.3-m TCT data at Mach 0.7; $\alpha = 10.6°$ flight, 8.2° tunnel.
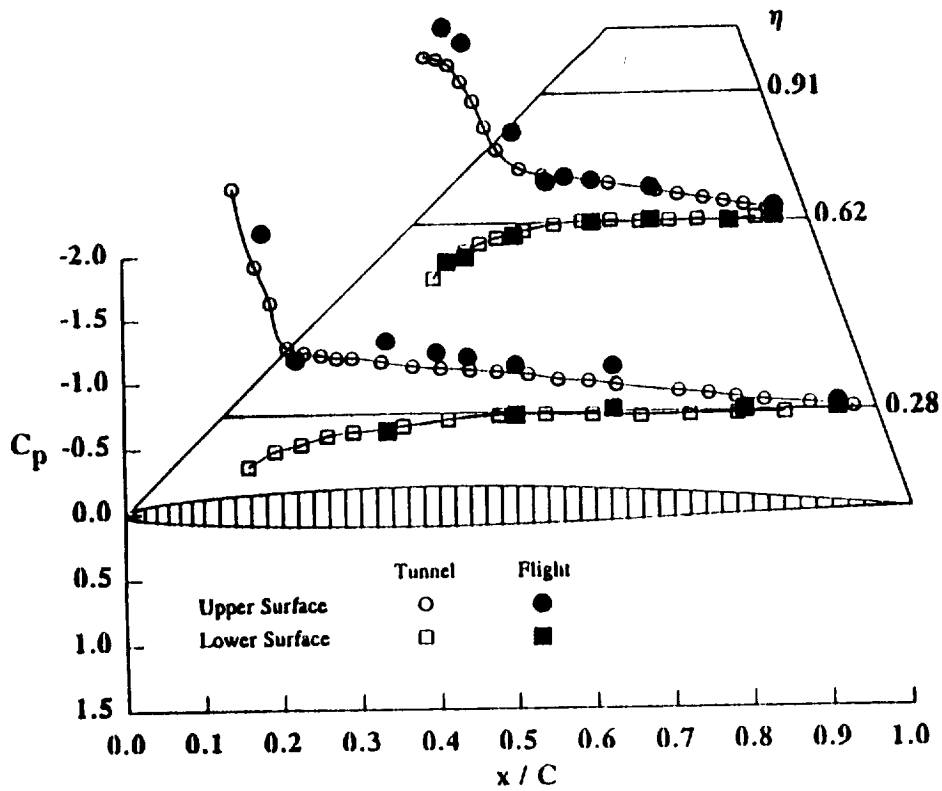
Figure 15. Comparison of flight and 0.3-m TCT data at Mach 0.7; $\alpha = 12.6°$ flight, 8.2° tunnel.
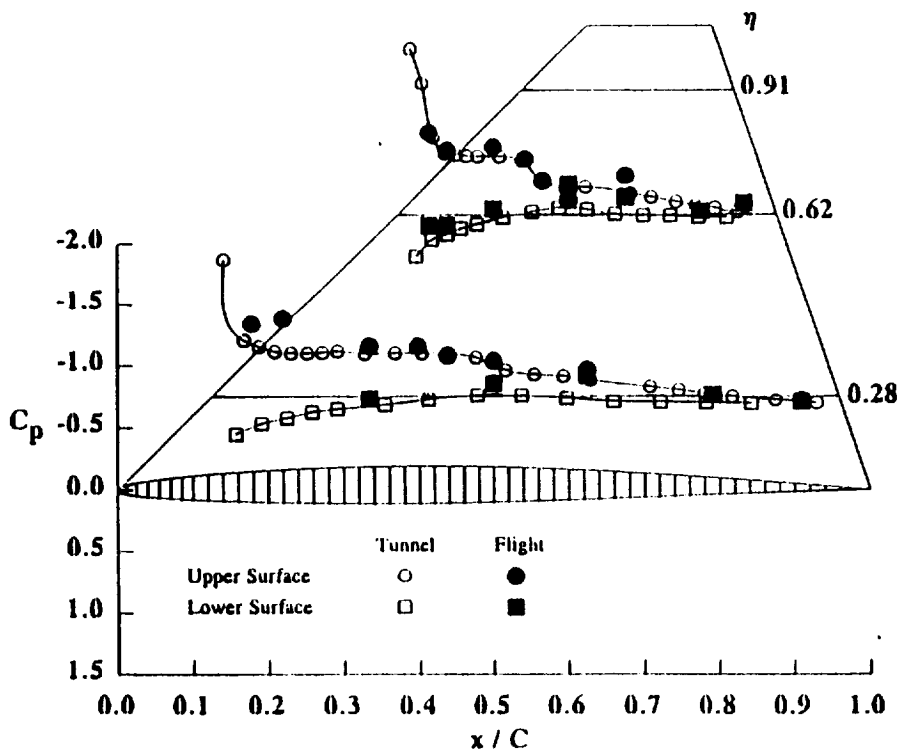
Figure 16. Comparison of flight and 0.3-m TCT data at Mach 0.9; $\alpha = 6°$.
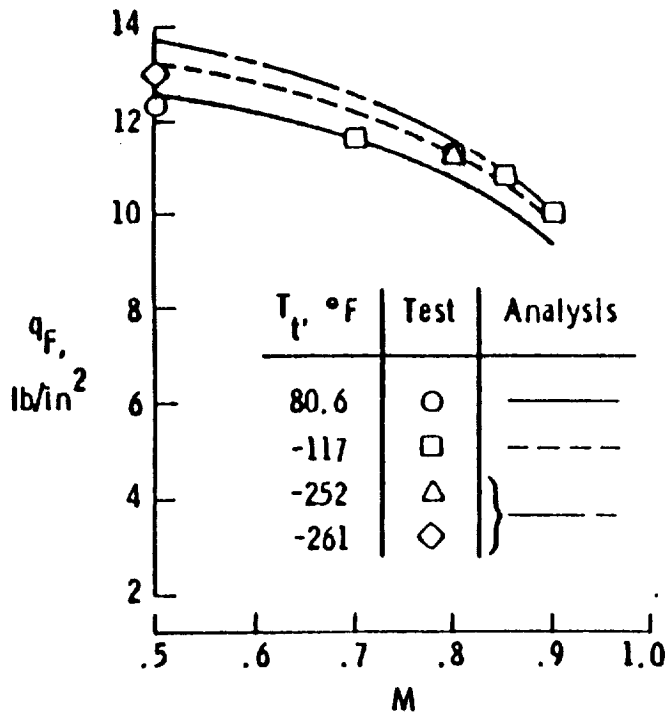
Figure 17. Experimental and calculated flutter results.
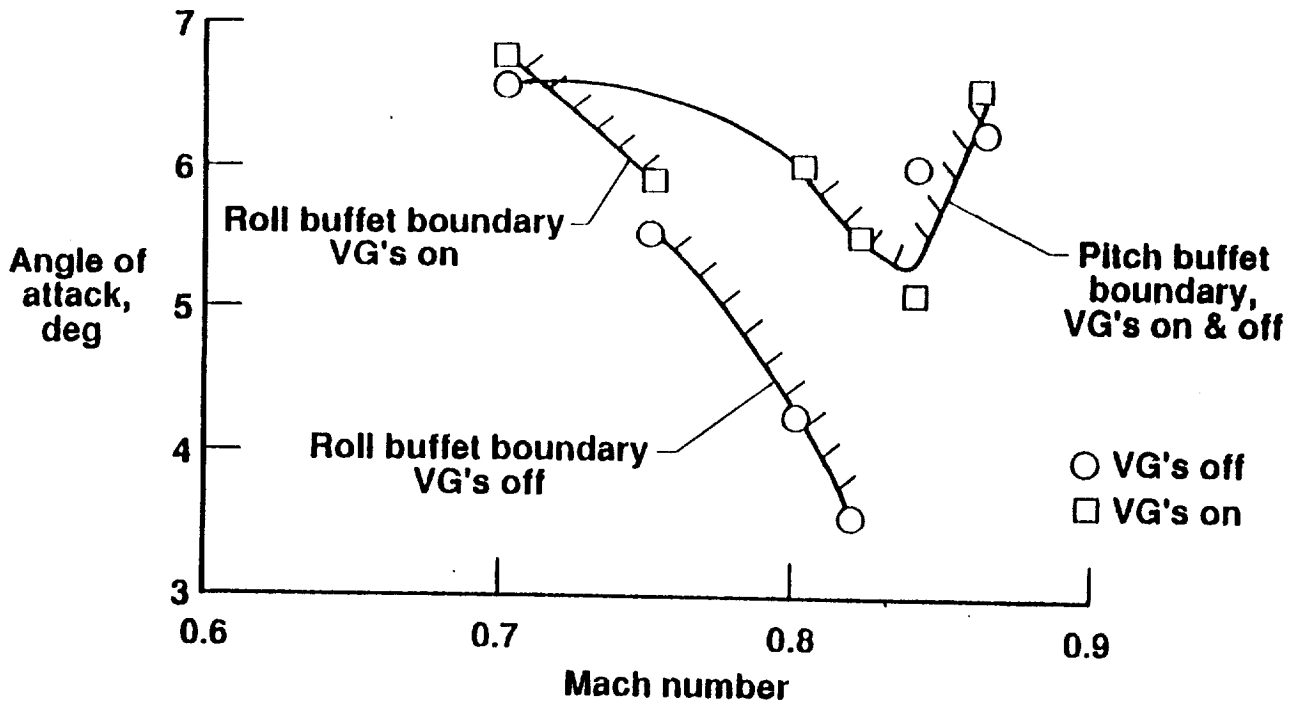
Figure 18. Model buffet boundaries at Reynolds number of 67 million.
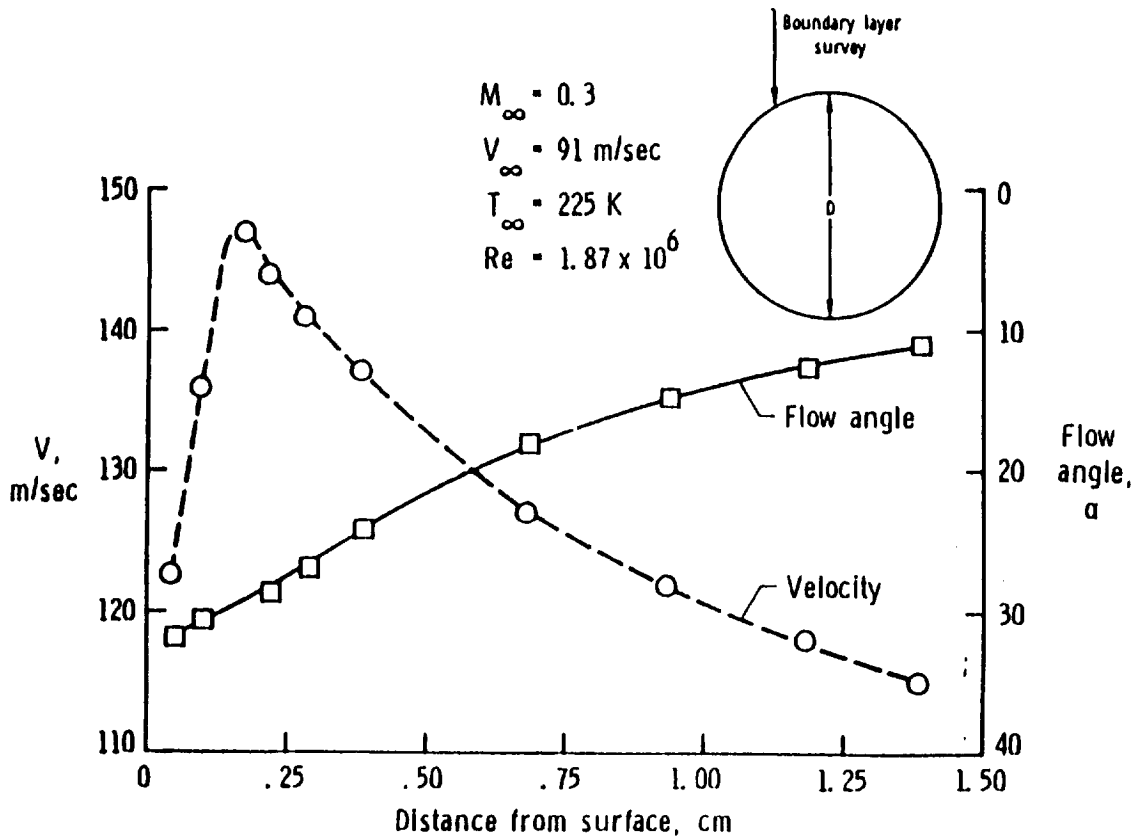
Figure 19. Velocity and flow angle as a function of vertical distance from the surface along the indicated scan line.
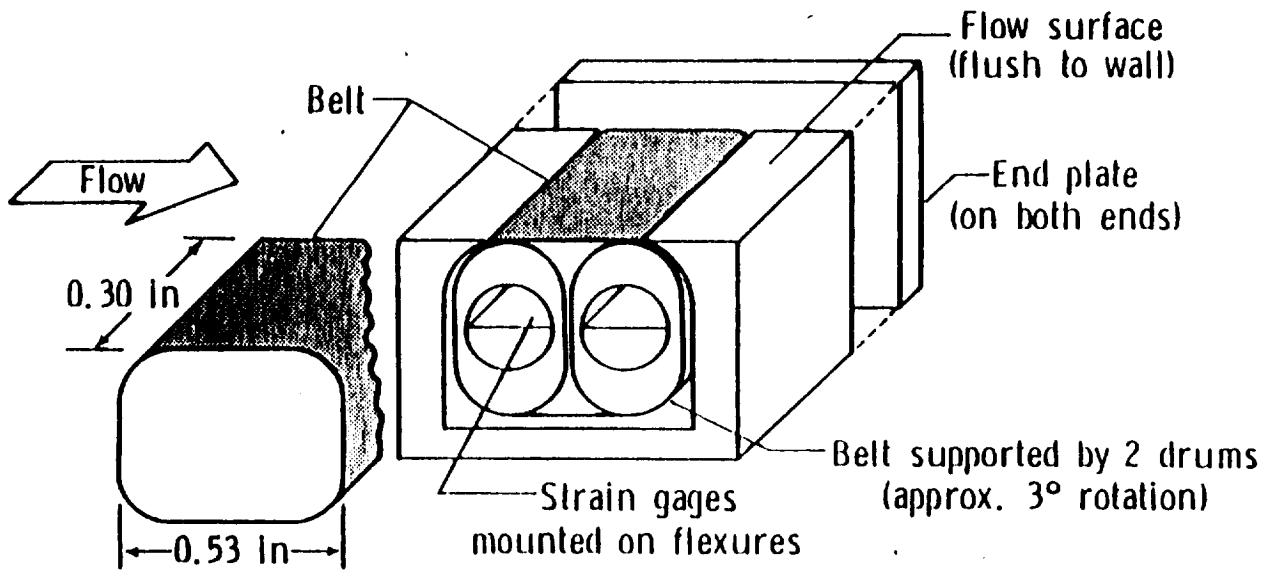
Figure 20. Schematic drawing of UTSI skin friction balance illustrating the moving belt concept.
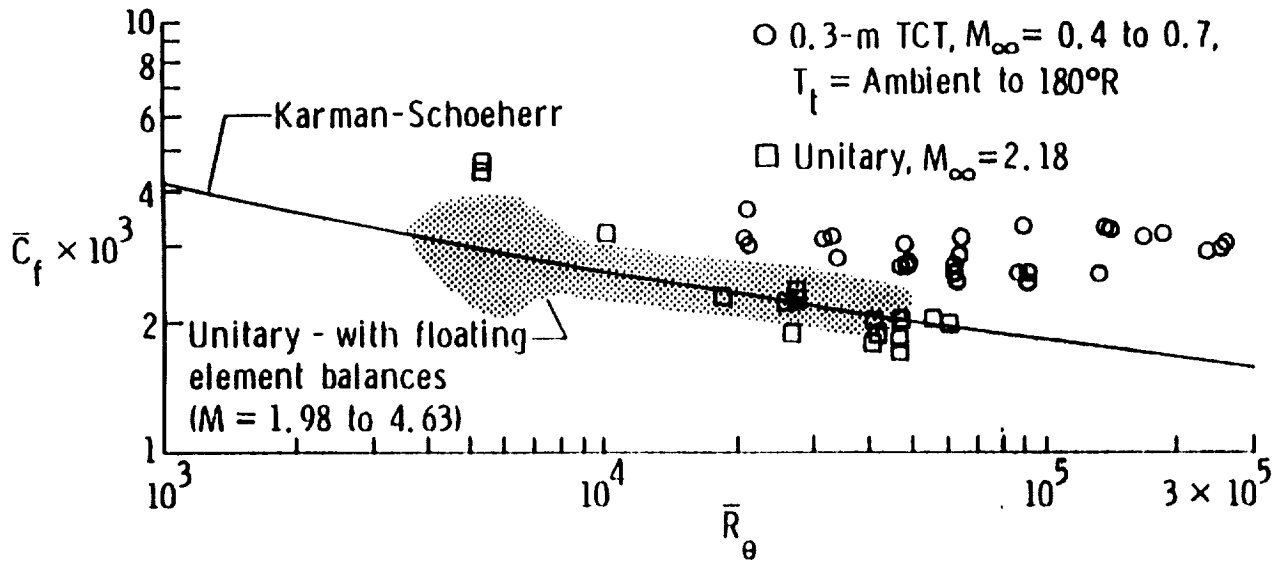
Figure 21. UTSI skin friction balance measurements compared to the history of floating element balances in Langley's Unitary Plan Wind Tunnel.
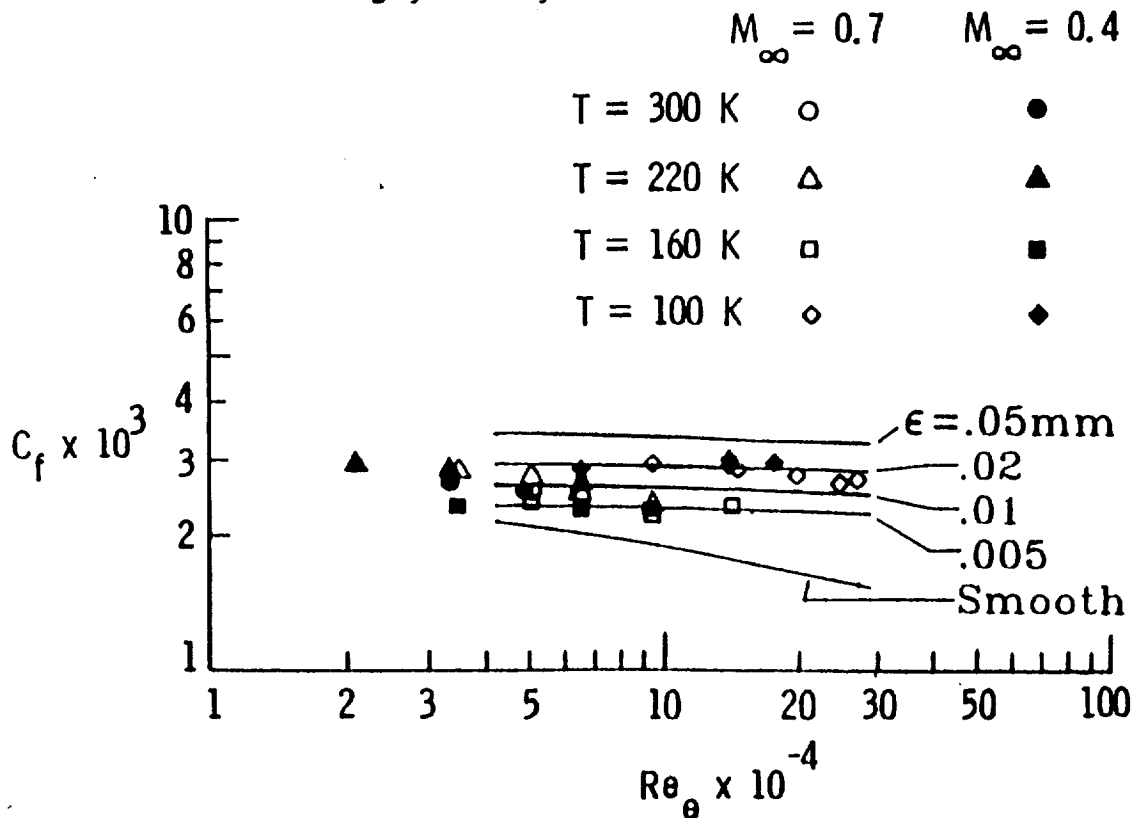
Figure 22. UTSI skin friction balance measurements compared with wall roughness theory in the 0.3-m Transonic Cryogenic Tunnel.
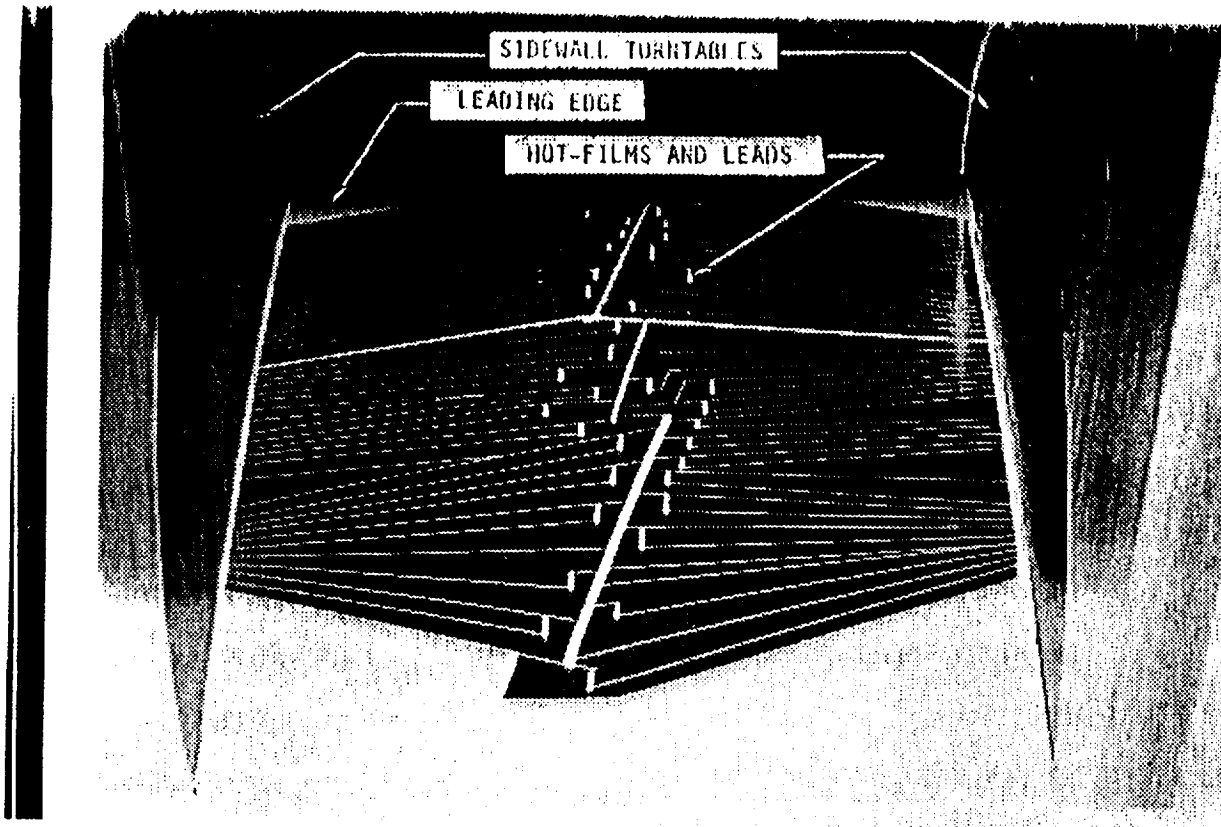
Figure 23.- Airfoil model instrumented with hot film gages shown mounted in 0.3-m TCT test section.

Transition Location by Fluctuating Pressure Measurement
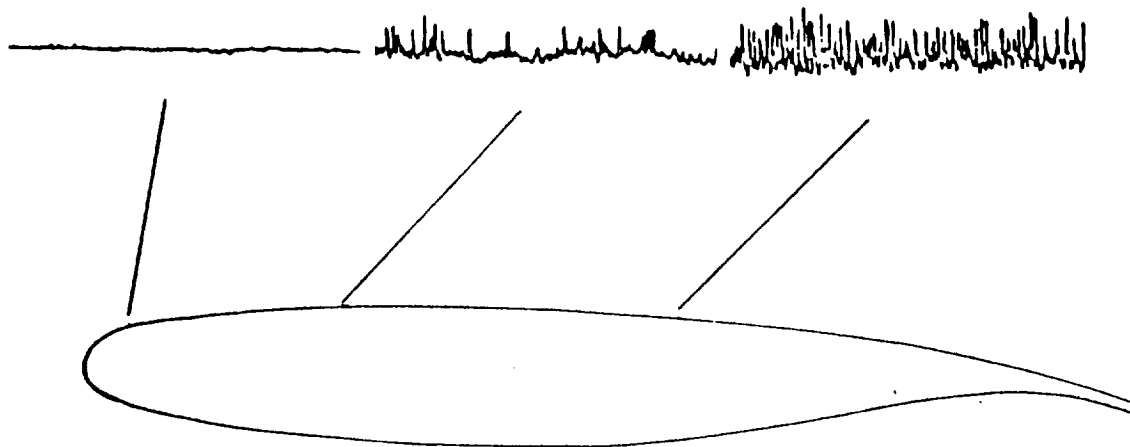
Figure 24.- 14% supercritical airfoil outline and sample fluctuating pressure traces.

67

REYNOLDS NUMBER EFFECTS ON UNSTEADY AERODYNAMICS

John T. Batina
Unsteady Aerodynamics Branch
Structural Dynamics Division
NASA Langley Research Center
Hampton, Virginia 23665-5225

Outline

1. Introduction

2. General characteristics

   a) Experimental aspects

   b) Computational aspects

3. Recommendations

   a) Experimental challenges

   b) Computational challenges

4. Concluding remarks

5. References

Introduction

Generally speaking, the field of unsteady aerodynamics embodies various aspects of time-dependent fluid flows, many of which are interesting as well as important, and consequently are worthy of study.[1] However, the present chapter on Reynolds number effects on unsteady aerodynamics, will limit the discussion to time-dependent flows about airfoils and wings, mainly because of the subsequent safety-of-flight consideration due to aircraft aeroelasticity. Aeroelasticity, defined as the structural response of the aircraft due to aerodynamic loading, involves phenomena such as static divergence, flutter, aileron reversal, aileron buzz, buffeting, and limit cycle oscillations. These phenomena can be studied and much can be learned by investigating more simply the associated unsteady aerodynamics.

Studies of unsteady aerodynamics for airfoils and wings can be divided into two general categories including experimental and analytical work. The experimental work concerns mostly tests performed in wind tunnels, such as the Transonic Dynamics Tunnel (TDT) at NASA Langley Research Center (a facility dedicated to experimental research in unsteady aerodynamics and aeroelasticity),[5] although some interesting as well as novel data have been acquired through flight testing.[6] The analytical work involves generally, theories that are too complicated to allow exact solutions, and consequently, computational methods of solution are employed.[7] Therefore this category of work will hereafter be referred to as computational.

With respect to Reynolds number effects on unsteady aerodynamics, compared to the effects on steady aerodynamics,[8] relatively little is known or understood either experimentally or computational (with noted exceptions to be discussed below). This general lack of knowledge for unsteady flows is largely due to the inherently greater complexity of measuring or computing time-dependent flows in comparison with steady flows. Further complicating the issue is the fact that wind tunnels such as the TDT are limited to Reynolds numbers in the range of 10^5 to 10^6, whereas flight Reynolds numbers can be as high as 10^7 or 10^8. (Admittedly, cryogenic tunnels such as the National Transonic Facility (NTF) at Langley, indeed exist which can test at Reynolds numbers much higher than available in conventional wind tunnels. However, the NTF does not presently have several necessary features that are required for unsteady aerodynamic and aeroelastic testing such as a data acquisition system to measure dynamic model response, by-pass valves in the wind-tunnel circuit to decrease quickly the dynamic pressure in case an aeroelastic instability is encountered, or a wire mesh safety screen to protect the tunnel fan blades from debris of damaged models). If Reynolds number effects are unimportant, then the issue is moot. Since this is obviously not the case, then the question

becomes: Can data be obtained that are consistent and monotonic with respect to Reynolds number (within the Reynolds number range allowed by a given wind tunnel), extrapolate the results to flight Reynolds numbers, and still have physically meaningful information relevant to flight?

Like the lack of knowledge of Reynolds number effects on unsteady aerodynamics through experimental means, little has been done to investigate such effects computationally. This is largely because most computer codes developed for unsteady aerodynamic and aeroelastic analyses are based on potential flow theory, either linear or nonlinear (transonic small-disturbance or full potential), although methods based on the Euler and Navier-Stokes equations are indeed being developed currently.[7] Most calculations that have been performed for unsteady applications to date, involve inviscid methods, and consequently are of no help in determining Reynolds number effects. Of course, only codes based on potential theory which include an interacted boundary layer capability and codes based on the Navier-Stokes equations are capable of predicting Reynolds number effects on unsteady aerodynamics. The comparatively few results obtained using these viscous methods have been computed at the same Reynolds numbers as the experiment to allow for direct comparison with the data. However, the calculations need to be repeated with different Reynolds numbers and possibly different transition locations to determine the sensitivity of the results to these parameters.

Noted exceptions to the above discussion are reported in the review paper by Mabey[9] on the so-called scale effects in unsteady aerodynamics. Two other noted reviews in unsteady aerodynamics are the discussion on practical problems for unsteady aerodynamics about airplanes by Cunningham[10] and the effects of transition on wind tunnel simulation of vehicle dynamics by Ericsson.[11] The paper by Mabey is a compilation of information on the known effects of Reynolds number from a wide range of unsteady aerodynamics tests with particular emphasis on flows about wings. This chapter will first summarize the excellent review by Mabey in the following section called General Characteristics. Both experimental and computational aspects are discussed. Recommendations are then made in the next section in the form of challenges to both the experimental and computational technical communities to include Reynolds number and transition location variations as an integral part of their studies. The chapter is summarized in a final section on Concluding Remarks.

General Characteristics

As suggested by Mabey,[9] the importance of scale effects involving Reynolds number or transition location is recognized generally in the area of steady aerodynamics,[8] but is often

ignored in unsteady aerodynamics. Hence, in this section, some general characteristics of scale effects are described, with consideration given to both experimental and computational aspects of the problem. The experimental aspects involve the origin, magnitude, and consequences of scale effects. The computational aspects involve limitations due to turbulence modeling.

Experimental Aspects

As for the origin of scale effects, there are two primary causes including failure to achieve full scale Reynolds number, and failure to achieve full scale transition location.[9] Scale effects result from the failure to achieve full scale Reynolds number since for wind tunnel models the Reynolds number is typically in the range of 10^6 to 10^7. The resulting scale effects are illustrated in the following example. Consider a simplified airfoil at high angle of attack, as shown in Fig. 1(a), which experiences flow separation along the upper surface at a point forward of midchord for a low Reynolds number. At a high Reynolds number, the boundary layer remains attached until a point that is say aft of midchord as shown in Fig. 1(b). Along the lower surface in either case, the boundary layer remains attached because of the favorable pressure gradient. However, because of the different separation locations on the upper surface due to low (Fig. 1(a)) and high (Fig. 1(b)) Reynolds number flows, the circulation about the airfoil differs, and consequently the pressure distributions along both of the upper and lower surfaces differ between the two cases.

Scale effects can also result because of the failure to achieve the full scale transition location, even if the Reynolds number is matched between the wind tunnel and flight.[9] For example, the transition position is located typically too far forward in comparison with the natural transition location encountered in flight, due to surface roughness or to flow unsteadiness in the wind tunnel. As diagrammed in Figs. 2(a) and 2(b), when the transition location is simulated incorrectly, the separation point may be located too far forward (advanced) or too far aft (delayed) depending upon the details of the problem (freestream flow conditions and geometry to name the simplest two). The thickness of the shear layers in the experiment will also be incorrect. Consequently, Mabey[9] has concluded that, "generally speaking, the failure to fix transition at an appropriate point on a wind tunnel model is probably more serious than the failure to reproduce the correct Reynolds number."

As for the magnitude of scale effects, for either steady or unsteady flows, it depends largely upon whether transition is fixed or free on the wind tunnel model.[9] For fixed transition location, the effects are typically small for fully attached or well-separated flows as suggested in the lift coefficient versus Mach number plots for a typical swept wing shown in Figs. 3.

71

Figure 3(a) uses data from steady measurements and Fig. 3(b) uses data from unsteady measurements. The effects can be large or medium for incipient separation as indicated in the middle part of Figs. 3(a) and 3(b), respectively. For free transition, however, the effects can be large for either attached or separated flows. And, unfortunately, many experiments in unsteady aerodynamics and aeroelasticity over the years have been performed with free transition. This practice can lead to unexpected results, as illustrated in the following example.[9] In an experimental investigation of the naturally oscillatory flow that occurs on rigid thick airfoils at transonic Mach numbers, wind tunnel tests were performed for a rectangular wing with a 14-percent-thick biconvex airfoil section, over a range of Reynolds number with the transition location first fixed (near the leading edge) and then with transition free. The data obtained with fixed transition, shown in Fig. 4(a), indicated that oscillatory flow occurs due to a periodic flow separation from the upper and lower surfaces (180° out of phase). This periodic flow occurs over a narrow range of Mach number and is relatively independent of Reynolds number, for the range of values that were considered. The data obtained with free transition, however, shown in Fig. 4(b), are quite different from the data obtained with fixed transition. With free transition, the range of Mach number in which the periodic flow occurs varies with Reynolds number. In fact, for a small range of Reynolds number near 4×10^6, the periodic flow no longer occurs. This obviously is an unexpected and disturbing result. It is disturbing since had the test been performed at a Reynolds number of only say 4×10^6, with free transition, the periodic flow phenomenon would not have been observed at all, and erroneous conclusions could have resulted.

Computational Aspects

Most computer codes developed for unsteady aerodynamic and aeroelastic analyses are based on potential flow theory, although methods based on the Euler and Navier-Stokes equations are being developed currently.[7] To determine Reynolds number effects on unsteady aerodynamics, either a potential flow method with an interacted boundary layer capability or a Navier-Stokes code is required. The potential flow method is desirable from a cost standpoint, whereas the Navier-Stokes code is regarded generally as being more accurate since it includes more of the flow physics. However, the accuracy of results obtained using a Navier-Stokes code is subject to the limitations of the turbulence modeling.[12, 13] Typically either equilibrium or nonequilibrium turbulence models have been used. Results obtained using both types of models are shown in Fig. 5 (taken from Ref. 13) for the NACA 0012 airfoil. Figure 5(a) shows steady pressure distributions for a case involving attached flow ($M_\infty = 0.7$ and

$\alpha = 1.49°$) and Fig. 5(b) shows distributions for a case involving separated flow ($M_\infty = 0.799$ and $\alpha = 2.26°$). For both cases, the Reynolds number was 9×10^6 and transition was fixed at five percent chord. The pressure distributions for the attached flow case shown in Fig. 5(a) indicate that the Baldwin-Lomax equilibrium turbulence model and the Johnson-King nonequilibrium model produce similar results. Both sets of calculated pressures also agree reasonably well with the experimental data, with noted differences near the shock wave on the upper surface of the airfoil. The pressure distributions for the separated flow case shown in Fig. 5(b), however, indicate that the Johnson-King model produces results which agree better with the data than the Baldwin-Lomax model. This is because the Baldwin-Lomax equilibrium turbulence model assumes that the turbulent shear stress depends only on the local properties of the mean flow, and thus the eddy viscosity does not account for the nonequilibrium between the turbulence and the mean flow in the outer portions of the viscous layers.[14] Consequently, equilibrium models give poor predictions for flows involving strong shock-wave/boundary layer interactions with the shock located typically too far aft. Alternatively, the Johnson-King nonequilibrium model accounts for the history effects of the turbulence through an ordinary differential equation for the maximum of the shear stress.[14] This maximum is then used to scale the eddy viscosity, and consequently, the Johnson-King model has been found to give good predictions for transonic flows with strong viscous-inviscid interaction.[14]

In three-dimensions, for example, similar comparisons of steady pressures computed using the Baldwin-Lomax and Johnson-King turbulence models have been reported in Ref. 14. The case that was considered involves the ONERA M6 transport-type wing at $M_\infty = 0.84$, $\alpha = 6.06°$, and Re $= 11.7 \times 10^6$ (based on the mean aerodynamic chord). These calculated results along with comparisons with experimental pressure data are presented in Fig. 6 (taken from Ref. 14). The case that was selected involves shock-induced flow separation on the upper surface of the wing, with some reverse flow indicative of a recirculation bubble that is especially evident in the outboard region. Similar to the two-dimensional results of Fig. 5(b), use of the Baldwin-Lomax algebraic turbulence model, shown in Fig. 6, results in an underprediction of the size of the reverse flow region and consequently the shock wave on the upper surface of the wing is predicted to be downstream of the experimental location. Use of the Johnson-King equilibrium model, however, produces an upper surface shock that is positioned close to the experimental location as well as overall pressure distributions that agree well with the experimental pressure data.

For unsteady flows, far less is known or understood about the effects of turbulence modeling on the accuracy of the calculations. This is due in part to the fact that far fewer unsteady calculations have been performed using viscous methods in comparison with steady calculations. Also, the unsteady flow physics can be more complex, such that in addition to

attached flow and separated flow cases, periodically separating and reattaching flows may be encountered. These flows are inherently more difficult to analyze and thus little work has been done to assess the accuracy of turbulence models for such flows. A noted exception is the Navier-Stokes study of Refs. 12 and 13, where calculations were again performed using both the Baldwin-Lomax and Johnson-King turbulence models for a pitching NACA 0012 airfoil. For the results shown in Fig. 7 (taken from Ref. 13) the Mach number was 0.6, the angle of attack was 4.86°, the pitch amplitude was 2.44°, the reduced frequency was 0.081, and the Reynolds number was 4.8 x 10^6. Figure 7(a) shows the instantaneous pressure coefficient distribution at $\alpha = 6.75°$, and Fig. 7(b) shows the lift and moment coefficients during a cycle of motion. The calculated results, in comparison with the experimental data, do not seem to favor one turbulence model over the other, although the comparisons of lift coefficient suggest that the Baldwin-Lomax model produces a more accurate result. This uncertainty in the accuracy of turbulence modeling for this case as well as for others, suggests strongly that more computational work is necessary to assess turbulence models for unsteady flows.

Recommendations

In the past, many experiments as well as calculations in unsteady aerodynamics have been performed at conditions which involve attached boundary layers where the emphasis was placed on learning about the flow physics associated with moving shock waves. More recently, there is increased testing and computing of unsteady aerodynamics at conditions resulting in incipient flow separation as well as massively separated flow.[15] Consequently, greater attention should be paid to scale effects to help ensure that the results are physically meaningful and relate to physics that are expected to be encountered in flight. Therefore, specific recommendations are made in this section in the form of challenges to both the experimental and computational technical communities, some of which are from Mabey.[9]

Experimental Challenges

In the past, many unsteady aerodynamic experiments were performed with free transition. As discussed above, with free transition, scale effects can be very large and non-monotonic and possibly lead to unexpected results. With fixed transition, scale effects are much more likely to be monotonic and large effects are restricted typically to the onset of flow separation. Consequently, unsteady experiments should be performed with fixed transition.[9] Unsteady experiments should also be performed by varying Reynolds number and with various transition positions.[9] The experimental community is further challenged to reconsider unsteady aerodynamic testing in the NTF. Some exploratory type tests have in fact been

74

performed in recent years using very small models in a cryogenic wind tunnel to achieve higher Reynolds numbers (in the 0.3-Meter Cryogenic Wind Tunnel at NASA Langley) for unsteady aerodynamics,[16] and aeroelasticity[17] but general testing of much larger models should commence in the NTF. Testing in the NTF could be done at full scale Reynolds numbers and would leave only the issue of transition to be resolved.

Also, although some work indeed has been done on comparing unsteady aerodynamic data obtained in the wind tunnel to similar data acquired in flight,[18] further research efforts should be made to perform such comparisons to help ensure that wind tunnel data is relevant to flight. A possible safety-of-flight issue that is related to this recommendation involves flutter clearance tests performed in wind tunnels such as the TDT. Specifically, dynamically scaled models of aircraft are aeroelastically tested at Reynolds numbers on the order of 10^6 and are typically found to be free of flutter. However, at much higher Reynolds numbers of say 10^8, which are encountered in flight, the shock waves on the vehicle may be much stronger. Stronger shock waves often have a detrimental effect on aeroelastic stability, and consequently, an aircraft model may be flutter free in the wind tunnel, when the full-scale vehicle flying at much higher Reynolds number (all other conditions similar) may be flutter critical.

Computational Challenges

In the past, most unsteady aerodynamic calculations have been performed at a single Reynolds number corresponding to experiment (say 10^6). However, unsteady calculations should also be performed at much lower (10^4 to 10^5) and much higher (10^7 to 10^8) Reynolds number as well as at fixed Reynolds number with varying transition location.[9] The computational community is further challenged to exercise the different turbulence models that are available currently to determine the sensitivity of the results to these models, as well as to develop new models that are more appropriate for time-dependent separated flows. Additionally, in all cases, effort should be made to determine the sensitivity of the calculation to numerical parameters such as the number of grid points, the grid point distribution, and the time step size. Every effort should be made to minimize the effect of these parameters on the final solutions.

Concluding Remarks

The chapter summarized the limited knowledge of Reynolds number effects in unsteady aerodynamics both experimentally and computationally. The discussion was restricted to time-dependent flows about airfoils and wings, mainly because of the subsequent safety-of-flight consideration due to aircraft aeroelasticity. The present survey focused primarily on transonic conditions involving attached, incipiently separated, and massively separated flows. Much

more research work is needed to investigate the origin, magnitude, and consequences of scale effects on unsteady aerodynamics in all speed regimes from incompressible to hypersonic. Other conditions and geometrical situations should also be considered such as helicopter blades, internal flow problems, laminar flow control designs, and complete aircraft configurations including component interference effects.

References

1.   Bisplinghoff, R. L.; Ashley, H.; and Halfman, R. L.: Aeroelasticity, Addison-Wesley, 1955.

2.   Mabey, D. G.; and Chambers, J. R.: Unsteady Aerodynamics-Fundamentals and Applications to Aircraft Dynamics, AGARD AR-222, 1986.

3.   Nixon, D., (editor): Unsteady Transonic Aerodynamics, vol. 120 of the AIAA Progress in Astronautics and Aeronautics, 1989.

4.   Edwards, J. W.: Unsteady Aerodynamics: Physical Issues and Numerical Predictions, proceedings of the Third International Congress of Fluid Mechanics, Cairo, Egypt, January 2-4, 1990, vol. 1, pp. 99-115.

5.   Ricketts, R. H.: Selected Topics in Experimental Aeroelasticity at the NASA Langley Research Center, proceedings of the Second International Symposium on Aeroelasticity and Structural Dynamics, Aachen, Germany, April 1-3, 1985, pp. 244-256.

6.   Murrow, H. N.; and Eckstrom, C. V.: Drones for Aerodynamic and Structural Testing (DAST) - A Status Report, Journal of Aircraft, vol. 16, no. 8, August 1979.

7.   Edwards, J. W.; and Malone, J. B.: Current Status of Computational Methods for Transonic Unsteady Aerodynamic and Aeroelastic Applications, Paper No. 1, proceedings of the AGARD Structures and Materials Panel Specialists' Meeting on Transonic Unsteady Aerodynamics and Aeroelasticity, San Diego, California, October 9-11, 1991.

8.   Elsenaar, A.: On Reynolds Number Effects and Simulation, AGARD CP-429, October 1987.

9. Mabey, D. G.: A Review of Scale Effects on Surfaces in Unsteady Motion, Paper No. 27, proceedings of the AGARD Structures and Materials Panel Specialists' Meeting on Transonic Unsteady Aerodynamics and Aeroelasticity, San Diego, Calfornia, October 9-11, 1991.

10. Cunningham, A. M., Jr.: Practical Problems: Airplanes, chapter 3 of Unsteady Transonic Aerodynamics, Nixon, D. (editor), vol. 120 of the AIAA Progress in Astronautics and Aeronautics, 1989.

11. Ericsson, L. E.: Effects of Transition on Wind Tunnel Simulation of Vehicle Dynamics, Prog. Aerospace Sci., vol. 27, 1990, pp. 121-144.

12. Rumsey, C. L.; and Anderson, W. K.: Some Numerical and Physical Aspects of Unsteady Navier-Stokes Computations Over Airfoils Using Dynamic Meshes, AIAA Paper No. 88-0329, January 1988.

13. Rumsey, C. L.; and Anderson, W. K.: Parametric Study of Grid Size, Time Step, and Turbulence Modeling on Navier-Stokes Computations Over Airfoils, Paper No. 5, proceedings of the AGARD 62nd Meeting of the Fluid Dynamics Panel Symposium on Validation of Computational Fluid Dynamics, Lisbon, Portugal, May 2-5, 1988.

14. Abid, R.; Vatsa, V. N.; Johnson, D. A.; and Wedan, B. W.: Prediction of Separated Transonic Wing Flows with a Non-Equilibrium Algebraic Model, AIAA Paper No. 89-0558, January 1989.

15. Edwards, J. W.: Unsteady Airloads Due to Separated Flow on Airfoils and Wings, Paper No. 16, AGARD CP-483, Aircraft Dynamic Loads Due to Flow Separation, Sorrento, Italy, April 1990.

16. Hess, R. W.; Seidel, D. A.; Igoe, W. B.; and Lawing, P. L.: Highlights of Unsteady Pressure Tests on a 14 Percent Supercritical Airfoil at High Reynolds Number Transonic Condition, AIAA Paper No. 87-0035, January 1987.

17. Cole, S. R.: Exploratory Flutter Test in a Cryogenic Wind Tunnel, AIAA Paper No. 85-0736, April 1985.

18. Reed, W. H.: Comparisons of Flight Measurements with Predictions from Aeroelastic Models in the NASA Langley Transonic Dynamics Tunnel, paper presented at the 46th AGARD Flight Mechanics Panel Symposium, Valloire, Savoi, France, June 9-12, 1975.

Pressure gradient - upper surface adverse
- lower surface favourable
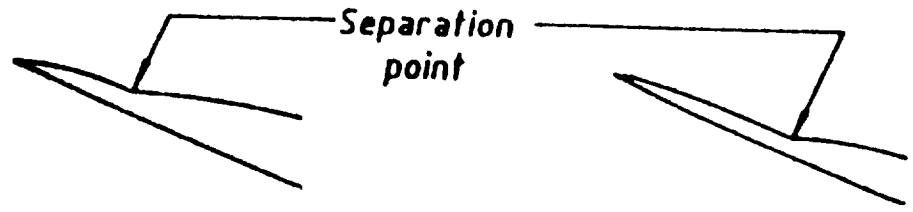

(a) Low Reynolds number   (b) High Reynolds number

Fig. 1   Simplified airfoil at high angle of attack illustrating scale effects which result from the failure to achieve the full scale Reynolds number (Ref. 9).
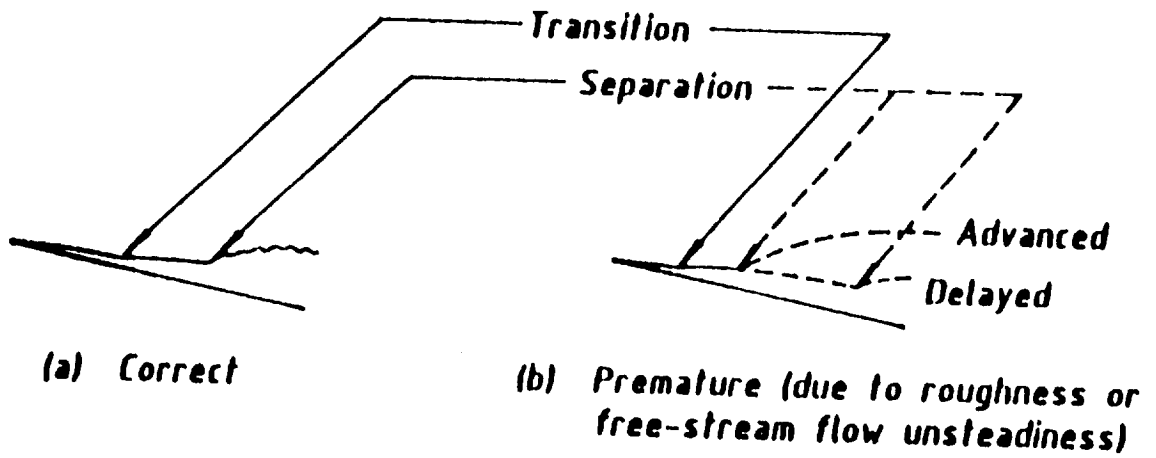
(a) Correct

(b) Premature (due to roughness or free-stream flow unsteadiness)

Fig. 2   Simplified airfoil at high angle of attack illustrating scale effects which result from the failure to achieve the full scale transition position (Ref. 9).
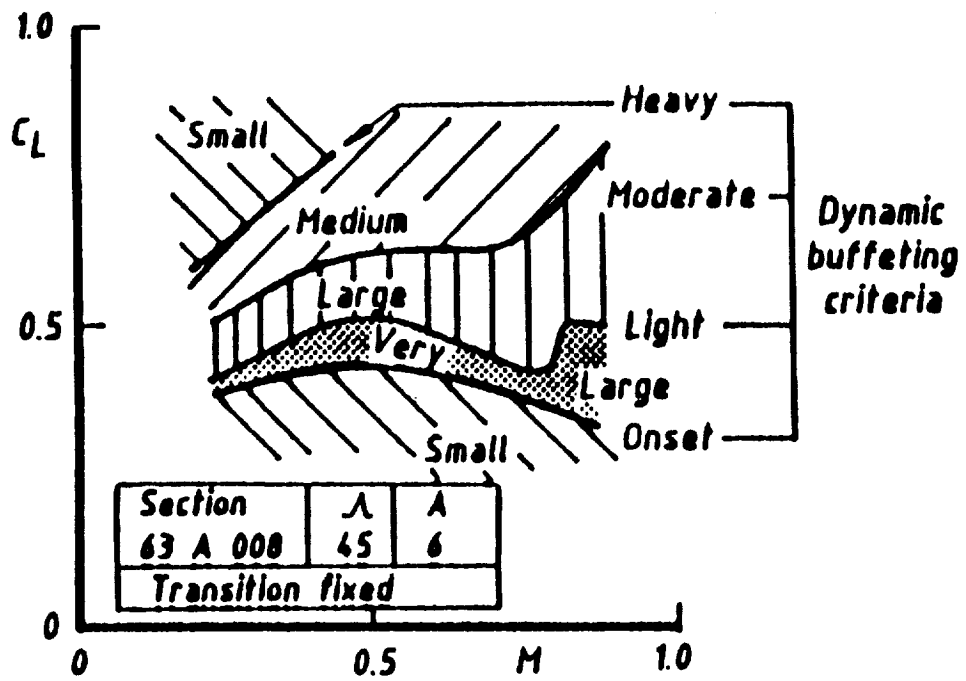
(a) from steady measurements.
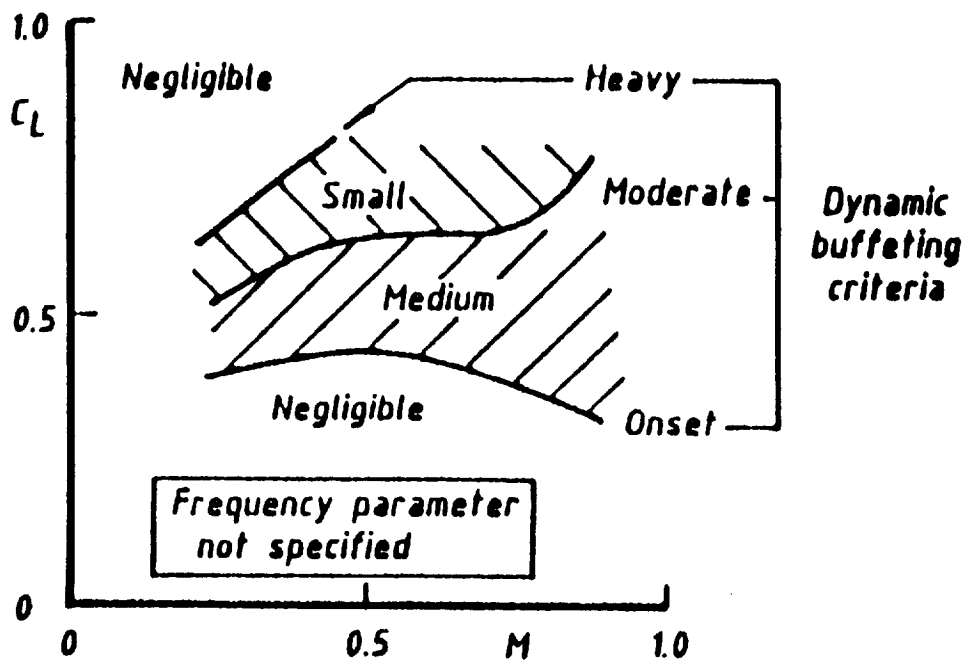
(b) from unsteady measurements.

Fig. 3   Lift coefficient versus Mach number for a typical swept wing illustrating the magnitude of scale effects (Ref. 9).
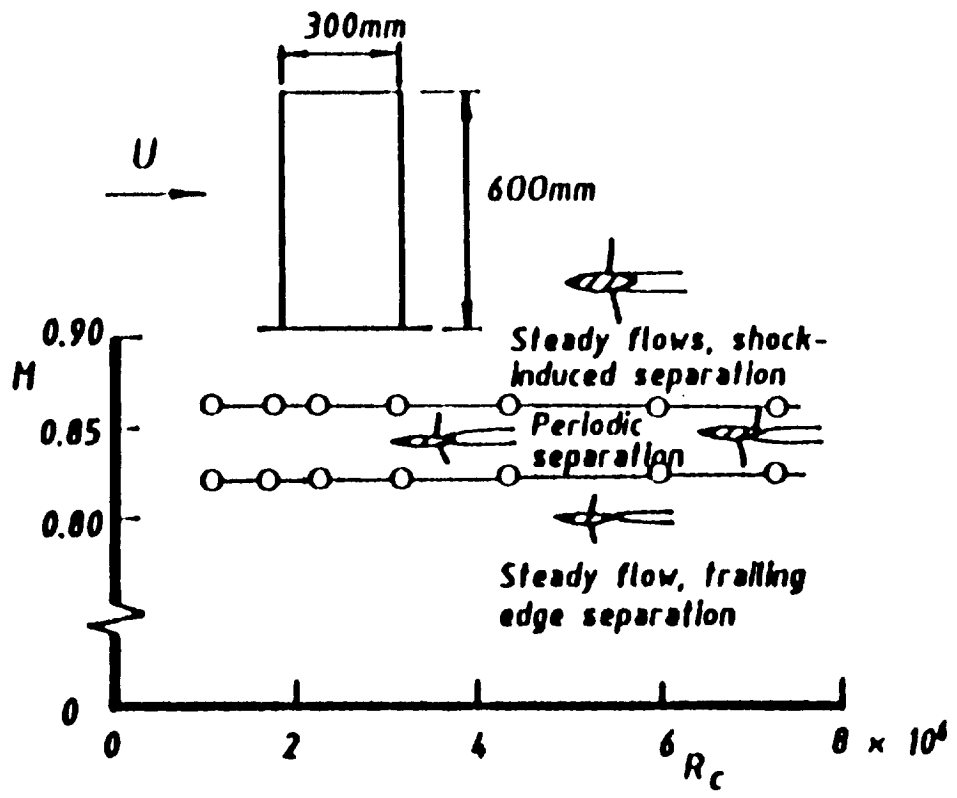
(a) with fixed transition.
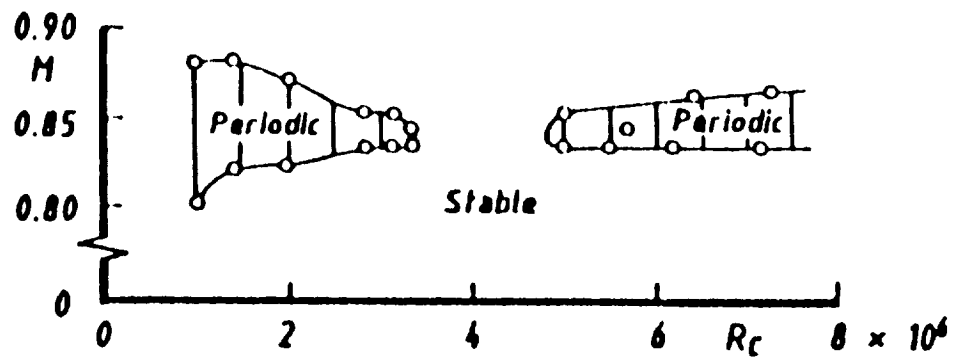
(b) with free transition.

Fig. 4   Boundaries of periodic flow for a rectangular wing with a 14-percent-thick
biconvex airfoil section illustrating transition effects (Ref. 9).

81
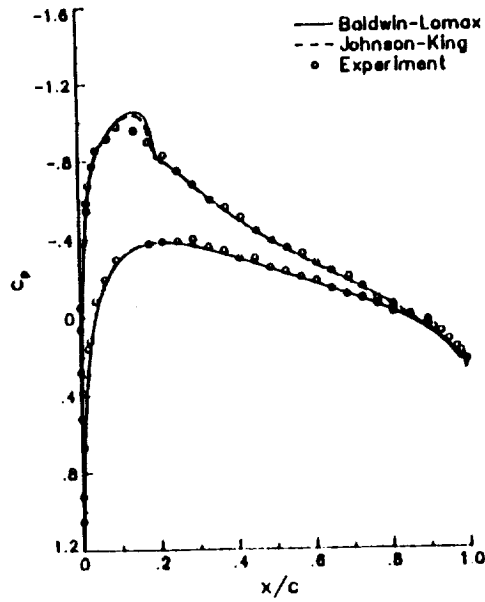
(a) case with attached flow
($M_\infty = 0.7$ and a = 1.49°).
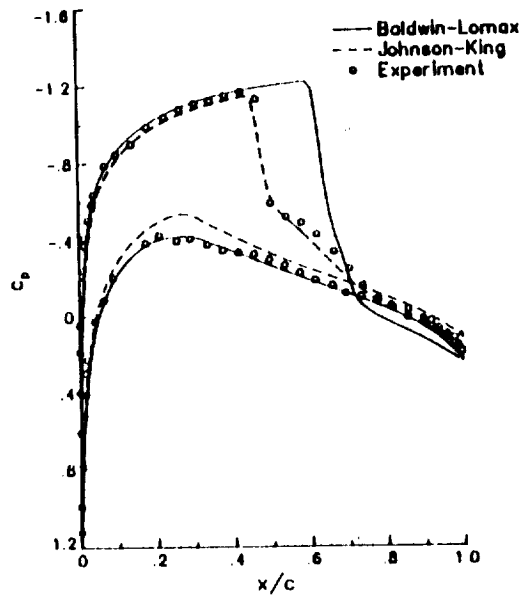
(b) case with separated flow
($M_\infty = 0.799$ and $\alpha = 2.26°$).

Fig. 5   Steady pressure coefficient distributions for the NACA 0012 airfoil computed at
Re = 9 x 10⁶ with transition fixed at 5 percent chord illustrating sensitivity with
respect to turbulence model for a separated flow case (Ref. 13).
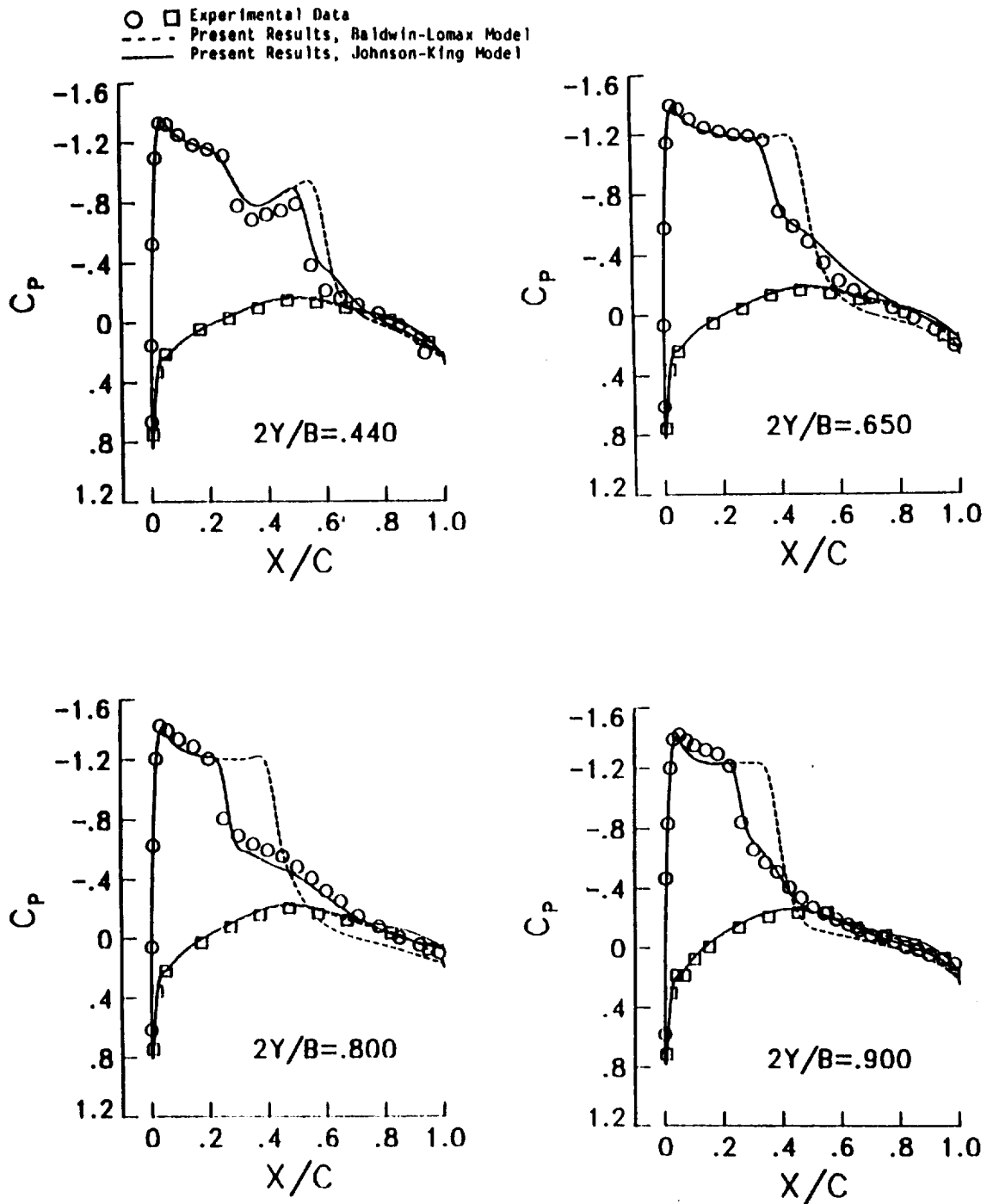
Fig. 6   Effects of turbulence model on steady pressure coefficient distributions for the ONERA M6 wing at $M_\infty = 0.84$, $\alpha = 6.06°$, and Re = 11.7 x 10^6 (Ref. 14).
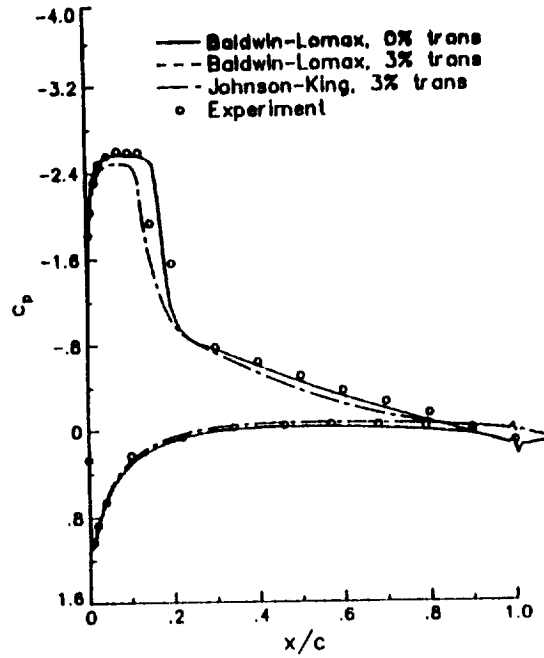
(a) instantaneous pressure coefficient
distribution at α(t) = 6.75° ↓.
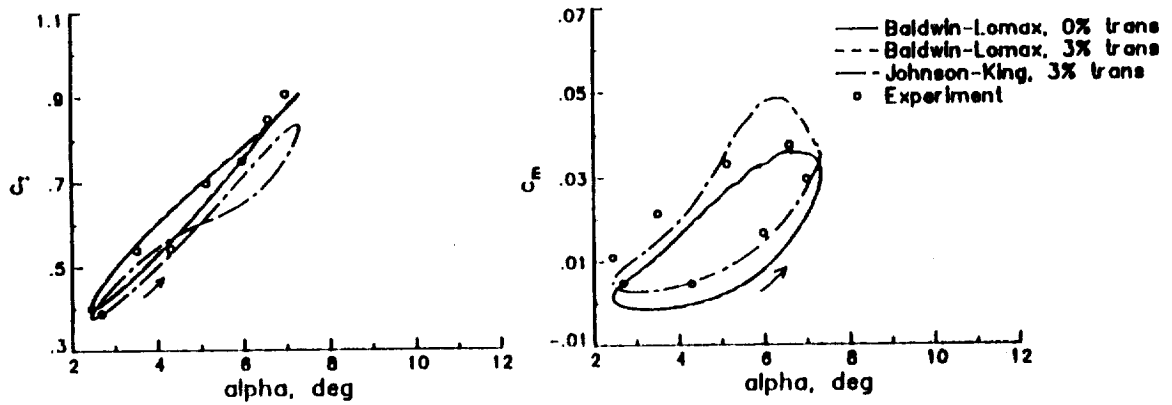
(b) lift and moment coefficients during a cycle
of motion.

Fig. 7   Unsteady results for the NACA 0012 airfoil at $M_\infty = 0.6$, $\alpha_o = 4.86°$,
$\alpha_1 = 2.44°$, k= 0.081, and Re = 4.8 x 10⁶, illustrating sensitivity with
respect to turbulence model (Ref. 13).

THE ROLE OF REYNOLDS NUMBER IN AEROACOUSTICS

Jay C. Hardin

INTRODUCTION

Acoustics is generally considered to be an inviscid fluid phenomenon, although all sound is ultimately dissipated into heat by viscosity. The reason for this apparent anomaly is that if viscous terms are included in the standard linear analysis, one finds that the viscous attenuation is so slight that audible frequency acoustic waves must travel many thousands of wavelengths before significant energy dissipation is observed. For example, a 1 kHz wave, traveling in still air at uniform temperature and pressure, would have its amplitude reduced by 0.32 percent in a distance equal to 1000 wavelengths[1]. Thus, dissipative losses only become important for high frequency sound propagation over long distances.

On the other hand, if one considers the generation of sound by flows rather than just the propagation of sound through flows, one might expect to see a significant Reynolds number effect. For example, probably the most common source of sound in flows is the acceleration of vorticity[2], which would not be present except for the action of viscosity. Even here, however, a curious independence is observed, which is apparently due to the fact that the large scale, efficient sound generation structures in the flow change little with Reynolds number. Thus, as will be seen, only in certain special cases and for certain measures, such as spectra, does Reynolds number become critically important in aeroacoustics.

EXPERIMENTAL OBSERVATIONS

One of the most studied sound generating flows is produced by uniform flow over a cylinder. At Reynolds numbers based upon cylinder diameter above about sixty, this flow becomes unstable developing the characteristic von Karman vortex street wake with its accompanying Aeolian tone. If one looks at steady state aerodynamic properties of this flow, one finds significant Reynolds number dependence. For example, the drag coefficient, shown in Fig. 1[3], changes by a factor greater than five over the range $60 < Re < 10^6$, most notably at the so-called drag crisis near $Re = 5 \times 10^5$. However, if one looks at the peak frequency f of noise radiation, plotted on Fig. 2[4] in terms of the Strouhal number:

$$St = \frac{fD}{U} \quad \text{where D = cylinder diameter and U = incoming flow velocity}$$

one finds that the Strouhal number is nearly constant, equal to 0.2, over the entire range, even through the drag crisis.

Perhaps a more telling measure is to look at the spectra of the radiated sound, such as shown in Figure 3. These data were collected by Revell[5] over the range

$0.89 \times 10^5 < Re < 4.44 \times 10^5$. Note that, over this variation in Reynolds number by a factor of five, while the peak frequency and peak level both increase with Reynolds number, the spectral shape remains essentially the same, although the broadband levels do increase somewhat more than the tones. It has already been shown that the frequency shift can be normalized by Strouhal number. Figure 4 shows that a similar relationship holds for the mean square pressure, i.e. integral of the spectrum. Figure 4 displays the overall sound pressure level in decibels, i.e

$$OASPL = 10\log_{10}\left(\frac{\overline{p^2}}{p_o^2}\right)$$

where $\overline{p^2}$ is the mean square acoustic pressure and p_o is a reference pressure, normalized by

$$60 \log_{10}M$$

where M is the Mach number. This normalization is based on the concept that the cylinder exerts a force on the fluid which should produce a dipole-type source of sound which theoretically scales as the sixth power of some characteristic flow velocity. Note that this scaled pressure level, for both smooth cylinders as well as those with various amounts of boundary layer tripping, varies little over the entire Reynolds number range. Again this scaling depends upon inviscid flow properties.

The variation of acoustic spectra over a wider Reynolds number range is shown in Figure 5.[6] These are spectra of supersonic jet noise ($M\sim2$) over the Reynolds number range $7.9 \times 10^3 < Re < 5.2 \times 10^6$ plotted as a function of Strouhal number. Note that all the spectra peak at the Strouhal number of approximately 0.2, but the spectral shapes are very different. At the lowest Reynolds number, nearly all of the sound energy is concentrated in a single tone, while at the higher Reynolds numbers, the spectra show a more broadband "haystack" type behavior. Nevertheless, in spite of this change in spectral shape and change in Reynolds number by a factor of 10^3, Figure 6 shows that the OASPL values are reasonably invariant. Figure 6 is a directivity pattern or polar plot of the OASPL level in dB at a distance of R/D=40 versus angle from the jet axis ($\theta=0°$). Note that here no velocity scaling based on source type was necessary since the Mach number is nearly the same in all cases. In these tests, the jet diameter D did vary some from jet to jet, although the Reynolds number was primarily changed by density variations.

These data illustrate the surprising fact that, even though the source of the sound is the acceleration of vorticity[2] or equivalently, the fluctuating Reynolds stress gradients[7], both of which depend upon viscosity, only the spectra of the sound which is generated vary substantially with Reynolds number. Apparently, a characteristic instability is present and responsible for the sound generation at low Reynolds numbers. As the Reynolds number is increased, a broader band of similar instabilities is excited by the flow. Of course, the use of the decibel, where a change in the mean square pressure by a factor of 2 only changes the level by 3 dB may obscure Reynolds number variation.

Another example of change in spectral shape with Reynolds number is shown in Figure 7. These are spectra of noise radiation by a helicopter main rotor[8]. In part a of the figure, the rotor speed is 1050 rpm while in part b it has been lowered to 525 rpm. Note that this reduction in Reynolds number by a factor of two causes a peak to appear in the spectrum with the higher thrust coefficient (C_T) in the range 5-10 kHz which was not present at the higher Reynolds number. This peak is apparently due to an airfoil tone phenomenon that can occur through feedback when the boundary layer on at least one side of the airfoil is laminar. Since Reynolds number varies linearly along the span of a rotor blade, precautions must be taken in rotor testing to eliminate this tonal phenomenon which would not be present at full scale.

As a final example of the relative invariance of aeroacoustics over wide Reynolds number ranges, Figure 8[9] presents spectra of fluctuating pressures inside a cavity in an aerodynamic surface. These fluctuating cavity pressures lead directly to an intense sound source known as cavity tones. Note that over the Reynolds number range $6 \times 10^6 < Re_L < 99 \times 10^6$, where Re_L is the Reynolds number per foot of cavity length, there is little variation of the spectra when normalized by the dynamic pressure $q = 1/2\rho U_\infty^2$ and plotted as a function of Strouhal number.

TRANSITIONAL FLOWS

In the previous discussion, it has been seen that Reynolds number has very little effect upon aeroacoustics as long as the turbulent flows are fully developed. However, in transitional flows, acoustics can have a significant impact, sometimes changing the entire development of the mean flow field. A dramatic example of this is shown in Fig. 9[10] where a completely stalled airfoil at high angle of attack has its flow reattached by the addition of a sound field of the proper frequency. Of course, this is a very low Reynolds number flow where the small perturbations introduced by the sound field are significant compared to the turbulent fluctuations. At higher Reynolds numbers, the sound field perturbations would be irrelevant. However, a similar behavior has been observed in high Reynolds number turbulent jets where the sound is introduced just at the jet exit where the flow instabilities are still small. The downstream development of the jet can be made much more orderly by the proper frequency acoustic excitation during this transitional stage.

The sensitivity of transitional flows to sound may be important in certain fields such as laminar flow control. In addition, the experimentalist needs to be aware of such phenomena and cautious such that they do not occur inadvertently.

CONCLUSION

Aeroacoustic phenomena have been shown to be reasonably insensitive to Reynolds number except in transitional flows. Spectral shape displays some dependence if Reynolds number changes are large, but overall levels and directivity are essentially unchanged if properly normalized. This invariance can be utilized to great potential advantage both experimentally and computationally.

It should be mentioned that there are still areas of aeroacoustic concern, such as the conversion of acoustic energy into vortical energy by sound absorbing materials, where Reynolds number dependence may be important. As research delves more deeply into such phenomena, the role of Reynolds number in aeroacoustics will become clearer. To date, aeroacousticians have paid little attention to Reynolds number as it has not been an obvious parameter affecting noise generation.

REFERENCES

1. Temkin, S.: Elements of Acoustics, Wiley and Sons, New York, 1981.

2. Powell, A.: Theory of Vortex Sound, JASA, Vol. 36, No. 1, pp. 177-195, Jan. 1964.

3. Schlichting, H.: Boundary Layer Theory, McGraw-Hill, New York, 1968.

4. Lenharth, W. and Corell, R. W.: Thoughts on the Relationship of Reynolds and Strouhal Numbers, J. Sound Vib., Vol. 36, No. 1, pp. 147-149, 1974.

5. Revell, J. D., Prydz, R. A. and Hays, A. P.: Experimental Study of Airframe Noise vs. Drag Relationship for Circular Cylinders, Final Report, Contract NAS1-14403, 1977.

6. Seiner, J. S., McLaughlin, D. K., and Lin, C. H.: Supersonic Jet Noise Generated by Large Scale Instabilities, NASA TP-2072, Sept. 1982.

7. Lighthill, M. J.: On Sound Generated Aerodynamically. I. General Theory, Proc. Roy Soc. Ser. A., Vol. 211, No. 1107, pp. 564-587, 1952.

8. Brooks, T. F., Jolly, J. F., Jr. and Marcolini, M. A.: Helicopter Main-Rotor Noise, NASA TP 2825, Aug. 1988.

9. Tracy, M. D., Plentovich, E. G., Chu, J., and Shearin, J. G.: Cavity Acoustics in High Reynolds Number Transonic Flow, 8th JOCG Aircraft/Stores Compatibility Sym., Eglin AFB, Fla., Oct. 22-25, 1990.

10. Ahuja, K. K., Whipkey, R. R. and Jones, G. S.: Control of Turbulent Boundary Layer Flows by Sound, AIAA Paper 83-0726, 1983.
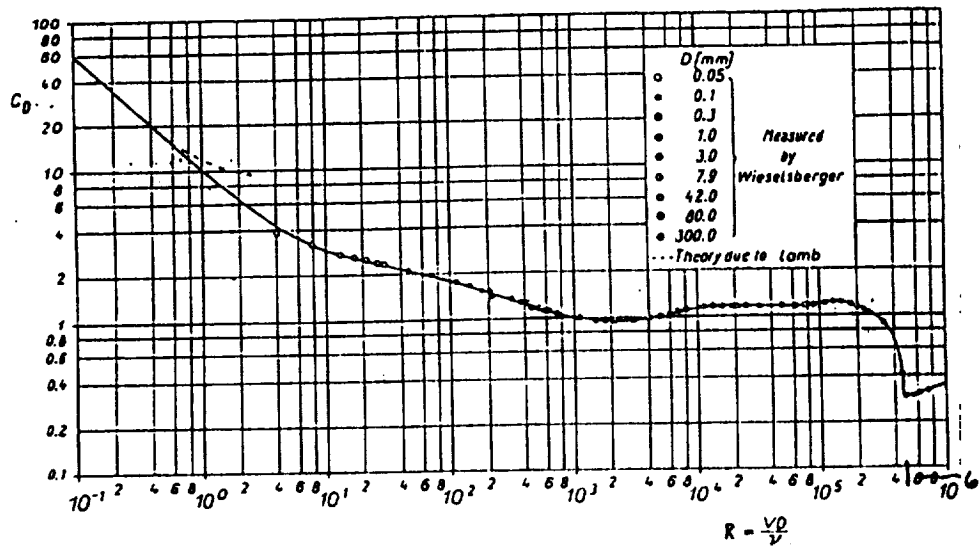
Figure 1:   Drag Coefficient for Cylinder
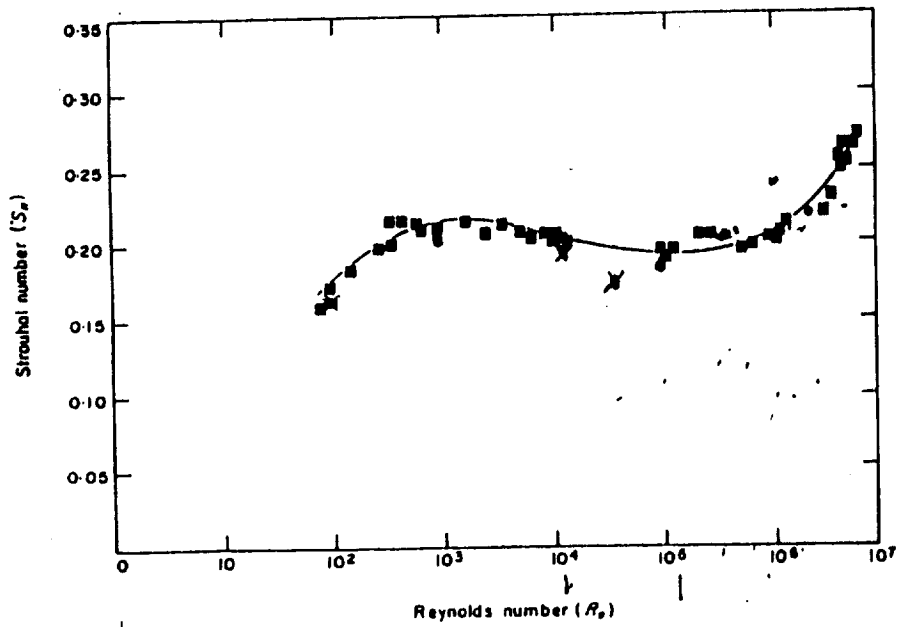
Figure 2:   Strouhal Number of Aeolian Tone
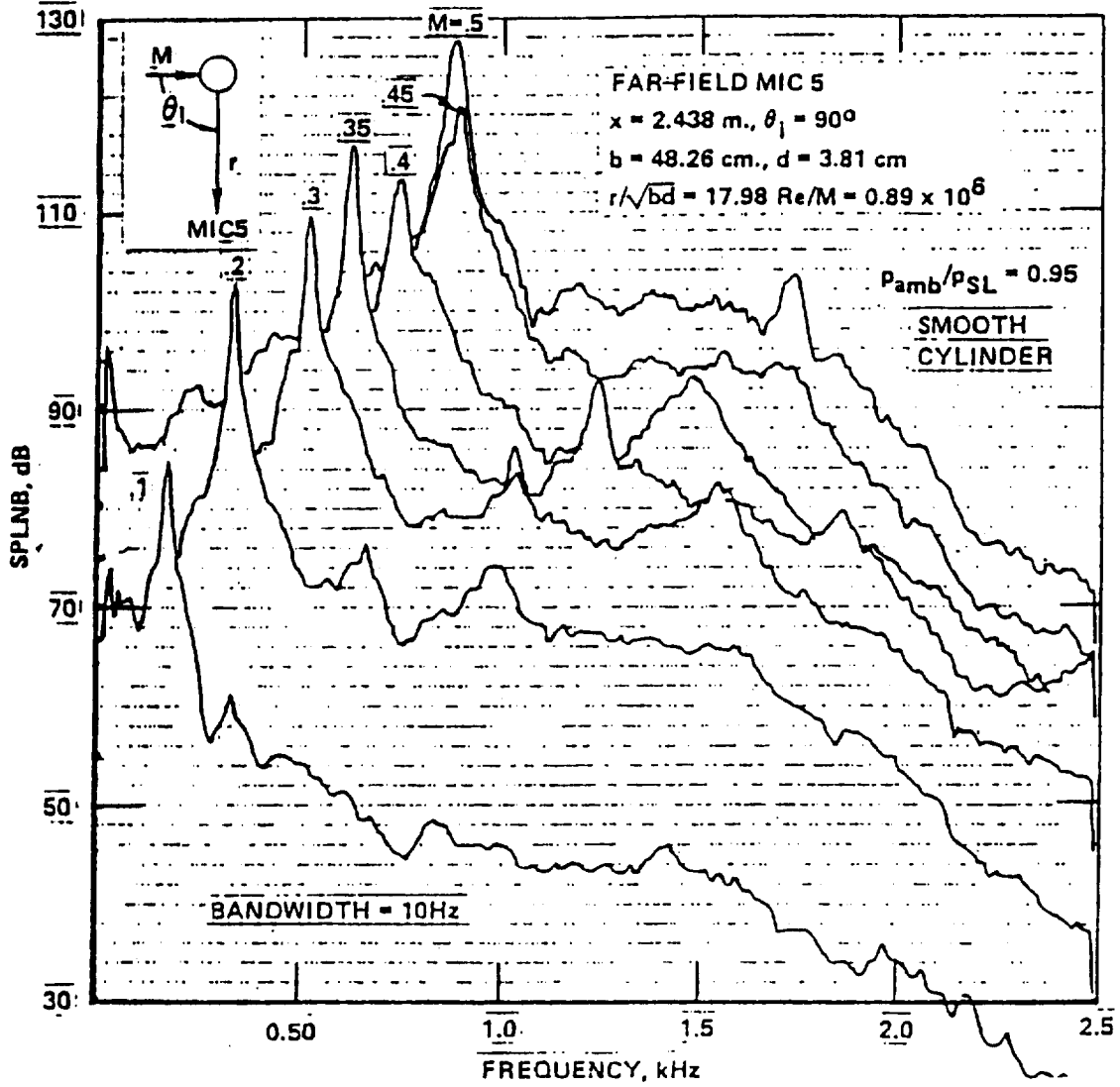
Figure 3:   Spectra of Radiated Sound
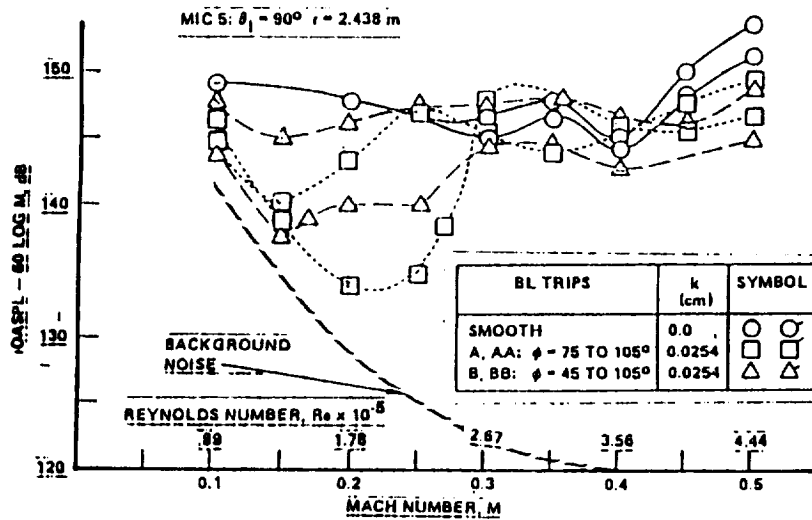
Figure 4:   Normalized OASPL
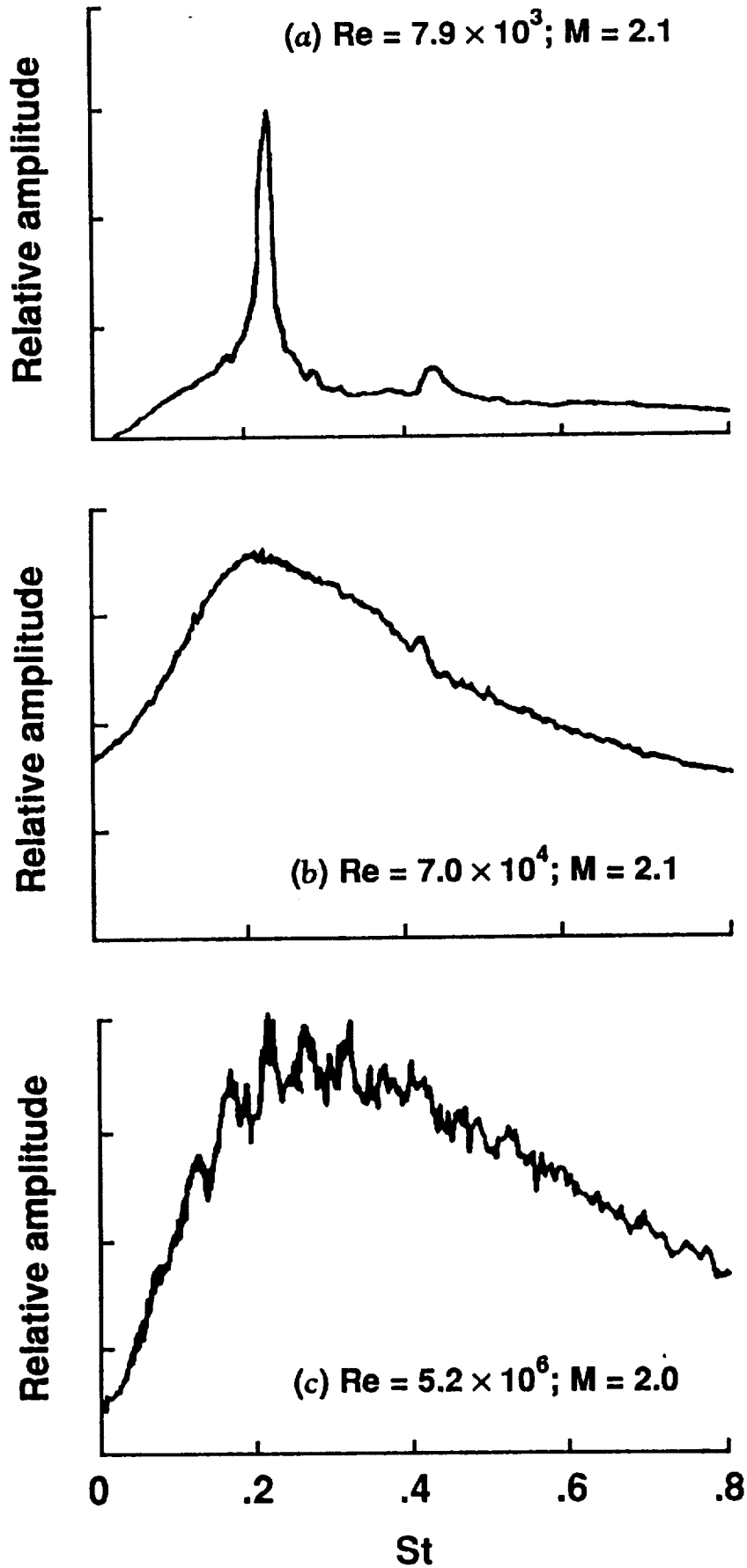
Figure 5: Spectra of Supersonic Jets
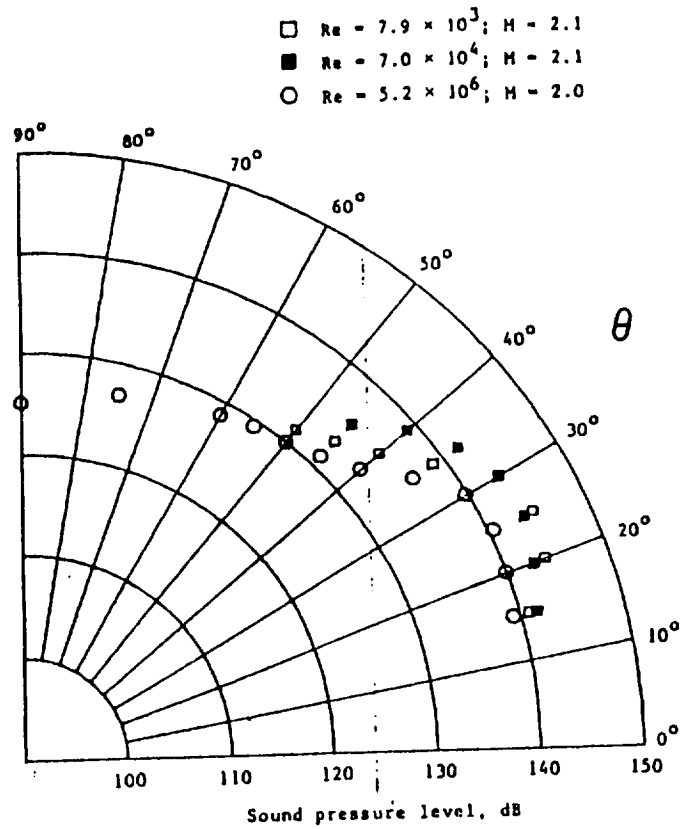
Figure 6: Directivity of Supersonic Jets
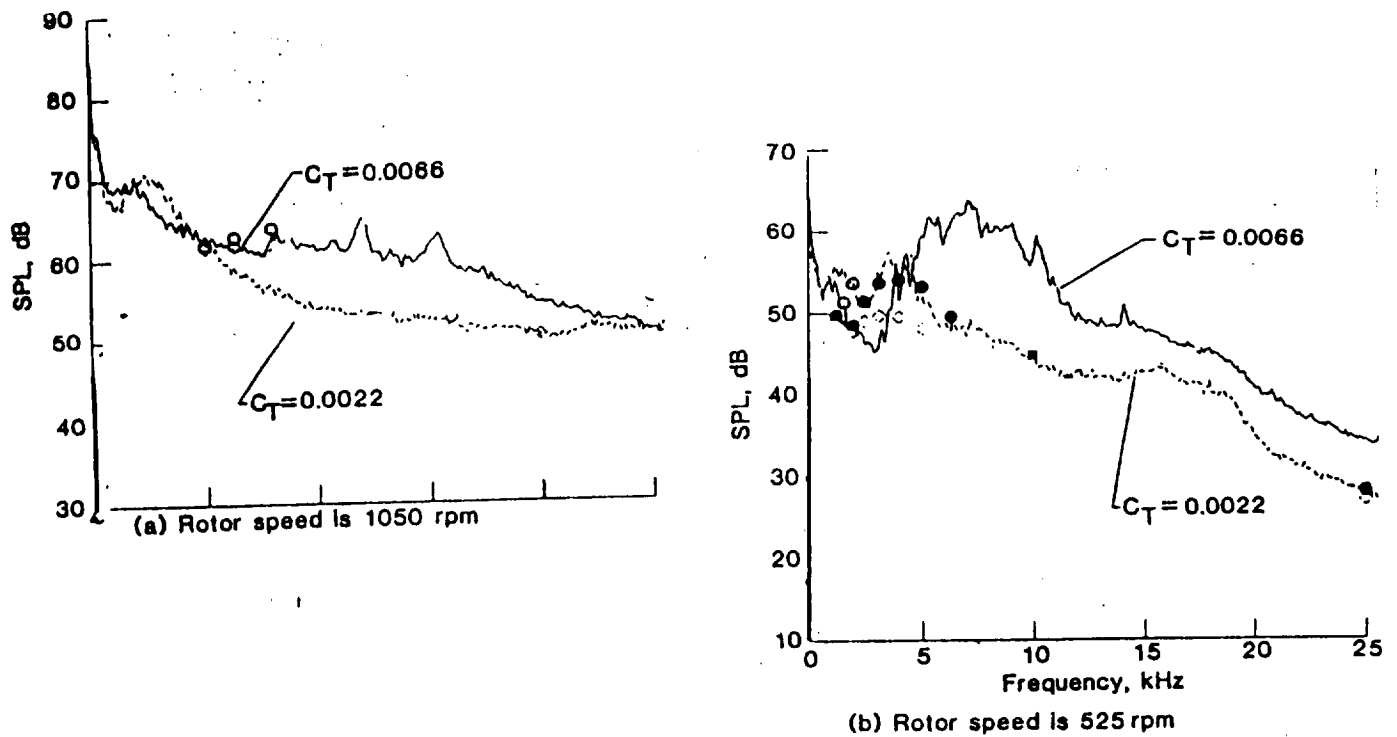

Figure 7: Spectra of Rotor Noise
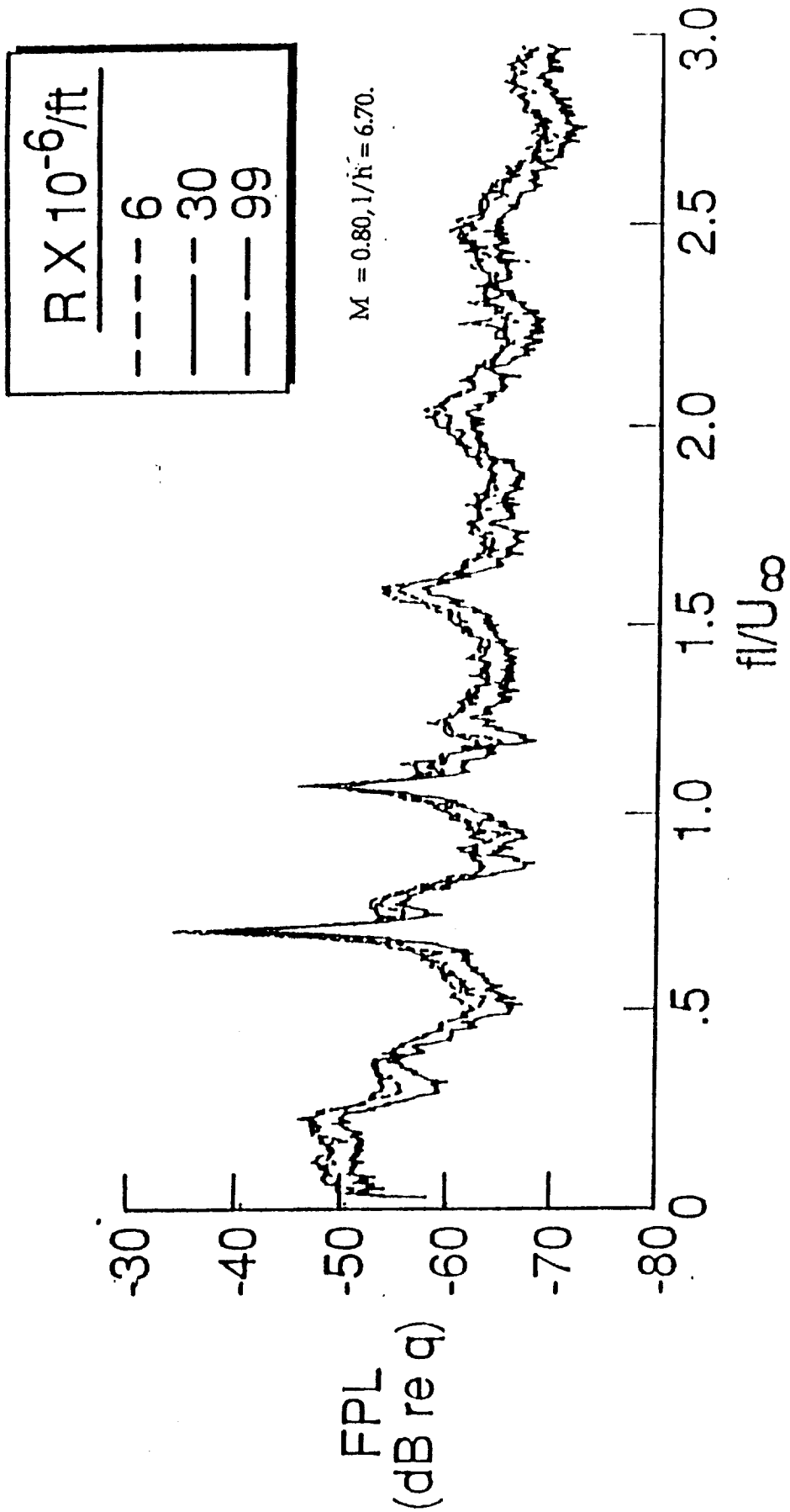
Figure 8: Spectra of Cavity Pressure Fluctuations

FPL
(dB re q)

R X 10^{-6}/ft
6
30
99

M = 0.80, l/h = 6.70.

fl/U$_\infty$

94

C-2
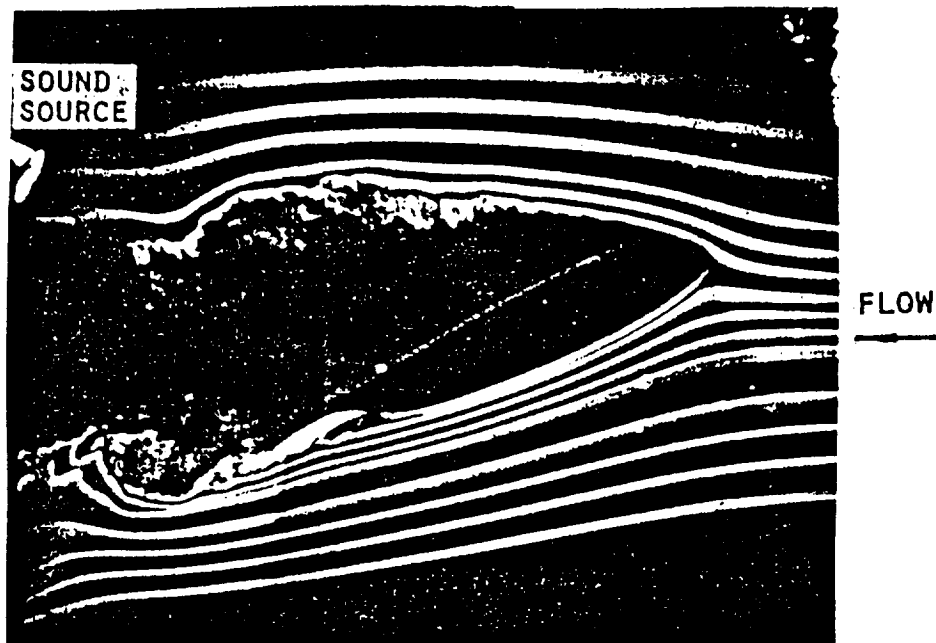
UNEXCITED

$\alpha = 26°$, $U = 13$ m/s, $f_e = 640$ Hz

EXCITED
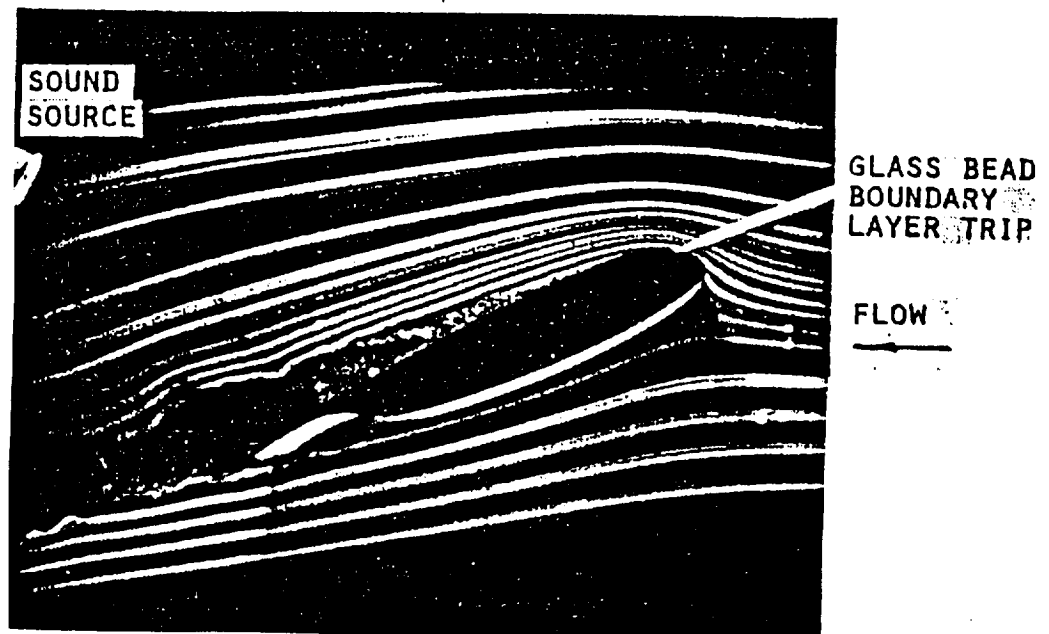
Figure 9: Acoustic Control of Separation

95

Reynolds Number Influences in Hypersonics

By

Thomas J. Horvath

Summary

This chapter identifies several hypersonic fluid dynamic phenomena which are influenced by viscous effects (i.e., Reynolds number). Reynolds number is a measure of the ratio of the inertia to viscous force and by definition is $Re = \rho UL/\mu$ where ρ is density, U is velocity, L is a characteristics length, and μ is the coefficient of viscosity. Specifically, this chapter provides a brief survey of those phenomena encountered in the hypersonic flow regime which are, or are thought to be influenced by viscous effects. It is not intended to be all inclusive, but rather provide a stimulus for identifying areas of deficiency in the understanding of the fluid physics driving these phenomena. A brief overview of hypersonics relevant to the topic of this chapter is included so as to allow the reader a more thorough understanding of the concepts to be discussed. Where appropriate, suggestions are made for the direction of future research.

I. INTRODUCTION

This section of the chapter is intended for the non-specialist who may not be familiar with some of the physical aspects of hypersonic flow. A working definition of hypersonic flow and how it is physically different from that encountered at

subsonic, transonic, or supersonic conditions is useful for the subsequent discussions of Reynolds number effects. The hypersonic vehicle designer is concerned with Reynolds number effects as they may influence the aerodynamic and aerothermodynamic characteristics of the vehicle under consideration. The subsequent review is to a large extent from Anderson 1989, and the interested reader is referred to this reference for a much more thorough introduction to hypersonics.

The study of hypersonic aerodynamics and aerothermodynamics is associated with high-speed flows and is of particular interest to the design of missiles, spacecraft such as the shuttle, and air-breathing aircraft currently under study such as the National Aero-Space Plane (NASP). Simulation parameters exist which allow the designer to relate measurements made on scaled wind tunnel models to those which occur in flight. Four of the more important simulation parameters in hypersonic testing include

Mach number (M)	a measure of compressibility effects
Reynolds number (Re)	a measure of viscous effects
Density ratio or ratio of specific heats (γ)	simulation of one aspect of a real/gas
Wall-to-adiabatic wall temperature ratio (T_w/T_{aw})	measure of energy driver potential

The relative importance of these parameters is dependent on several factors with the most important factor being model shape

(blunt versus slender) which in turn dictates the speed regime (subsonic, transonic, supersonic, and hypersonic) characterizing the flow field about the model. Anderson states that there is a conventional rule of thumb that defines hypersonics as the case when the vehicle velocity is greater than 5 times the local speed of sound or the free stream flow velocity in a hypersonic wind tunnel exceeds the free stream speed of sound by a factor of 5. He acknowledges, however, that the definition of hypersonics as M > 5 is somewhat arbitrary. More realistically, hypersonic flow is defined as that flow regime where certain physical phenomena become important that were not found or were not significant at lower speeds. For example, consider the flow field about a body moving through the atmosphere at a velocity which exceeds the local speed of sound (M > 1). One of the many differences between a subsonic and the supersonic/hypersonic flow is the formation of a detached bow wave which forms ahead of the body and wraps around it. In a subsonic flow (M < 1) disturbances are communicated upstream via pressure waves and random molecular motion alerting the flow to the approaching body. At supersonic/hypersonic speeds these disturbances cannot propagate upstream and instead coalesce at a finite distance from the body forming what is generally referred to as a shock wave. The post shock region, that is, the flow field between the shock wave and the body is defined as the shock layer. Major changes in flow properties (pressure,

98

temperature, density, velocity) and composition (at sufficiently high velocities take place across this shock wave, the largest changes occurring where the shock is normal to the oncoming flow.

Thin Shock Layers

Shock waves are characteristic of hypersonic flow. From theory, it can be shown that for a given flow deflection angle, the density ratio (ρ_2/ρ_1) across the shock wave becomes asymptotically larger as the free stream Mach number is increased. This increase in density ratio would be expected to produce a decrease in the shock wave deflection angle. (From mass conservation principles, as the density in the postshock region increases, the shock layer thickness would have to be decreased in order for the mass flow across the shock to remain nearly constant.) Consider the Mach 3 flow of a perfect gas with a ratio of specific heats or gamma equal to 1.4 ($\gamma = C_p/C_v = 1.4$) over a wedge of 15° half angle. From standard oblique shock wave theory, the shock wave angle will be approximately 32° relative to the free stream flow. By comparison, a Mach 36 perfect gas flow over the same wedge will produce a shock wave angle of 18°, as shown in fig. 1. If high temperature, chemically reacting effects (commonly referred to as real gas effects) are included, the shock wave angle will be even smaller. Discussed subsequently, real gas effects produce changes in the shock density ratio which ultimately governs the shock detachment distance and wave angle.

This shock layer is thin and it is a basic characteristic of hypersonic flows. At low Reynolds numbers (to be discussed at a later point), shock wave and boundary layer thicknesses increase substantially and become an appreciable portion of the shock layer itself and viscous effects may become more dominate on the aero/ aerothermodynamic characteristics of a hypersonic vehicle under consideration.

Viscous Interaction

Consider a boundary layer on a flat plate in a hypersonic flow, as shown in fig. 2. A high velocity hypersonic flow contains a large amount of kinetic energy; when this flow is slowed (the no-slip boundary condition dictates that V = 0 at the wall) by viscous effects within the boundary layer, the lost kinetic energy is transformed into internal energy of the gas (temperature for a perfect gas)--this is called viscous dissipation. Generally speaking, hypersonic boundary layers are characterized by such temperature increases. One consequence of this temperature increase is a thickened boundary layer. Assuming the static pressure is constant through the boundary layer normal to the surface, the increase in temperature corresponds to a decrease in the fluid density (through the equation of state). From mass flow conservation principles, as the density in the boundary layer decreases the boundary layer thickness (or velocity) must increase. The above argument is highly simplified and neglects, for example, three-dimensional effects; however, it

100

does illustrate that hypersonic boundary layers can grow more rapidly than their counterparts at lower speeds (or Mach numbers). It can be shown that for laminar compressible flow along a flat plate the boundary layer thickness δ grows as

$$\delta \propto \frac{M_e^2}{\sqrt{Re_x}} \qquad (1)$$

where M_e is the local edge Mach number, and Re_x is the local Reynolds number based on distance from the leading edge X. Since δ varies as the square of M_e, boundary layers can become quite thick at hypersonic conditions.

Thick boundary layers can exert a displacement effect on the inviscid flow outside the boundary layer, causing a given body shape to appear much thicker to the approaching flow. Due to the "effective" increase in thickness, the outer inviscid flow is altered; the inviscid flow field changes in turn feed back into the boundary layer affecting its growth. This cycle of inter-action is referred to as viscous interaction which may result in first order effects on both aerodynamic and aerothermodynamic characteristics. The hypersonic viscous (as opposed to inviscid) flow over a flat plate is often used to illustrate this point. In the viscous case, a boundary layer develops initially from the leading edge and the rate of growth of the boundary layer displace-ment thickness in this region is generally quite large. As a

result, a locally strong shock is formed in the region of the leading edge with accompanying increases in pressure and density (in contrast to the inviscid case where, in the absence of a boundary layer, the pressure is constant with distance X). These pressure and density increases tend to make the boundary layer thinner than would be expected (although the boundary layer itself is still thick on a relative scale) and result in velocity and temperature gradient increases at the wall. As a direct consequence, skin friction and heat transfer levels are enhanced (particularly at the leading edge) when viscous interactions are present. Enhanced heating is of utmost importance to the aerothermodynamicist who is concerned with incorporating an effective thermal protection system (TPS) into his design. The implications for a slender or moderately slender hypersonic vehicle imply that lift, drag, and stability of the vehicle may be influenced. Consider fig.3, which illustrates the viscous interaction on a sharp right-circular cone at 0° angle of attack. Here, the pressure distribution on the cone surface p is given as a function of axial distance. If there were no viscous interaction, the inviscid pressure would be constant and equal to P_c (indicated by dashed line). Because of viscous interactions, the pressure in the vicinity of the nose exceeds the inviscid value (the surface pressure decays further downstream, ultimately approaching the inviscid value far downstream).

The degree to which viscous interactions affect the flow field characteristics increase with Mach number and decrease with

Reynolds number and thus can be particularly important for slender vehicles flying at high altitudes. At very low Reynolds numbers it is possible for the hypersonic boundary layer and shock wave to become so thick that they essentially form a merged shock layer. This type of condition can also arise for both slender and blunt bodies. At high altitudes, the shock wave itself becomes smeared (as opposed to being infinitesimally thin) and results in a merged shock layer.

High Temperature Flows

The higher temperatures associated with hypersonic flight have been alluded to in the earlier discussion of viscous dissipation. These high temperatures occur within hypersonic shock layers and boundary layers and can lead to imperfect gas effects (e.g., vibrational excitation, dissociation and recombination, and ionization) and will be referred to herein as real gas effects. The onset of appreciable real gas effects in flight in air occurs when the vehicle velocity approaches 10,000 ft/sec. It is possible in ground-based facilities (e.g., wind tunnels) to achieve high Mach number flows without these high velocities (or enthalpy levels) by expanding the test media to very low values of free stream static temperature, hence speed of sound. For this reason, vehicles flying or models subjected to velocities in excess of 10,000 ft/sec are often referred to as being in the hypervelocity regime. If the surface of a hypersonic/ hypervelocity vehicle is protected by an ablative heat shield,

103

then the products of ablation will be present in the boundary layer giving rise to additional chemical reactions; surfaces of hypersonic vehicles can be wetted by a chemically reacting boundary layer.

For example, consider the nose region of a blunt body (or the nosecap of a slender configuration) as sketched in fig. 4. At the stagnation region, the bow shock wave is locally normal to the flow, and as a result, the temperature increase behind the shock at high speeds can be quite significant. Anderson 1989, calculates that for an Apollo lunar return capsule traveling at Mach 32.5 (altitude 53 km) the temperature immediately behind the bow shock is approximately 12,000 K. This calculation was based on the assumption of a chemically reacting flow in thermochemical equilibrium (see next paragraph). If chemical reactions are ignored the calculated post shock temperature will be much higher; for this particular example one will erroneously compute temperatures on the order of 58,000 K behind the shock wave. This is because the energy that goes into chemical kinetic processes (e.g., rotational and vibrational excitation, dissociation...) is not accounted for. At hypervelocity conditions this energy can be quite large resulting in the erroneously high temperature calculations. So for a high velocity hypersonic flow, not only can the boundary layer be chemically reacting, but the entire shock layer can be dominated by chemically reacting flow.

The reaction rates of dissociation and recombination processes are important to the understanding of a hypervelocity

104

flow. The residence time of molecules and/or atoms in the vicinity of body compared to the time for a chemical reaction to occur is a key factor in real gas phenomena. If the temperature of the shock layer is increased to a high enough level where chemical reactions are important then time itself becomes a critical factor. If chemical reactions take place very rapidly in comparison to the time it takes for a typical fluid element to traverse the flow field of interest then the flow is in chemical equilibrium. If the chemical reactions occur over a much longer time period than it takes a fluid element to traverse the flow field of interest then nonequilibrium conditions exist (or in the limit "frozen").

Another aspect of the entry-body flow field is sketched in fig. 5. If the shock layer temperature is high enough, the fluid will begin to emit radiation. The thermal radiation emitted by the gas gives rise to a radiative heat flux to the vehicle surface (and is referred to as radiative heating, q_r). This radiative heat transfer augments the convective heating, q_c, which is already present by virtue of the frictional dissipation within the boundary layer. For example, during the Apollo re-entry, radiative heat transfer was more than 30 percent of the total heating. For a space probe entering the atmosphere of Jupiter, the predicted radiative heating will account for over 95 percent of the total heat load.

Low Density Flows

The discussion thus far has assumed the flow is in continuum. That is, the mean free path (distance) that molecules or atoms travel before colliding with each other is small relative to same characteristics length of interest in the flow field. However, there are certain hypersonic applications which involve densities low enough that the continuum assumption is no longer valid. Consider the Space Shuttle reentry. As it descends from orbital altitudes it passes from a free molecular regime to a much denser portion of the atmosphere which is referred to as the continuum regime. Somewhere in between is termed the transitional regime (this is not to be confused with boundary layer transition). In free molecular flow the mean distance a molecule moves between collisions can become as large as the scale of the body itself. Aerodynamic characteristics are then determined by individual scattered molecular impacts. The transition regime is characterized by "slip" conditions at the body surface. Slip conditions refer to the fact that the viscous flow boundary conditions at the wall fail (that is, the velocity at the wall is not zero and the gas temperature immediately adjacent is not equal to the wall temperature). More relevant to this chapter is the fact that in this regime shock layers are characterized by relatively thick boundary layers and thick shock waves.

The similarity parameter that is used to characterize these different regimes (free molecular, transitional, continuum) is the

Knudsen number, defined as Kn = λ/L, where L is a characteristic

dimension of the body and λ is the mean free path length discussed

earlier. The values of Kn in the different regimes are noted in

fig. 6, taken from Moss and Bird, 1984. Note that for Kn < 0.2

the continuum assumptions are valid and the Navier-Stokes

equations are applicable. However, slip effects must be included

in these equations when Kn > 0.03. The effects of free molecular

flow begin around a value of Kn = 1, and extend out to the limit

of Kn becoming infinite. Hence, the transitional regime is

essentially contained within 0.2 < Kn < 1.0. The Knudsen number

is the commonly employed criterion to determine if low-density

effects are important, and to what extent. For example, if Kn is

very small, the flow will be in continuum; if Kn is very large,

the flow will be free molecular. A hypersonic vehicle entering

the atmosphere from space will encounter the full range of these

low-density effects, down to an altitude where continuum

aerodynamics takes over. Because Kn = λ/L is the governing

parameter, the altitude below which continuum assumptions are

valid is dependent on the characteristic length. Hence, large

vehicles experience continuum flow to higher altitudes than small

vehicles. Moreover, if we let the characteristic length be a

running distance x from the nose or leading edge of the vehicle,

then Kn = λ/x becomes infinite when x = 0. Hence, for any vehicle

at any altitude, the flow immediately at the leading edge is

107

governed by low-density (low Reynolds number) effects. For most practical applications in aerodynamics, this leading edge region is very small, and is usually ignored. However, for high-altitude hypersonic vehicles, the proper treatment of the leading edge flow by low-density methods can be important.

Hypersonic Flow Summary

Hypersonic flow can be defined as that flow regime where all or some of the previously discussed physical phenomena become important as the Mach number and/or velocity is increased to high values. This overview, taken from Anderson, has been intentionally restricted to those topics relevant to the topic of this chapter--namely, Reynolds number effects. It is hoped that the subsequent discussions in this document will be easier to follow. To help reinforce the physical phenomena outlined, fig. 7, high-lights some physical aspects associated with hypersonic flight.

The remainder of the paper focuses on identifying several physical phenomena that are or are speculated to be influenced by Reynolds number or viscous effects. Because the basic aim of any wind tunnel test is to determine the full-scale aerodynamic/ aerothermodynamic performance of a particular concept, the hyper-sonic Reynolds number trends are identified by highlighting discrepancies between laboratory and flight data. Emphasis is placed on but not strictly limited to the Gemini/Apollo and shuttle flight programs.

II. HYPERSONIC SIMULATION

Many aerodynamic phenomena are adequately simulated in wind tunnel by achieving the Mach and Reynolds number corresponding to actual flight conditions. The transition to the hypersonic regime significantly complicates the simulation problem, as the changes in air properties at high temperatures must now be taken into account. The larger number of simulation criteria for hypersonic flight makes it virtually impossible to completely simulate flight conditions in a conventional hypersonic wind tunnel (e.g., stationary model, moving air stream). As reviewed by Witcofski and Scallion, 1987, ballistic ranges can duplicate velocities and densities associated with hypervelocity entry into planetary atmospheres and Earth entry from planetary return. This is achieved by firing scaled model through a well defined quiescent test gas. Model size for a facility of this nature makes it difficult, however, to duplicate phenomena associated with a real gases (e.g., atomic recombination - wall catalysis, combustion, radiation).

In a conventional hypersonic blowdown wind tunnel, a steady isentropic expansion from stagnate reservoir conditions is employed to accelerate the flow to the desired conditions. As the flow is expanded to hypersonic conditions (in air) the Reynolds number decreases primarily due to a decrease in fluid density. Thus, in order to achieve a given Reynolds number at high Mach numbers large stagnation densities (pressures) and temperatures are required. The large temperatures are required to prevent

condensation of the test medium during the expansion process. The maximum obtainable Reynolds number in a hypersonic wind tunnel is dependent on the structural ability to contain high pressures and temperatures; hence limiting high Reynolds number hypersonic research. Probstein, 1961, illustrates this point by analyzing the requirements to study the aerodynamic/aerothermodynamic characteristics of a vehicle 6 m long flying at an altitude of 40 km and a speed of 3 km/sec. He assumes a wind tunnel model length of 0.4 m. To match flight Mach and Reynolds numbers, the air in the wind tunnel reservoir must be compressed to 150 atm and heated to a temperature of approximately 800 K to avoid condensation. For the proposed wind tunnel simulation, the stagnation temperature of 800 K will only mildly excite the molecular internal energies. Because the actual flight vehicle flies at 3 km/sec the air temperature in the vicinity of the nose during flight will be on the order of 3,000 K. For such high temperatures, the internal degrees of freedom of the molecules will become excited and dissociation of the oxygen molecules can occur. Therefore, flow phenomena for the wind tunnel simulation will take place under conditions which do not correspond to the enthalpy levels of flight.

This is not to imply that the classical Mach-Reynolds number similitude parameters are not important. Chemical processes in flight are often restricted to localized regions of the flow and the resultant effects on the aerodynamics of the vehicle can be small. Figure 8 taken from Lukasiewicz, 1973, illustrates the

110

Reynolds number/Mach number regimes encountered by various vehicles. This figure should be compared with fig. 9 (obtained from Witcofski, LaRC) which indicates the Agency (NASA) capability to simulate free stream Reynolds number in air, nitrogen, and helium wind tunnels via an isentropic expansion from a stagnate high temperature and pressure gas. The free stream Reynolds numbers shown in this chart are based on nominal model lengths for each NASA facility. For reference purposes, a shuttle descent trajectory along with a proposed NASP trajectory are shown. Up to Mach 10, the capability to simulate Mach/Reynolds number for reentry is good. However, for proposed airbreathers such as NASP on ascent, there appears to be a lack of agency facilities to properly simulate viscous effects particularly above Mach 8.

Simulation of the free stream Reynolds number for a given Mach number, however, does not insure that boundary layer development over the wind tunnel model will be equivalent to that over the actual flight vehicle. Boundary layer development (and hence viscous interactions) are dependent upon several factors; some of the primary factors are boundary layer edge Reynolds and Mach numbers, the ratio of the wall temperature to boundary layer edge temperatures, and, the existence of entropy gradients. (As discussed by J. C. Adams, 1975, entropy gradients develop as streamlines pass through a highly curved shock and can effect the local edge conditions as these streamlines merge with the developing boundary layer - often referred to as entropy swallowing). It is generally accepted that correlating wind

111

tunnel data with flight data using a Reynolds number based on free stream conditions is not always appropriate. For example, at the same value of free stream Reynolds number, large differences between wind tunnel and flight values for edge Reynolds and Mach numbers have been calculated by Thomas, 1967, fig. 10 for sharp flat plates. At high angles of incidence, differences of up to 80 percent can be expected. Since boundary layer characteristics and in particular transition are strongly influenced by the local edge conditions differences of this magnitude can be important. Hence, the first problem to be solved in a flight/laboratory data comparison is to determine what correlation parameter(s) are relevant.

III. EARLY BLUNT BODY EXPERIENCE

Gemini program

On March 23, 1965, the third Gemini mission was completed with Grissom and Young splashing down after completing three Earth orbits. One significant aspect of this flight is that the capsule fell 60 miles short of the targeted recovery area. Like the Apollo command capsule it preceded, the Gemini capsule was designed with a center of gravity offset from the geometrical axis of symmetry. This allowed the vehicle to trim at angle of attack and develop lift. A comprehensive preflight wind tunnel data base was established to provide an accurate knowledge of the Gemini stability characteristics. After the flight, a variety of explanations were postulated to explain the undershoot during

112

reentry. Existing wind tunnel data was re-examined and new experimental information obtained. The ensuing test program (reexamination) and results are detailed by Griffith, 1967. Previous research had indicated that correlation of viscous effects on slender bodies was best accomplished through a viscous interaction parameter (the interested reader is referred to Anderson, 1989 page 302-320 for a detailed discussion of this parameter). However, for a blunt body such as the Gemini capsule during reentry, the primary flow field of interest to the designer becomes the flow behind the bow shock wave. Figure 11 gives a qualitative sketch of the flow field characteristics. It follows that a Reynolds number based on the properties behind the shock becomes a more meaningful correlation parameter than the free stream Reynolds number. From Griffith's investigation, it was determined that significant viscous effects occurred in the separated flow region about the Gemini capsule. At low Reynolds number (high altitudes-low densities), the flow on and around the corner of the heat shield is believed to have remained attached for $R_{e,2d}$ = 2400-5400, resulting in a rearward shift in the center of pressure. This shift is summarized in figs. 12 and 13. At small angles of attack, a large shift in the center of pressure is observed. Figure 13, shows an increase of 4.7° in trim angle was evident with a corresponding 60 percent overestimate in L/D. The correctly correlated data agreed very well with the actual splash down location experienced by Gemini 3. Correctly selecting the proper correlation parameter (Reynolds number based on post shock

113

conditions) and recognizing the potentially significant viscous effects at low Reynolds on separated flows was extremely important for hypersonic blunt body analysis. Although viscous effects are speculated to have been the primary cause of the rearward shift in the center of pressure, the influence of real gas effects on the flow expansion around the heat shield corner has not been adequately addressed.

Apollo Program

Approximately 1.5 years later a similar flight anomaly occurred during re-entry of Apollo AS202 (an unmanned flight) which resulted in the capsule being recovered 200 miles from the intended recovery point. As with the Gemini case, a comprehensive post-flight wind tunnel test program examined the discrepancies concerning the original aerodynamic data base. It was determined that the actual flight L/D ratio was significantly less than predicted. Although viscous effects were believed to have been a contributor to the trajectory discrepancy, it is recognized that unlike the Gemini experience, several other factors may have led to the unexpected loss in L/D. As discussed by Lukasiewicz 1973, the geometry of the Apollo heat shield was not preserved between preflight wind tunnel models and the actual flight vehicle which resulted in significant changes (20 percent in L/D) to the stability characteristics. Lukasiewicz believed that real gas effects on Apollo stability characteristics were not significant at velocities up to 27 kft/sec and that Mach number influences

114

were observed up to approximately M = 14 (substantially higher than indicated in previous blunt body investigations). To this date, there remains much controversy in the aerodynamic community regarding these conclusions concerning the interpretation of the early Apollo hypersonic data base. It was determined by Griffith and Boylan that viscous effects were present at high altitude/low post shock Reynolds numbers (for the Apollo geometry), fig. 14. At a given α, L/D nearly doubled as simulated altitude decreased from 350,000 to 130,000 ft which may illustrate the importance of viscous effects on the Apollo capsule at high altitude.

The discussion up to this point has been limited to low density (low Reynolds numbers) viscous effects on the aerodynamic characteristics of blunt bodies. Because of the expected large lunar return velocities for Apollo, the issue of aerodynamic heating was also of primary concern. Prior to the flights of the Apollo, an effort was made to determine the radiative heat-transfer rates to the blunt capsule heat shield. As discussed by Park, 1985, it was found that laboratory results indicated that radiation would be significantly enhanced in the low density (high altitude) low Reynolds number regime because of the lack of chemical equilibrium. In direct contrast, flight tests conducted aboard a subscale Apollo configuration (known as Project Fire) yielded results that indicated limited radiation enhanced heating in the low density low Reynolds number regime. To this date, the apparent discrepancy between laboratory data conducted in shock

tubes and ballistic ranges, and flight data has not been resolved completely. Our lack of understanding of this phenomena will have consequences for the future design of vehicles referred to as ASTV's (Aeroassisted Space Transfer Vehicles). ASTV's are designed to perform orbital changes or planetary aerocapture missions by flying through the outer portion of the atmosphere and decelerate/maneuver using aerodynamic forces (as opposed to using chemical propellants). ASTV concepts are discussed in detail by Walberg 1982. More recently, Jones 1987, pointed out several key issues involving ASTV's and the impact of the conflicting data obtained from the Apollo era on their design. Jones points out that the radiation heating levels measured by Project Fire may have been significantly reduced before reaching the wall by absorption in the ablation layer. Furthermore, data were obtained on a much smaller scale vehicle, where the shock layer may not have been thick enough to suppress the viscous effects experienced at higher altitudes. That is, at the low Reynolds numbers experienced at high altitudes, the viscous boundary layer occupied a large fraction of the shock layer thickness, and as a result, suppressed the temperatures significantly through much of this region. This reduced the radiative heating measured on the subscale Apollo configuration. The situation is qualitatively illustrated in fig. 15. Consider a hypersonic blunt body as depicted at the top of the figure. The large amount of kinetic energy associated with the hypersonic free stream (or vehicle) is converted to thermal energy across the strong bow shock wave. The

116

vibrational mode can become excited, and at sufficiently high enough speeds, the energy will be sufficient to dissociate and ionize the air in the shock layer. Atomic and molecular species become important sources of radiation which promote additional heating above and beyond the convective component found at slower speeds. A series of collisions is required to establish thermo-dynamic and chemical equilibrium; however, the time associated with these processes varies depending on the reaction involved. Thus, the amount of radiation received at the vehicle wall depends on the transient time a radiating fluid element spends in the shock layer. This is depicted in the lower half, fig. 15, where the gas temperature and associated radiation intensity levels are plotted as a function of distance to the vehicle surface. During the initial compression (immediately behind the shock wave) the temperature attains values approaching those values associated with an ideal molecular gas since the translational modes are rapidly excited. As energy is diverted to the less rapid excitational modes of vibration and rotation and finally to dissociation and ionization, the tempera-ture drops off with time (and hence distance) and eventually reaches an equilibrium value. The strong upsurge in radiation immediately behind the shock results from the fact that several of the internal energy models have not yet absorbed their share of energy; the excess energy appearing as thermal energy. If the air density in the shock layer is low enough, an insufficient number of molecular collisions to achieve equilibrium conditions exists. The

117

radiation will then be principally from the gas which is in nonequilibrium. If the density of the gas in the shock layer is increased, the radiation may well be approximated by equilibrium values. If the density of the gas is high enough, strong reabsorption of the emitted radiation can occur. Reabsorption reduces the radiative heating from the value it would otherwise have. It is speculated that the Project Fire radiative heating was suppressed in such a manner by virtue of the presence of a very thick ablating boundary layer. At high altitudes (low Reynolds number) this ablative boundary layer occupied a significant portion of the boundary layer attenuating the radiative heat flux directed towards the surface. It should be noted that other factors could have contributed substantially to the observed phenomenon. Park, 1983, pointed out that there are problems with the shock tube and ballistic range data which may have resulted in erroneous conclusions.

The situation in regards to Reynolds number effects on hypersonic blunt bodies is complex. It appears that at low Reynolds numbers hypersonic L/D is reduced somewhat by viscous effects. In terms of predicting the radiative heating that may be experienced by large, blunt aerobraking configurations, the picture is not clear. Miller and Wells, 1990, summarized the current dilemma: If the conclusions reached in the early 1970s and based on the analysis of Apollo and Project Fire flights are essentially correct, then radiative heating will be a contributing, but not a dominating consideration, and the prospects look very bright for

the successful development of large, very blunt aerobrakes. If, however, these prior data were significantly altered by the effects of ablation and the viscous layer, and the more recent estimates are essentially correct, then the blunt ASTV would produce a high radiative heating level which might not be tolerable with lightweight nonablating thermal protection materials.

There is little possibility of settling the blunt body radiative heating issue with new ground based data; there are no agency facilities capable of producing the high energy (velocity), low density (low Reynolds number) test conditions with sufficient run times to perform aero and aerothermodynamic assessments of advanced aerospace vehicle concepts. The inadequacy or lack of ground based data dictates that computational methods be utilized to predict the ASTV environment. However, computational models of viscous effects on blunt body aerodynamics and radiative heat transfer have not been thoroughly validated. A flight experiment seems to be the only method to obtain data needed to verify current computational models. Indeed, a flight experiment was advocated to collect data for the anticipated flight velocity and Reynolds number ranges and is detailed by Jones, 1987.

IV. HYPERSONIC BOUNDARY LAYERS

Two additional phenomena that exhibit a strong influence with Reynolds number, and probably the most important aerodynamic/ aerothermodynamic concerns for a designer are boundary layer

119

transition and flow separation/reattachment. In high speed flight, the state of the boundary layer can strongly influence the design of vehicles through its effect on skin friction drag and aerodynamic heating. At hypersonic speeds, all things remaining equal, turbulent boundary layer heating can be several times greater than laminar heating. We have seen how a sustained flow attachment around the Gemini/Apollo heat shields contributed to significant changes in the stability characteristics. The next section of this paper highlights specific instances which occurred during the Shuttle program which emphasize just how difficult it is to predict the orbiter entry environment where boundary layer transition is concerned.

Transition

Boundary layer/shear layer transition phenomena, although studied extensively, is not well understood (the interested reader is referred to Bushnell, 1989 for additional reference material). The flow physics of transition is very complicated particularly at hypersonic speeds where a variety of variables not found at lower speeds, are present. Accurate knowledge of transition phenomena and the transition Reynolds number are essential for the optimum design of a thermal protection system. An excellent overview of the hypersonic transition problem is given by Stetson, 1990. Stetson points out that in the past, most hypersonic transition problems have been associated with re-entry vehicles (e.g., shuttle orbiter, missiles), where transition initially developed

on the aft section of the vehicle and moved forward in only a few seconds. The vehicle subsequently experienced an all turbulent boundary layer flow. For the Shuttle Orbiter, boundary layer transition from laminar to turbulent flow along the windward centerline nominally occurs 1100 to 1200 seconds following entry corresponding to a nominal Mach number of 10 and a Reynolds number of 6×10^6 (STS 1-5), Goodrich et al., 1983.

During the STS-28 entry a particularly asymmetrical boundary transition occurred on the windward surface and required excessive control surface movement, usage of more than a normal amount of RCS propellant, and TPS tile damage. Postflight analysis of surface temperature measurements on the orbiter indicated that transition to turbulent flow occurred at Mach 18. What was unique about this flight was the fact that transition patterns were very asymmetrical with all indications pointing to early tripping on the orbiter left wing. It was found that the flight control system responded to compensate for the resulting induced sideslip and rolling moment through the use of the orbiter ailerons and reaction control jets and adequate flight control margins were maintained at all times during descent. Early investigations indicated that external disturbances (protruding gap fillers on the left forward area of the orbiter) most likely resulted in the asymmetric transition patterns. The incident clearly illustrates the influence the state of the boundary layer can have on hypersonic entry aerodynamics and our need to understand and predict more accurately transition phenomena.

Because transition occurred approximately 300 seconds earlier on this mission, the orbiter windward surface was exposed to a substantially longer period of increased aerodynamic heating. Peak temperatures on the vehicle surface and internal substructure were within ranges experienced on previous flights; however, there was a concern that the high heating levels experienced during STS-28 entry, coupled with tile damage experienced on an earlier mission (STS-27), could result in substantial damage to the Thermal Protection System.

The ability to predict the transition Reynolds number at hypersonic speeds is important to reducing the risks involved. For hypersonic airbreathing configurations such as the National Aero-Space Plane (NASP), where the vehicle may spend prolonged periods in the atmosphere and experience a turbulent boundary, the need for accurate prediction becomes crucial (to optimize propulsion and TPS requirements).

Predicting the Reynolds number for the onset of transition has always been a challenge regardless of the speed range. Anderson, 1989, attempted to functionally define (in a qualitative sense to illustrate the complexity of the problem) the hypersonic transition Reynolds number

$$Re_T = f\left(M_e, \theta_c, T_w, \dot{m}, \alpha, k_R, E, \frac{\partial p}{\partial x}, R_N, Re_\infty/ft, \frac{x}{R_N}, V, C, \frac{\partial w}{\partial z}, T_O, d^*, \tau, Z\right) \qquad (2)$$

where M_e is the Mach number at the edge of the boundary layer, θ_c is a characteristic defining the shape of the body (for a cone, θ_c would be the cone angle), T_w is the wall temperature, m is mass addition or removal at the surface, α is the angle of attack, k_R is a parameter expressing the roughness of the surface, E is a general term characterizing the "environment" (such as free-stream turbulence, or acoustic disturbances propagating from the nozzle boundary layer in a wind tunnel), $\partial p/\partial x$ is the local pressure gradient, R_N is the radius of a blunt nose tip, Re_∞/ft is the unit free stream Reynolds number, x/R_N is the location of the boundary layer while it is immersed in the entropy layer generated by the nose (effects of the entropy layer can be felt more than a hundred nose radii downstream of the tip), V is an index of the vibration of the body, C is the body curvature, $\partial w/\partial z$ is the cross-flow velocity gradient, T_o is the stagnation temperature, d* is a characteristic dimension of the body, τ is a chemical reaction time, and Z is an index of the magnitude of chemical reactions taking place in the boundary layer.

It is beyond the scope of this paper to address the effect of each of the variables on the transition Reynolds number; however, the functional relationship outlined above highlights several parameters unique to the hypersonic problem. Fortunately, for a given situation, not all transition mechanisms are of equal

123

importance and it is up to the researcher to make an intelligent judgement as to which mechanism(s) will dominate. It is commonly accepted that at the present time there is no transition theory; the complexity of the physics of transition prohibits this Stetson, 1990. To date, all transition methods are empirical and have a large degree of uncertainty associated with their use. A major contributor to this problem lies in the limited Reynolds number range capability of hypersonic wind tunnels and the availability of dynamic instrumentation from which to explore the physics of transition.

On subscale wind tunnel models, the boundary layers are typically laminar or transitional, whereas, for a full scale configuration a turbulent boundary layer can be expected to "wet" nearly the entire vehicle. In order to properly simulate aerodynamic characteristics associated with a turbulent boundary layer at subsonic speeds, methods of artificially producing a turbulent boundary layer through the use of small roughness elements has been developed (see for example Braslow, Hicks, and Harris, 1966). Hypersonic boundary layers have been artificially tripped turbulent by roughness elements up to local Mach numbers of approximately 9, Sterrett, et al., 1967. However, the size of the roughness elements required can be of the same order of magnitude as the boundary layer thickness itself. The use of such relatively large trips at hypersonic speeds can create large spanwise disturbance effects in the boundary layer and produce undesirable effects by generating shocks, altering pressure

distributions and erroneously increasing the overall pressure drag (e.g., Sterrett, 1967, Nestler and McCauly, 1981, and Whitehead, 1969).

Even when transition Reynolds numbers are obtained in ground based wind tunnels at flight Mach numbers, it is generally not possible to duplicate velocity or high temperature effects. Thus, it is not possible to obtain boundary layer profile similarity between wind tunnel and flight (boundary layer stability characteristics are very sensitive to the velocity profiles). The effects of high temperatures where chemical reactions can occur on boundary layer transition is just now starting to be addressed computationally (Masad and Nayfeh 1991, Malik and Anderson 1991, Bushnell and Malik 1988). Bushnell acknowledges that little is known in the area concerning the detailed physics of the influence of chemistry upon the transition process; whether or not chemistry specific instability modes exist can only be speculated on as research in this area is, at the present time, limited. It should be noted that at high altitudes and velocities, when thermal non-equilibrium conditions prevail, boundary layer transition may not occur or may not necessarily be the driving aerothermodynamic issue.

The author is aware of at least one case where radiation, dissociation, ablation, and the state of the boundary layer all had a dramatic influence on the predicted aerothermodynamic heating loads for a planetary entry probe. In his paper, Moss 1982, looked at the aerothermal environment that the Galileo space

probe heat shield would encounter during the 48 km/sec entry into the Jovian hydrogen-helium atmosphere. His computations indicated that shock layer temperatures approaching 20,000 K would be encountered with radiative heat transfer as the dominating energy transfer mechanism. As a consequence of the high heating, the carbon-phenolic heat shield will experience massive ablation. A number of flow field phenomena were investigated in this study among them being the adverse impact that turbulence has on predicted radiative heating to the probe surface. Calculations were made assuming instanteous transition from laminar to turbulent flow when the local boundary layer edge Reynolds number reached 1×10^5. Under massive ablation, it was found that turbulent flow produced substantially higher radiative heating than the corresponding laminar results. It was determined that turbulence brought the higher temperature gases much closer to the surface than for the laminar case. In turn, the higher temperatures promoted the dissociation of molecules (C_2, C_3) that served as primary radiation absorbers. Because the mole fractions of these molecules were reduced, the radiation reaching the space probe surface increased. Although substantial insight into the effect of turbulence on radiative heating was gained, it was concluded that turbulence modeling for chemically reacting gases under massive ablation is still poorly understood and experiments must be devised to construct and challenge future turbulence models.

Some problems with wind tunnel/flight transition data

Hypersonic wind tunnels have limitations such as operational deficiencies in Mach number, Reynolds number, and velocity ranges. They are also known for their "noisy" disturbance environment that is produced by turbulent nozzle wall boundary layers. During the late 1950s and 1960s, the recognition of the significance of wind tunnel free stream disturbances provided some explanation as to why flight transition Reynolds numbers are generally larger than those obtained in wind tunnels (see Pate 1969, Morkovin 1959). This eventually led to the development of a "quiet" (low disturbance) tunnel at Langley (Beckwith et al., 1983) to obtain transition Reynolds numbers comparable to flight values. Typical transition onset data for cones in the Mach 3.5 Pilot Quiet Tunnel are shown fig. 16. The quiet tunnel data for low noise conditions are in good agreement with the lower range of flight data up to Re $\approx 1 \times 10^6$ inch^{-1}. Generally speaking, wind tunnel testing is more conducive to systematic control of the test environment than flight; however, due to the limitations in operational capability and noise environment, extrapolation to flight can be quite difficult and misleading. In flight testing the desired Mach and Reynolds numbers are obtained at flight velocities; however, typically there is very little parametric control of the variables influencing the phenomena of interest (e.g. angle of attack, ablation, wall waviness) or definition of the atmospheric environment. Unfortunately, flight instrumentation is costly, lacks the spatial resolution needed for proper analysis and the

measurements of fluid parameters of interest are difficult if not impossible to obtain (e.g., flow field information, boundary layer surveys). Neither technique is ideal.

It is the opinion of the author that future experimental work related to hypersonic transition should be conducted in a manner so as to not only provide parametric trends but to identify the instability phenomena itself. This would require fast response 2-D/3-D optical nonintrusive measurements and would necessitate accurate and detailed knowledge of the free stream environment as well as multi-facility testing and possibly even flight tests, if appropriate. It is important that reliable data be obtained to check models used in computational techniques. Real gas effects on transition will be difficult to assess. A large ballistic range proposed by Langley and referred to as AHAF (Advanced Hypervelocity Aero-physics Facility) would provide flight duplication (as opposed to simulation) of velocity and densities (see Witcofski and Scallion, 1989) but it is acknowledged that advances in remote measurement techniques, onboard model instrumentation/construction techniques, and model launcher systems must be made before any commitment for the construction of such a facility can be made.

Flow Separation

As noted previously, the state of the boundary layer (laminar, transitional, turbulent) can have a significant influence on the aerodynamics and aerothermodynamics of a

hypersonic vehicle. For example, at low Reynolds numbers where a laminar boundary layer exists, a deflected control surface can create an adverse pressure gradient strong enough to force the boundary layer to separate from the wall. This can degrade control surface effectiveness as well as creating high heating loads where the free shear layer reattaches. In addition, the high angle of attack ($\alpha \approx 40°$) attitude of the shuttle orbiter during reentry creates a highly three-dimensional and complex flow field on the upper (leeward) surface (see Baranowski and Kipp, 1983 and Helms III, 1981). The shuttle leeward flow is characterized by cross flow separation and the formation of one or more pairs of counterrotating vortices which eventually reattach along the leeward surface centerline. A vortex system also emanates from the shuttle wing-fuselage junction and scrubs along the fuselage side.

This complex leeward flow field was studied prior to the shuttle first flight without the benefit of CFD to provide an insight to the leeside flow field, it was necessary to use wind tunnel data and extrapolate to flight with empirical correlations. Figure 17 taken from Lee and Harthun 1982, depicts the side fuselage vortex movement with angle of attack as traced from data obtained on a 0.04 scale model. The position and strength of the vortex was highly sensitive to angle of attack and Reynolds number. After the second shuttle flight, a comparison of wind tunnel and flight heating data along the orbiter midfuselage side

was made at various Reynolds numbers, fig. 18. The heating to the fuselage side was significantly underpredicted. Lee and Harthun speculated that the discrepancy between the data and prediction is due to a difference in vortex behavior (strength and/or position) between flight and the wind tunnel. Recent in-flight temperature measurements made on the leeward surface of the shuttle orbiter Columbia (Throckmorton et al., 1992) may provide useful information for the proper interpretation of heating for this complex flow field. It is well recognized in the hypersonic community there is the need for benchmark data to validate turbulence models that are applicable to separated shear layer/vortical flows.

Probably the most well known disparity between ground based measurements and flight data is the so called "hypersonic nose up pitch anomaly" that was observed during the first flight of the shuttle orbiter. Extensive wind tunnel tests on the orbiter were conducted prior to the first flight and preflight estimates of the shuttle aerodynamic characteristics were made based on these tests. The tests indicated that nose-up pitching moments would occur due to real gas effects but that the incremental increase would be within the tolerances and variations established from the aerodynamic design data book (Woods, et al., 1983). Figure 19 shows the trimmed C_m in flight (which is zero) along with a predicted C_m value based on wind tunnel measured body flap effectiveness and the actual flap deflection measured in flight. It is evident that for $M_\infty > 15$ a difference of approximately +0.03

exists. During the shuttle return from orbit on the first flight, the body flap had to be deflected down by approximately double the predicted value (15° instead of 7.5°) to properly trim the vehicle.

The level of uncertainty in predicting the trimmed pitch characteristics was a concern to the aerodynamics community. For the interested reader, Koppenwallner 1987, reviews the published explanations of the shuttle pitching moment behavior. In addition, Woods, et al., 1983 provides an extensive historical overview of wind tunnel research that contributed to the shuttle aerodynamic design philosophy leading up to the first flight. A variety of explanations for the "anomaly" exist ranging from low Reynolds number viscous effects (Koppenwallner, 1987) to high velocity real gas effects (Yasuhiro and Hirotoshi, 1990). The intent here is not to survey the literature or resolve the so called "anomaly" but to highlight possible Reynolds number related effects which could possibly contribute to the observed nose-up pitch.

In his paper, Woods, concludes that the state of the boundary layer and its effect on body flap effectiveness may be an important contributor to the shuttle nose-up pitching behavior. The fact that Reynolds number can influence control effectiveness is well recognized. Penland and Romeo, 1971 reviewed the significant factors which can affect extrapolation of wind tunnel data at subscale Reynolds numbers to flight values (where laminar and turbulent boundary layers exist, respectively). They concluded

that additional work was required to determine viscous effects on control surface effectiveness over a wide Reynolds number range. Penland postulated that accurate knowledge of control effectiveness parameters would be required to predict reliable values of the trimmed performance at flight Reynolds numbers, and, because of flow separation over controls, viscous effects could be significant.

Woods indicates that shuttle preflight predictions projected that boundary layer transition on the windward surface would occur near Mach 16. Results from heating measurements on STS-1 implied that a laminar boundary layer existed to around Mach 10. Woods argued that for most of the hypersonic portion of reentry the body flap was immersed in the lower momentum environment of a laminar boundary layer. However, prior to obtaining flight data, a turbulent boundary layer was expected, and according to Woods, Mach 13.5 wind tunnel tests were advocated and conducted in NSWC Tunnel 9 for the express purpose of obtaining turbulent boundary layer control effectiveness data at close to flight Reynolds numbers. The presence of extensive regions of laminar flow can present the designer of hypersonic high altitude vehicles with several challenges. It is known that laminar boundary layers can separate more easily than their counterpart turbulent boundary layers. A separation bubble located ahead of a deflected control surface can significantly reduce control forces by effectively "fairing-in" the compression surface. Holden 1986, discusses briefly the shuttle nose-up pitch anomaly and concludes that to

132

reconcile the differences between flight and ground based measurements solely on the basis of an equilibrium inviscid code to correct for real gas effects (as suggested by Maus and Griffith 1984) might be misleading. Holden points out that the greater than expected pitching moment could also be explained directly in terms of decreased flap effectiveness as a result of the increased size of the interaction region (ahead of the body flap) at the lower Reynolds numbers encountered in flight. The exact nature of the phenomena producing the unexpected incremental increase in pitching moment continues, to this date, to be shrouded in controversy.

The increased stability of laminar boundary layers at high Mach number flows coupled with the fact that laminar boundary layers can separate easily poses a challenge not only to the aerodynamicist, but the aerothermodynamicist as well. The high heating rates associated with the reattachment of laminar separated flows can severely increase thermal protection system requirements. The role and influence of Reynolds number on the size and structure of separated regions is not clearly understood. This is particularly true for separated regions formed by a shock wave impingement on a turbulent boundary layer. The literature review conducted by Holden 1986, indicates that major experimental discrepancies exist in this area.

It is recognized by the aerodynamic community (subsonic - hypersonic) that more experimental work is needed to address the influence of Reynolds number on separated laminar/turbulent flows

as well as separated shear layers. In the supersonic/hypersonic regime emphasis should be placed on compression corner interactions as well as shock/boundary layer interactions. There remains a need for high Reynolds number studies with detailed steady and unsteady measurements.

V. CONCLUSIONS

Through the comparison of flight and ground based data, this paper has attempted to identify some hypersonic fluid dynamic phenomena which are, or may be, influenced by Reynolds number. It is not intended to be all inclusive, but rather it is hoped to stimulate questions concerning the availability of facilities to investigate, and the instrumentation to measure the fluid phenomena in question. Although not explicitly discussed, the impact of CFD as a tool to aid in the understanding and modeling of the fluid physics should not be overlooked.

Because of the high temperatures associated with hypersonic shock layer and boundary layers that occur in flight, the accurate determination of the heating environment becomes a primary concern for the vehicle designer. Emphasis in the paper has been placed on the influence the state of the boundary layer (laminar transition/turbulent, attached/separated) has on the aerothermodynamics as well as vehicle stability and control. Interest in blunt body reentry configurations has raised fundamental questions regarding the influence of viscous effects found at high altitude, low density (low Reynolds number) conditions on vehicle

aerodynamics, aerothermodynamics, and in particular radiative heating. The present uncertainty levels that exist regarding Reynolds number effects associated with hypersonic viscous interactions at high altitudes and boundary layer transition has dictated conservative design practices for thermal protection systems. The optimum design of future hypersonic vehicles such as the National Aero-Space Plane (NASP) and Aeroassisted Space Transfer Vehicles (ASTV's) will be achieved by reducing these conservative design margins.

The aerodynamic/aerothermodynamic fluid phenomena associated with high altitude rarefied flows is challenging to explore both experimentally and computationally. The limited experimental capability (for vehicle aerodynamic/aerothermodynamic assessment) that exists today lies outside the Agency and is restricted to low enthalpy facilities where very small models are used. Extreme demands are placed on measurement techniques employed in such facilities. Magnetic suspension systems and/or highly sensitive balances are required in these low dynamic pressure environments. The rarefied environment also poses many challenges in terms of the measurement of pressure. Computationally, Direct Simulation Monte Carlo (DSMC) methods model the real gas flow by tracking thousands of simulated molecules in a computer; however, this technique is restricted to low Reynolds number flows. Higher density flows, where the Reynolds number is higher, require far too much memory for this method to be practical.

The influence of Reynolds number on hypersonic transition and separation continues to be an issue for the aero/aerothermodynamic research community and has impacted manned and unmanned flight vehicle operations in a variety of unexpected ways. As with rarefied flow facilities, no ground based facility can simulate or duplicate all conditions experienced in flight. The limited Reynolds number range capability for hypersonic wind tunnels within the Agency continues to be a challenge for continued research. Even if full scale Reynolds number simulation were possible, the "noisy" environment produced in hypersonic wind tunnels is said to "taint" experimental data. The quiet tunnel capability at Langley is a step in the right direction but it does not provide high enthalpy flows. Flight testing does provide one with unique opportunities but it is generally regarded as too expensive and measurements are challenging to make.

With the success of such programs as Mercury, Gemini, Apollo, Shuttle, and X-15, it is clear that manned hypersonic flight is possible. Although Reynolds number effects can produce some undesired effects concerning stability and control and heating, these unknowns are accounted for through conservative design practices. It is hoped that continued research into low and high Reynolds number regimes can reduce the uncertainty bandwidth associated with future hypersonic vehicle design.

In summary, recommendations for future research in the area of hypersonic Reynolds number are as follows:

1. The limited Reynolds number range of current ground based hypersonic facilities within the Agency impedes our research efforts to explore and understand the physics of hypersonic viscous effects. Advocacy of facility development/refinement in three areas is suggested:

   a) A high Reynolds number hypersonic/hypervelocity (high enthalpy) device to investigate real gas and in particular radiation effects on viscous phenomena.

   b) A high enthalpy/low density (rarefied) flow facility to study aerodynamic/aerothermodynamic viscous effects for the high altitude/low Reynolds number flight regime.

   c) Quiet tunnel technology particularly at hypersonic/ hypervelocity conditions where the role of chemistry on the transition process is largely unknown.

2. The role of viscous effects and ablation on radiation enhanced heating for hypersonic blunt body re-entry is largely unknown. A flight experiment has been advocated in the past, Jones 1987, to obtain data needed to verify computational models for the anticipated velocity and Reynolds number ranges expected in flight.

3. Future experimental work related to hypersonic transition modeling should be conducted in a manner so as to provide not only parametric trends but to also identify the instability itself. This entails knowledge of the free stream test environment and multi-facility testing.

4. The role and effect of Reynolds number on hypersonic control surface effectiveness remain shrouded in controversy. Data to validate turbulence modeling for separated shear layer/vortical flows are needed.

VI. REFERENCES

[1]Adams, J. C.; et al.: Real-Gas Effects on Hypersonic Laminar Boundary-Layer Parameters Including Effects of Entropy-Layer Swallowing. AEDC-TR-75-2, 1975.

[2]Anderson, J. D.: Hypersonic and High Temperature Gas Dynamics. McGraw-Hill, Inc. 1989.

[3]Baranowski, L. C.; Kipp, H. W.: A Study of Leeside Flow Field Heat Transfer on Shuttle Orbiter Configurations. NASA CR NAS1-16839, 1983.

[4]Beckwith, I. E.; Creel, T. R.; Chen, F. J.: Free-Stream Noise and Transition Measurements on a Cone in a Mach 3.5 Pilot Quiet Tunnel. NASA TP-2180, 1983.

[5]Braslow, A. L.; Hicks, R. M.; Harris, R. V.: Use of Grit-Type Boundary-Layer Transition Trips on Wind Tunnel Models. NASA TN D-3579, September 1966.

[6]Bushnell, D. M.; and Malik, M. R.: Compressibility Influences on Boundary-Layer Transition. Invited paper, Physics of Turbulent Mixing, Princeton, New Jersey, 1988.

[7]Bushnell, D. M.: Applications and Suggested Directions of Transition Research. Fourth Symposium on Numerical and Physical Aspects of Aerodynamic Flows, Long Beach, California, January 1989.

[8]Goodrich, W. D.; Stephen, D. M.; and Bertin, J. J.: Shuttle Orbiter Boundary Layer Transition at Flight and Wind Tunnel Conditions. NASA CP-2283, Part 2, 1983.

[9]Griffith, B. J.; and Boulan, D. E.: Postflight Apollo Command Module Aerodynamic Simulation Tests. Journal of Spacecraft, vol. 5, no. 7, July 1968.

[10]Griffith, B. J.: Comparison of Aerodynamic Data from the Gemini Flights and AEDC-VKF Wind Tunnels. Journal of Spacecraft, vol. 4, no. 7, July 1967.

[11]Helms, V. T., III: An Empirical Method for Computing Leeside Heating on the Space Shuttle Orbiter. AIAA Paper No. 81-1043, June 1981.

[12]Holden, M. S.: A Review of Aerothermal Problems Associated with Hypersonic Flight. AIAA Paper No. 86-0267, January 1986.

[13]Jones, J. J.: The Rationale for an Aeroassist Flight Experiment. AIAA Paper No. 87-1508, June 1987.

[14]Koppenwallner, G.: Low Reynolds Number Influence on Aerodynamic Performance of Hypersonic Lifting Vehicles. AGARD-CP-428 Aerodynamics of Hypersonic Lifting Vehicles, 1987.

[15]Lee, D. B.; and Harthun, M. H.: Aerodynamic Entry Environment of the Space Shuttle Orbiter. AIAA Paper No. 82-0821, 1982.

[16]Lukasiewicz, J.: Experimental Methods of Hypersonics. Marcel Kekker, Inc., N.Y., 1973.

[17]Malik, M. R.; and Anderson, E. C.: Real Gas Effects on Hypersonic Boundary-Layer Instability. Phys. Fluids A, Vol. 3, No. 5, May 1991.

[18]Masad, J. A.; and Nayeh, A. H.: Effect of Heat Transfer on the Subharmonic Instability of Compressible Boundary Layers. Phys. Fluids A, vol. 3, no. 9, September 1991.

[19]Miller, C. G., III; and Wells, W. L.: Wind Tunnel Based Definition of the AFE Aerothermodynamic Environment. Third Joint Europe/US Short Course in Hypersonics, October 1990.

[20]Morkovin, M. V.: On Supersonic Wind Tunnels with Low Free Stream Disturbances. Journal of Applied Mechanics, Paper 59-APM-10, Vol. 26, 1959.

[21]Moss, J. N.: Advancements in Aerothermodynamic in Support of the Galileo Probe. Thirteenth International Symposium on Space Technology and Science. Tokyo, Japan, 1982.

[22]Moss, J. N.; and Bird, G. A.: Direct Simulation of Transitional Flow for Hypersonic Reentry Conditions. AIAA Paper No. 84-0223, 1984.

[23]Nestler, D. E.; and McCauly, W. D.: A Study of a Boundary Layer Trip Concept at Hypersonic Speeds. AIAA Paper No. 81-1086, 1981.

[24]Pate, S. R.; and Schueler, C. J.: Radiated Aerodynamic Nose Effects on Boundary Layer Transition in Supersonic and Hypersonic Wind Tunnels. AIAA Journal, vol. 7, no.3, 1969.

[25]Park, C.: Radiation Enhancement by Nonequilibrium in Earth's Atmosphere. Journal of Spacecraft, vol. 22, no. 1, January-February 1985.

[26]Penland, J. A.; and Romeo, D. J.: Advances in Hypersonic Exploration Capability-Wind Tunnel to Flight Reynolds Number. Journal of Aircraft, vol. 8, no. 11, November 1971.

[27]Probstein, R. F. (transl. and ed.): Introduction to Hypersonic Flow. Academic Press, New York, 1961.

[28]Sterrett, J. R.; Morrisette, E. L.; Whitehead, A. H., Jr.; and Hicks, R. M.: Transition Fixing for Hypersonic Flows. NASA TN D-4129, October 1967.

[29]Stetson, K. F.: Comments on Hypersonic Boundary-Layer Transition. WRDC-TR-90-3057, September 1990.

[30]Thomas, A. C.; and Perlbachs, A.: Application of Ground Test Data to Reentry Vehicle Design. AFFDL-TR-66-229, January 1967.

[31]Throckmorton, D. A.; Zoby, E. V.; Dunavant, J. C.; and Myrick, D. L.: Shuttle Infrared Leeside Temperature Sensing (SILTS) Experiment-STS-35 and STS-40 Preliminary Results. AIAA Paper No. 92-0126, January 1992.

[32]Walberg, G. D.: A Review of Aeroassisted Orbit Transfer. AIAA Paper No. 82-1378, 1982.

[33]Whitehead, A. H., Jr.: Flow-Field and Drag Characteristics of Several Boundary Layer Tripping Elements in Hypersonic Flow. NASA TN D-5454, October 1969.

[34]Witcofski, R. D.; and Scallion, W. I.: Advanced Hyper-velocity Aerophysics Facility Workshop. NASA CP 10031, May 1989.

[35]Woods, W. C.; Arrington, J. P.; and Hamilton, H. H. II: A Review of Preflight Estimates of Real-Gas Effects on Space Shuttle Aerodynamic Characteristics. NASA CP 2283, Part 1, 1983.

[36]Yasuhiro, W.; and Hirotoshi, K.: Numerical Simulation of Re-entry Flow Around the Space Shuttle with Finite Rate Chemistry. International Symposium on Space Technology, Tokyo, Japan, May 1990.
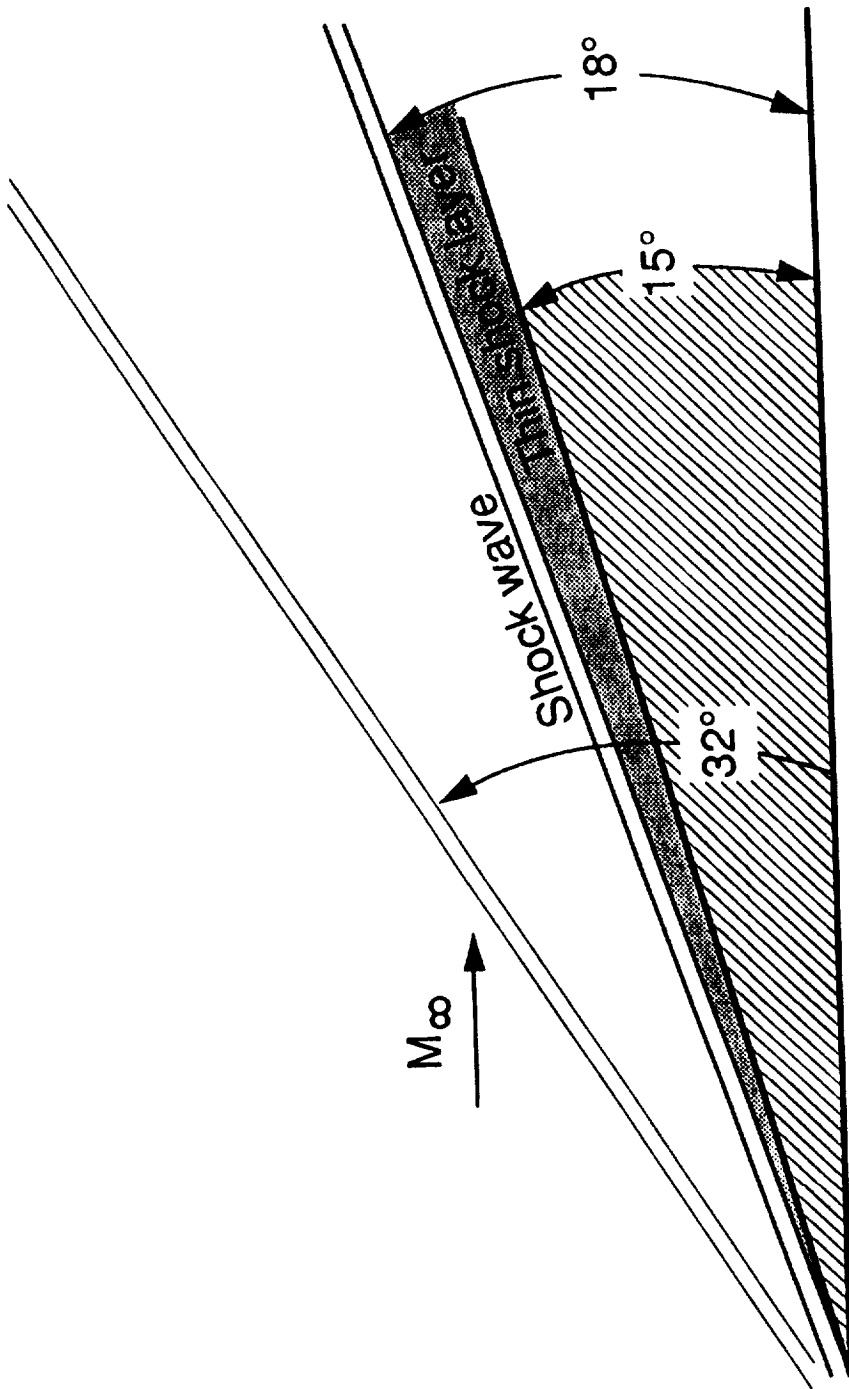
Fig. 1   Typical thin hypersonic shock layer
(from Anderson, 1989).
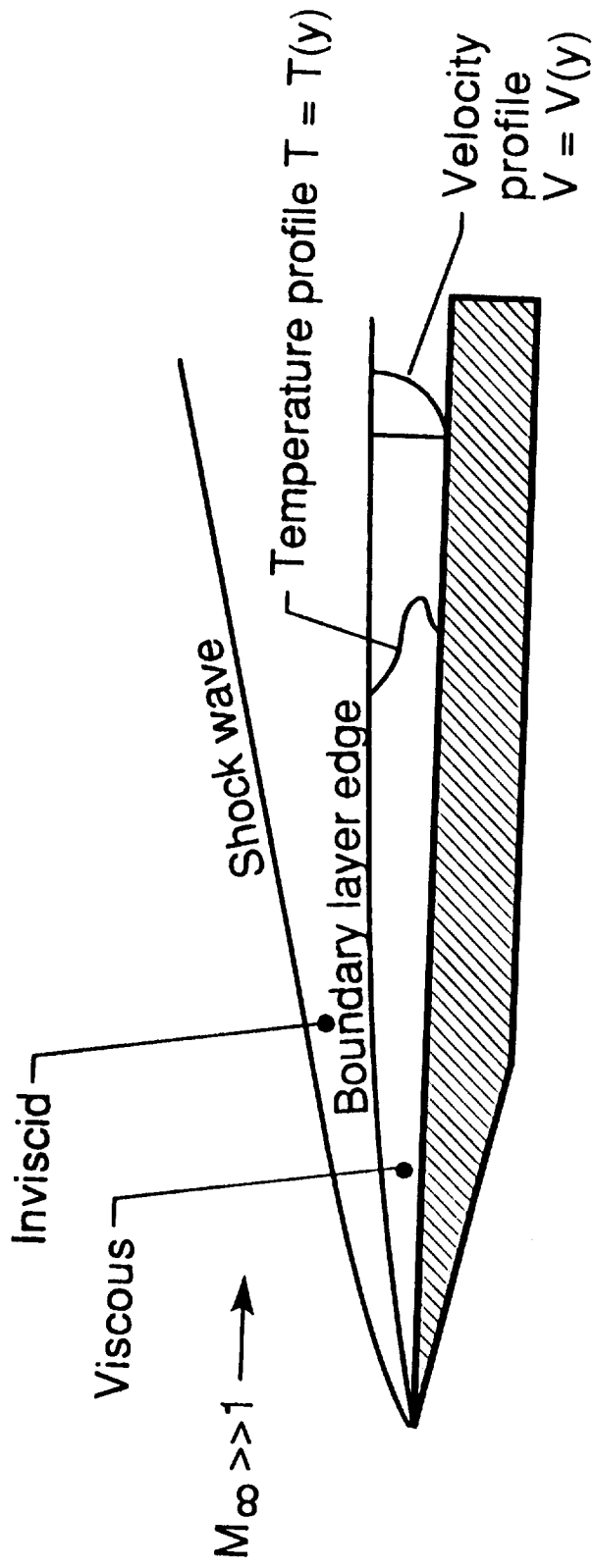
Fig. 2   Temperature and velocity profiles in a hypersonic boundary layer.
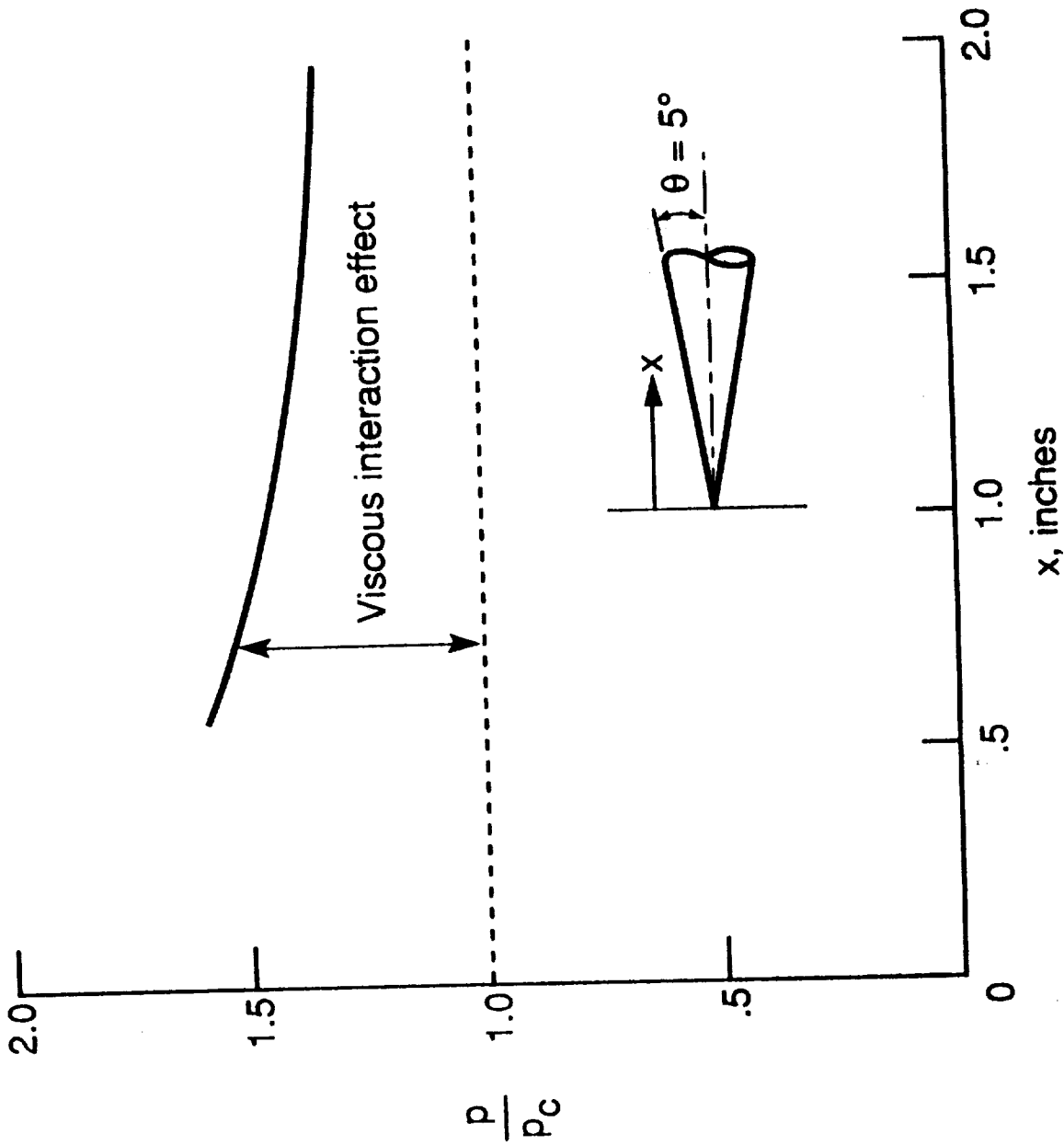
Fig. 3. Viscous interaction effect. $M_\infty = 11$, $Re_\infty/ft = 1.88 \times 10^5$ (from Anderson, 1989).

High-temperature boundary layer

Strong bow shock wave

$M_\infty \gg 1$

Entry body

High-temperature shock layer region
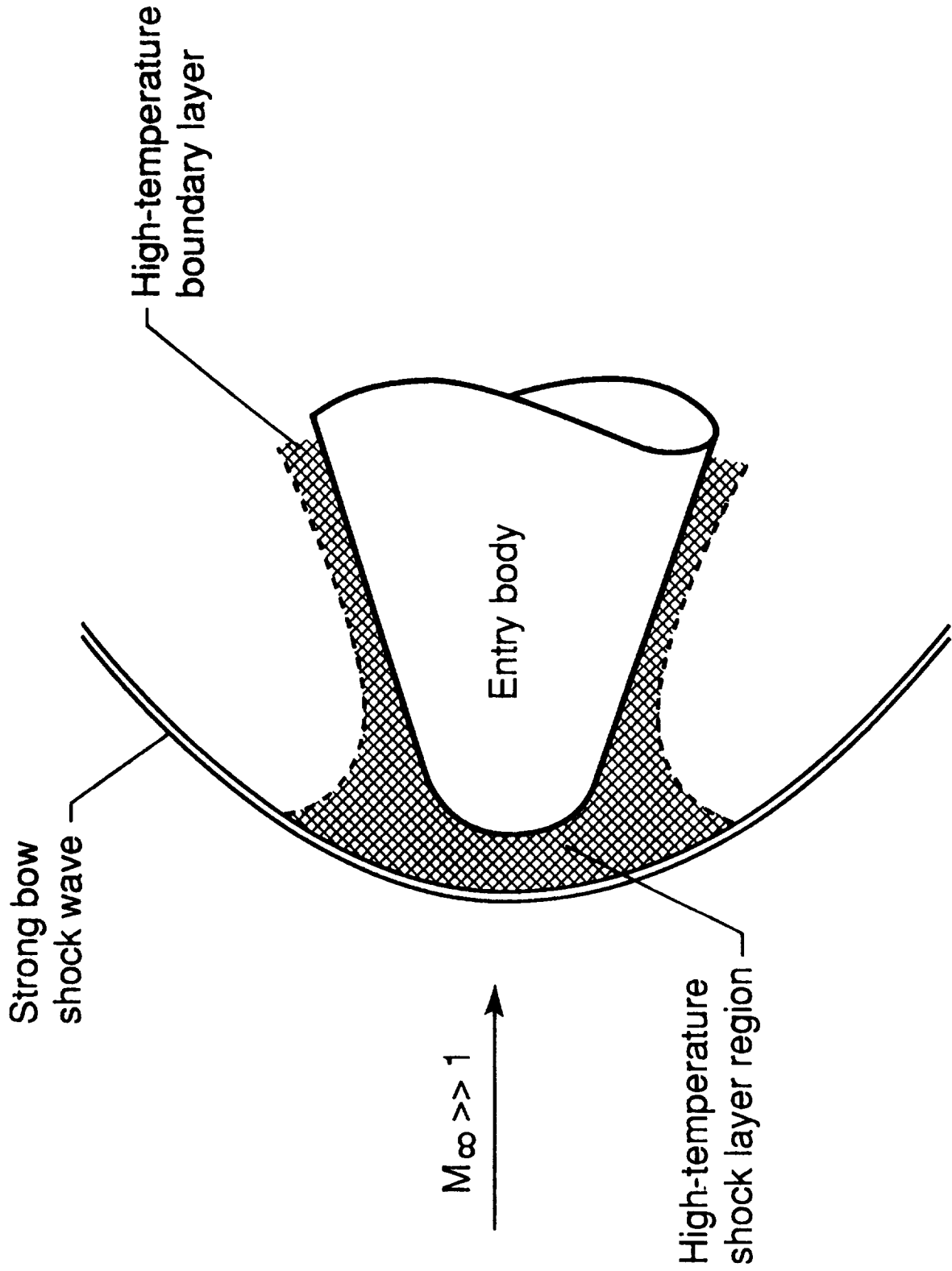
Fig. 4   Schematic of high temperature regions in a hypersonic blunt body flow field (from Anderson, 1989).

Strong shock wave

Body

Radiating fluid element

$M_\infty \gg 1$
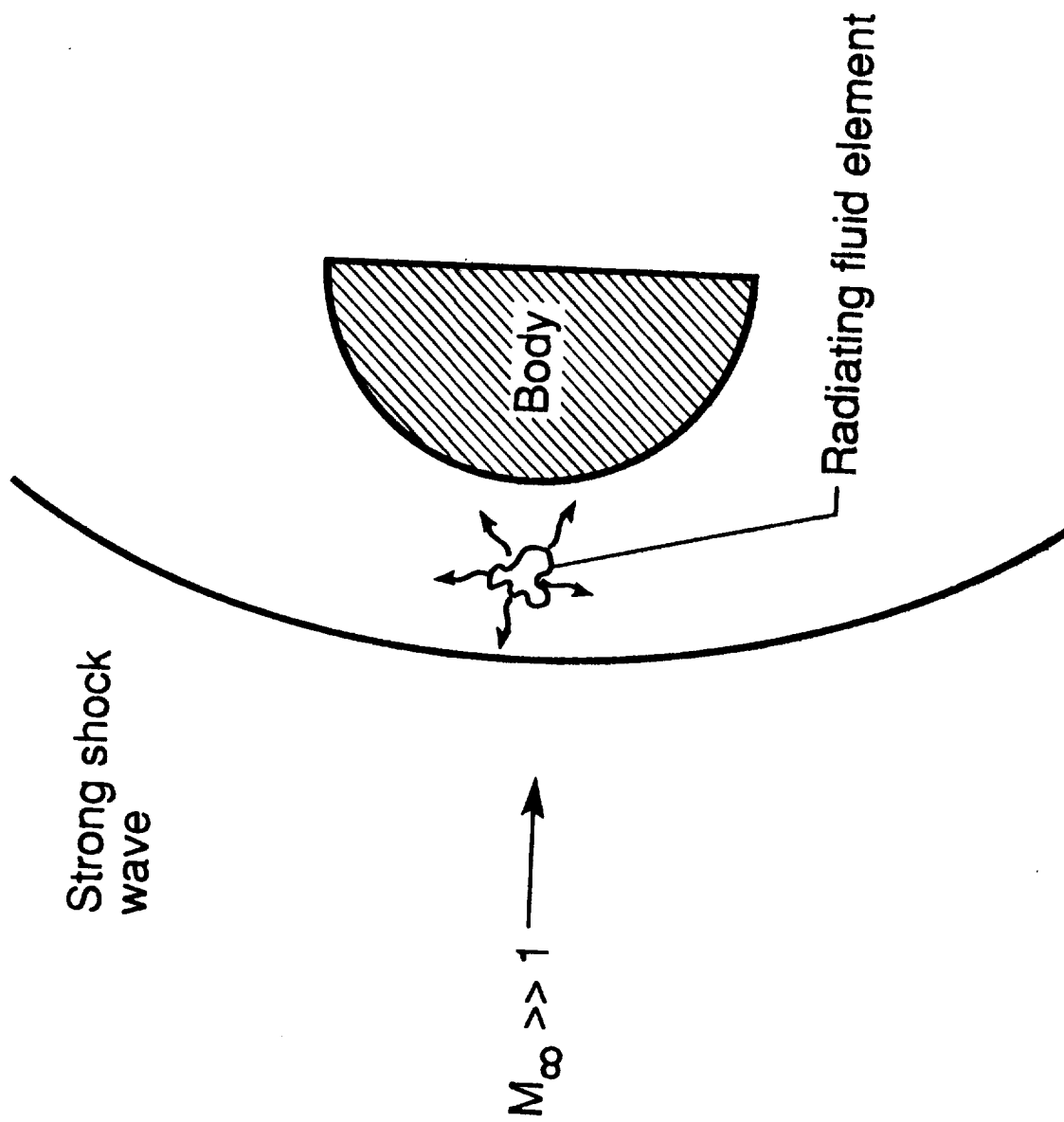
Fig. 5 Schematic of radiating flow field (from Anderson, 1989).
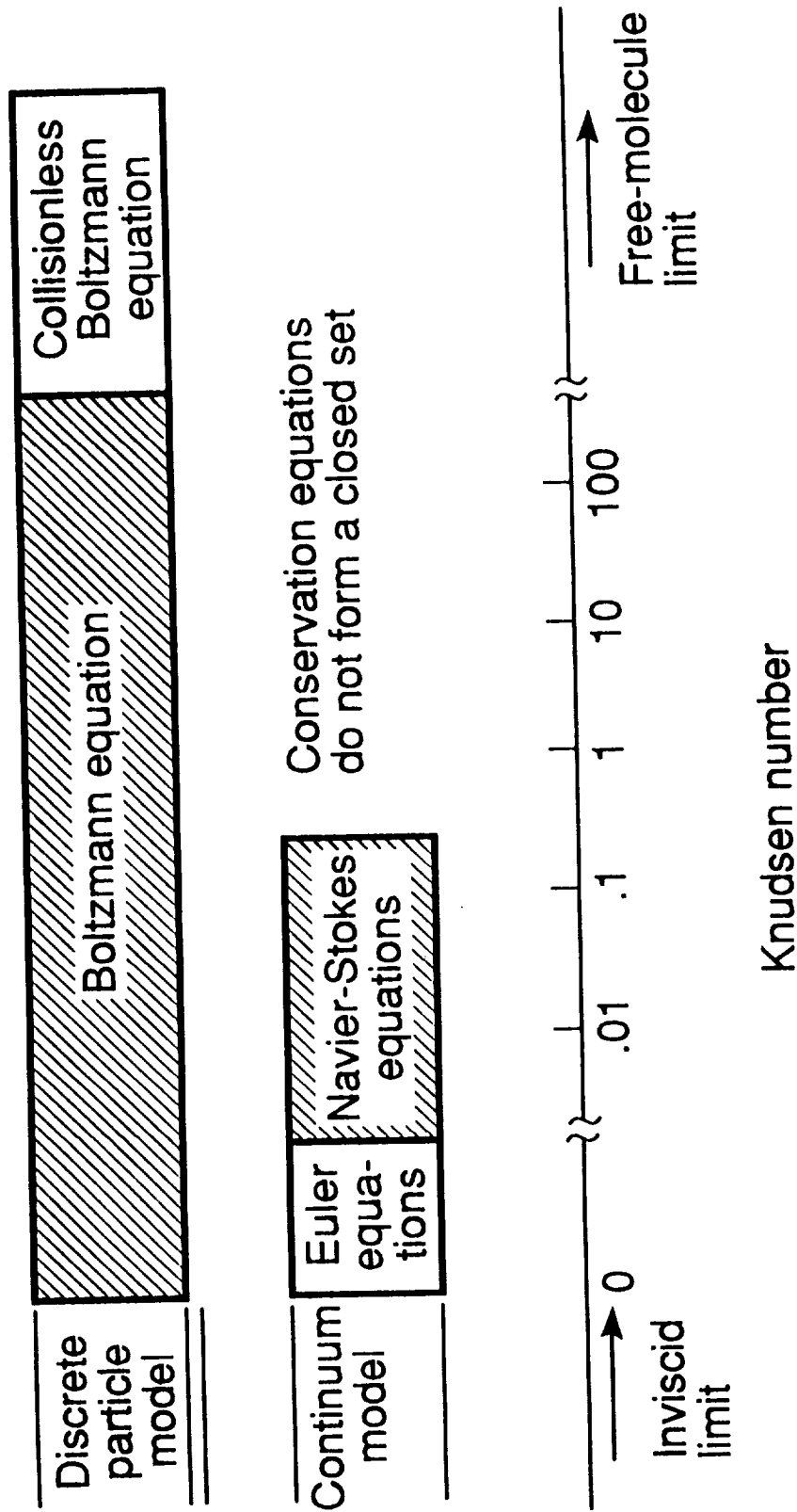
Fig. 6   Regimes of low density flow (from Anderson, 1989).

High-temperature effects
- Excitation of energy modes (vibrational, rotational, electronic)
- Chemical reactions
- Radiation
- Nonequilibrium
- Ablation

Boundary layers
- Thick boundary layer $\delta \propto \dfrac{M^2}{\sqrt{R_e}}$
- Transition

Low density effects (high altitudes)
- Thickened shock wave
- Merged shock layer
- Velocity and temperature slip

Thin shock layer
- Shock close to body
- Viscous interaction
- Vorticity

B.L. δ

B.L. δ

B.L.

Thickened shock

Fig. 7 Some physical characteristics of hypersonic flow.
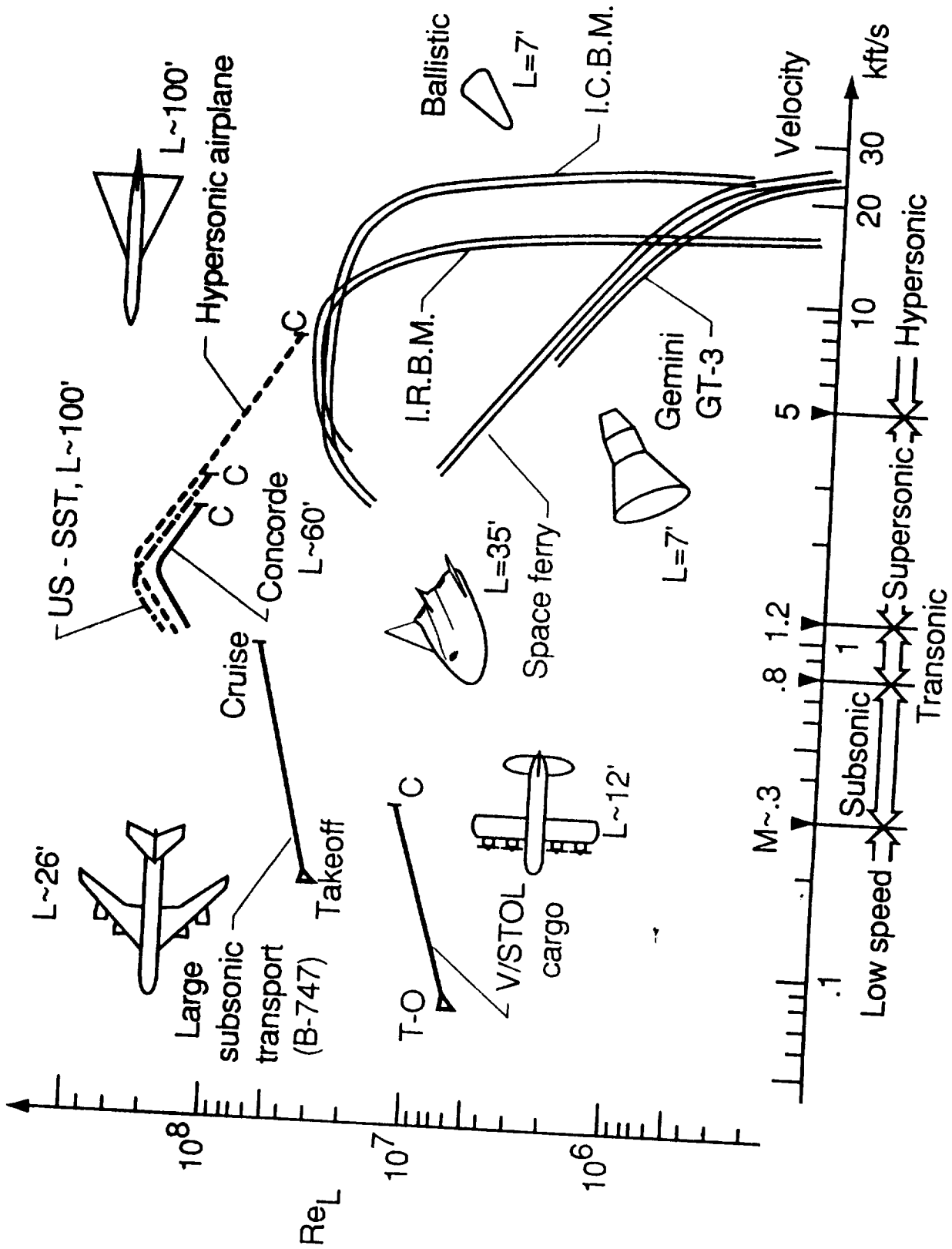
Fig. 8 Mach number/Reynolds number parameters for various vehicles (from Lukasiewicz, 1973).

CAPABILITIES OF NASA FACILITIES

NASP, ℓ=150 ft.

Ascent (q=1000 psf)

Descent

STS-1 descent

Length Reynolds number

Mach number

1   60-in. M18 He   (6-ft.)*
2   Ames 3.5-ft.   (2-ft.)
3   31-in. M10   (2.5-ft.)
4   20-in. M6 CF4   (1.5-ft.)
5   20-in. M17 N2   (1.5-ft.)
6   15-in. M6 HiT   (1.5-ft.)
7   22-in. M20 He   (2-ft.)
8   20-in. M6   (1.5-ft.)

9   M18 QHeT   (1.5-ft.)
10   M8 VDT   (2-ft.)
11   M6 HiReT   (1.5-ft.)
12   M6 NTC   (1.5-ft.)
13   CHSTF   (0.65-ft.)
14   AHSTF   (0.65-ft.)
15   LeRC HTF   (10-ft.)
16   8-ft. HTT   (10-ft.)
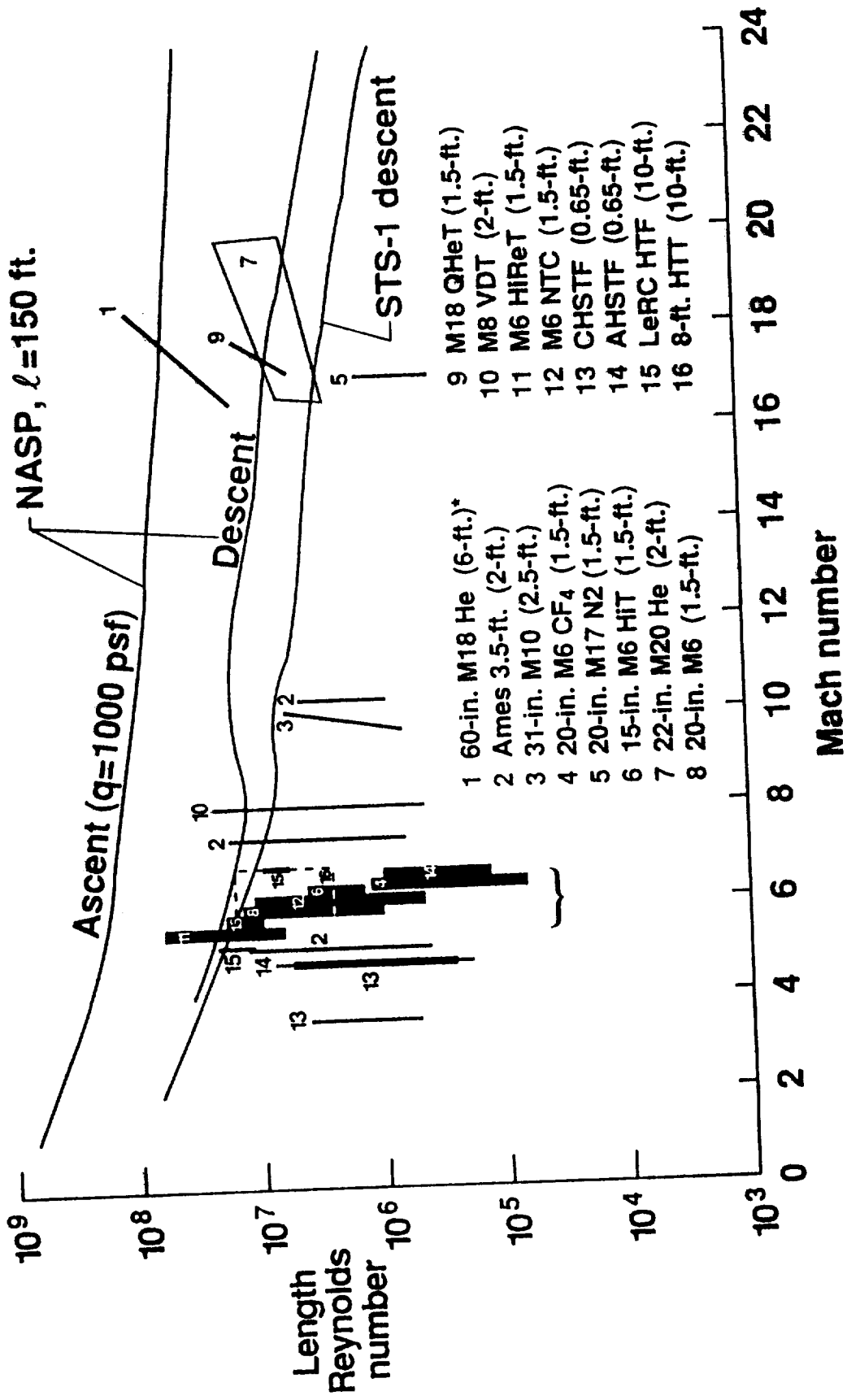
* Note: Number in parentheses represents model length.

Fig. 9   Reynolds number simulation in NASA ground-based facilities (developed by Witcofski, 1992).
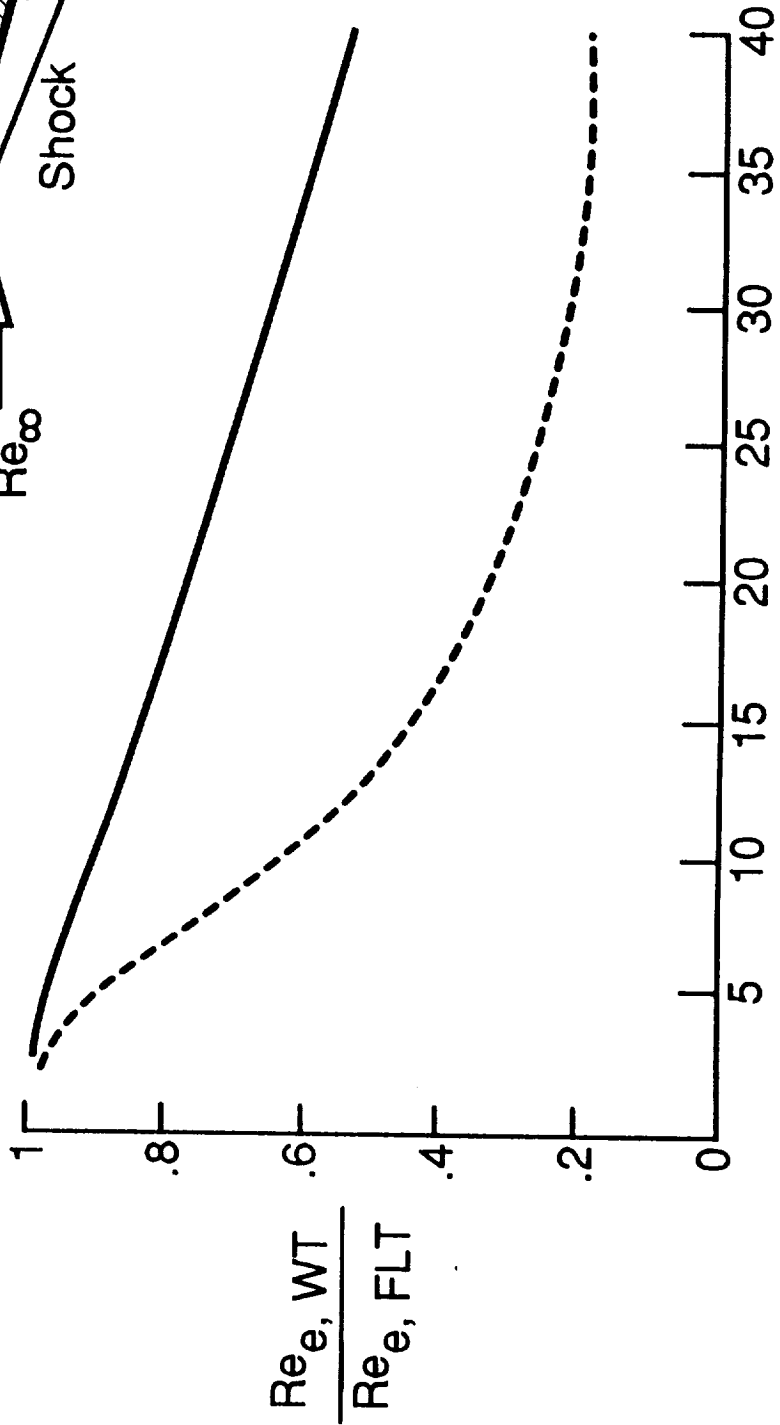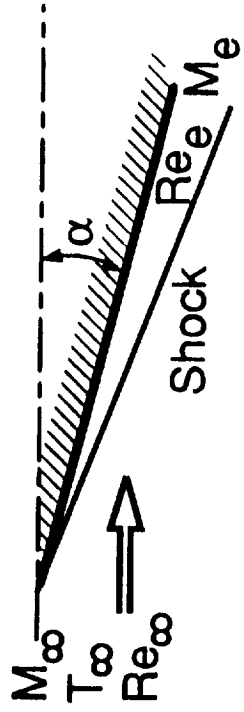
Fig. 10 Comparison of flight and wind tunnel
edge Reynolds numbers for M_∞ = 10 and
20 (from Thomas and Perlbachs, 1967)

153
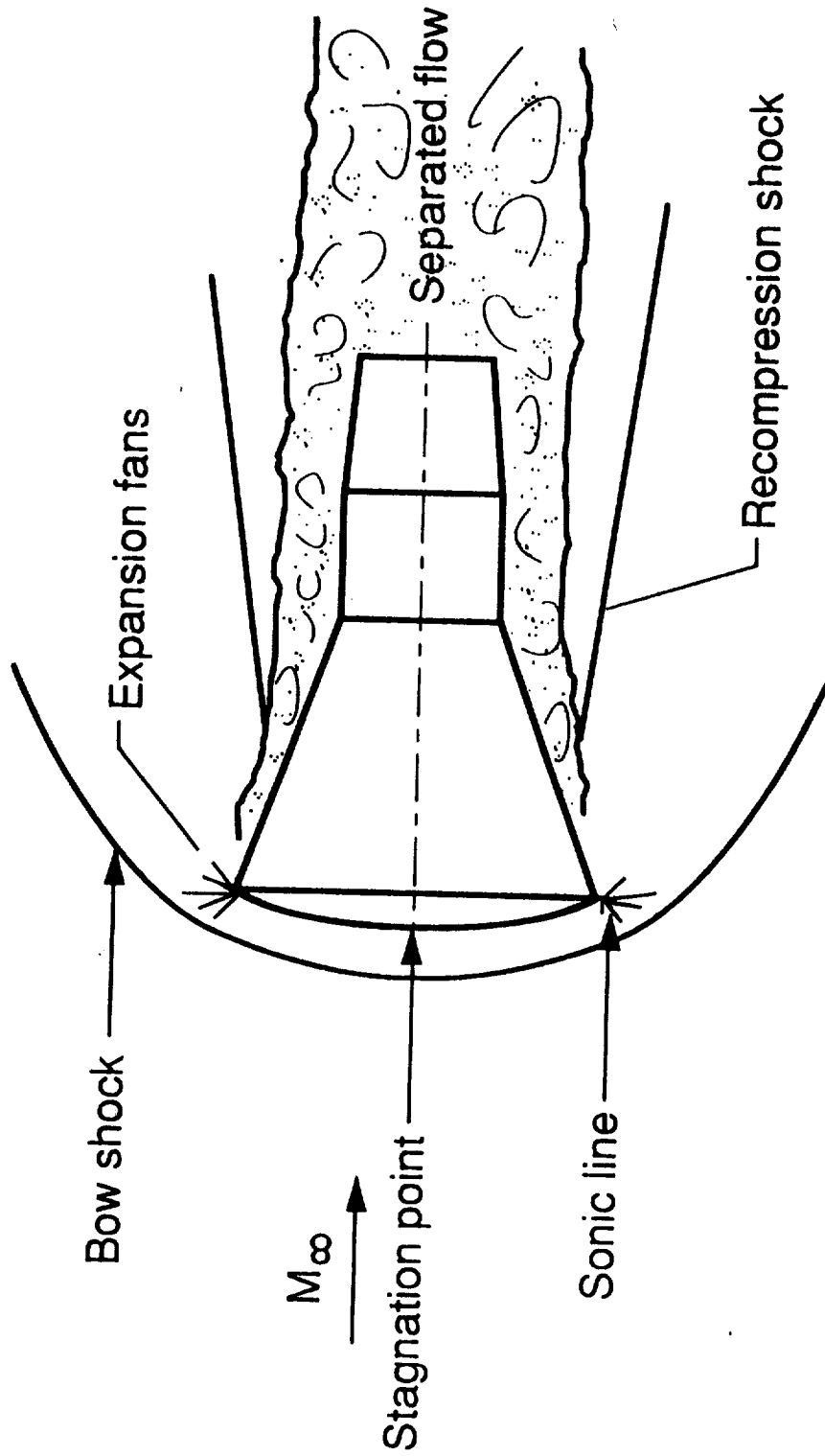
Fig. 11 Sketch of flow field characteristics for Gemini capsule (from Griffith, 1967).

154
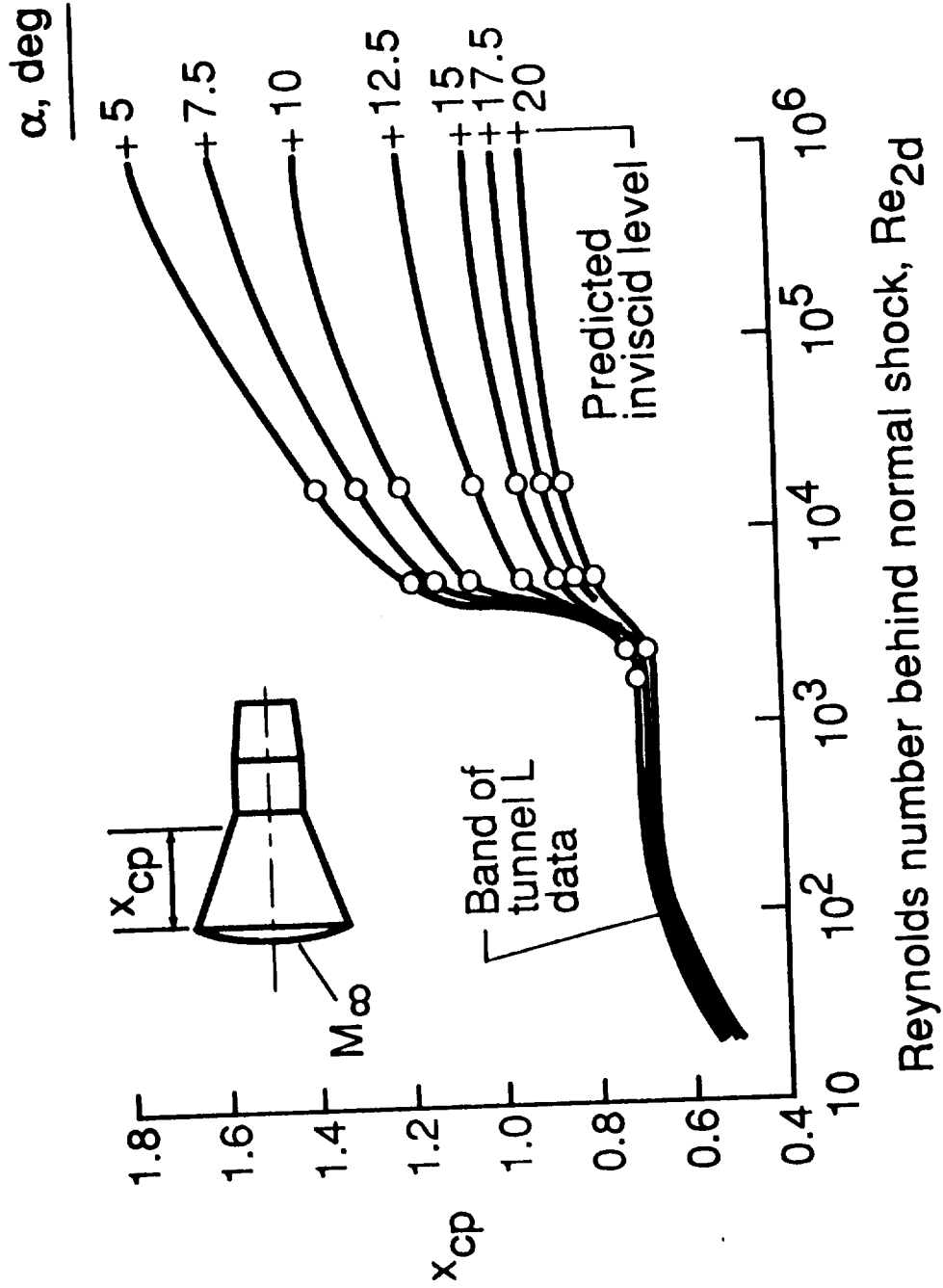
Fig. 12 Center of pressure movement with post-shock Reynolds number (from Lukasiewicz, 1973).
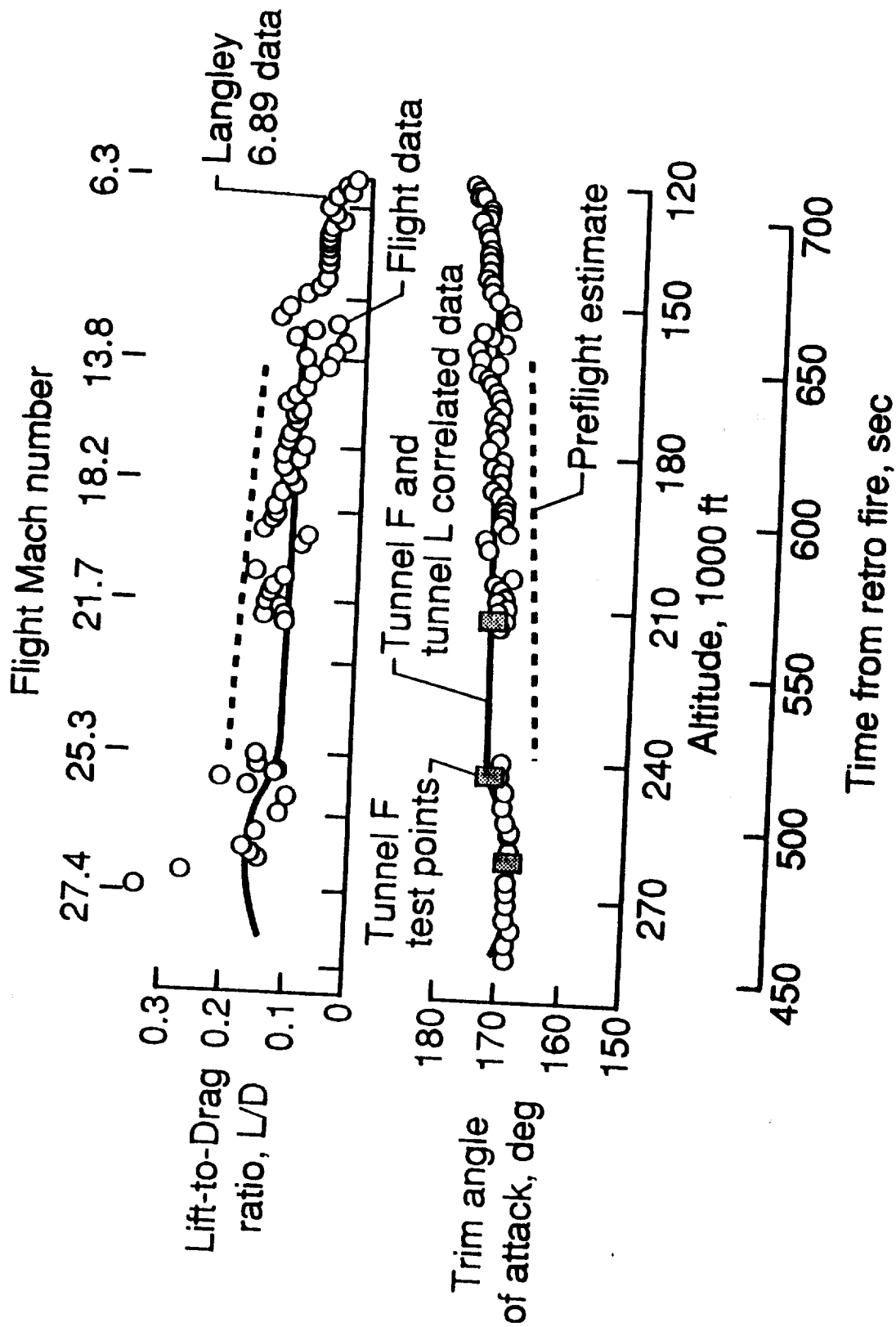
Fig. 13 Comparison of Gemini 3 flight data
with AEDC and Langley wind tunnel data
(from Lukasiewicz, 1973).
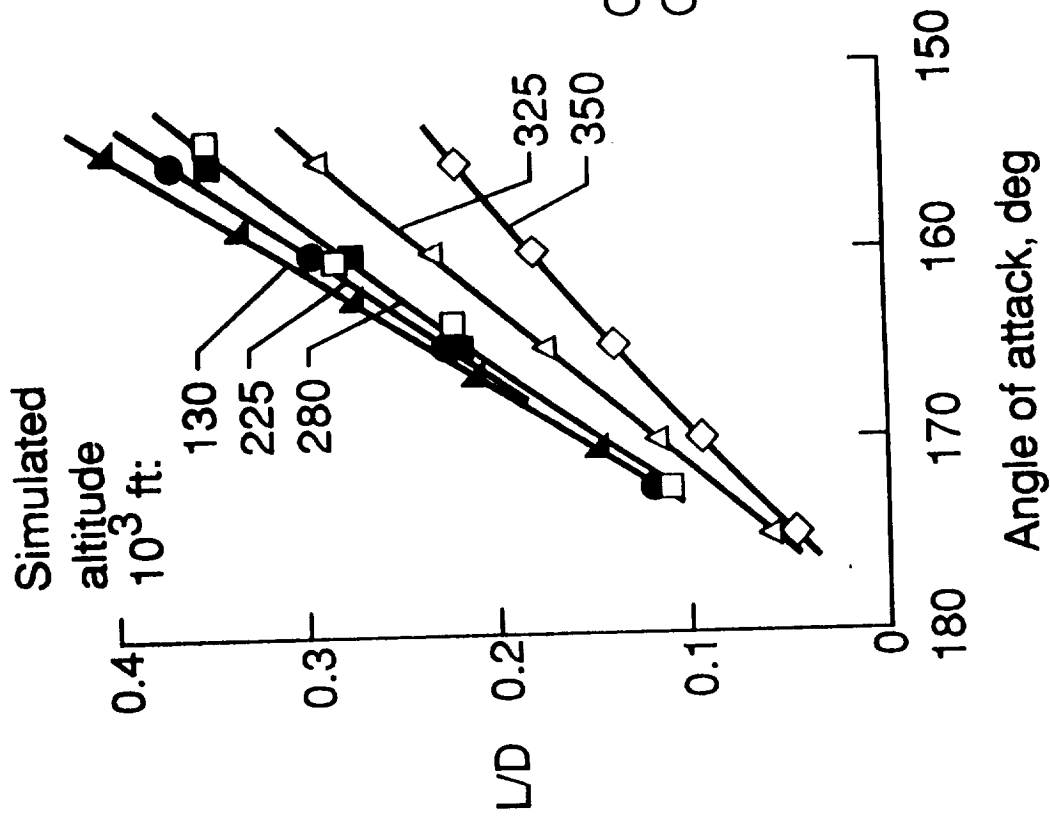
Fig. 14 Effect of post-shock Reynolds number on Apollo lift-to-drag ratio (from Griffith and Boylan, 1968).
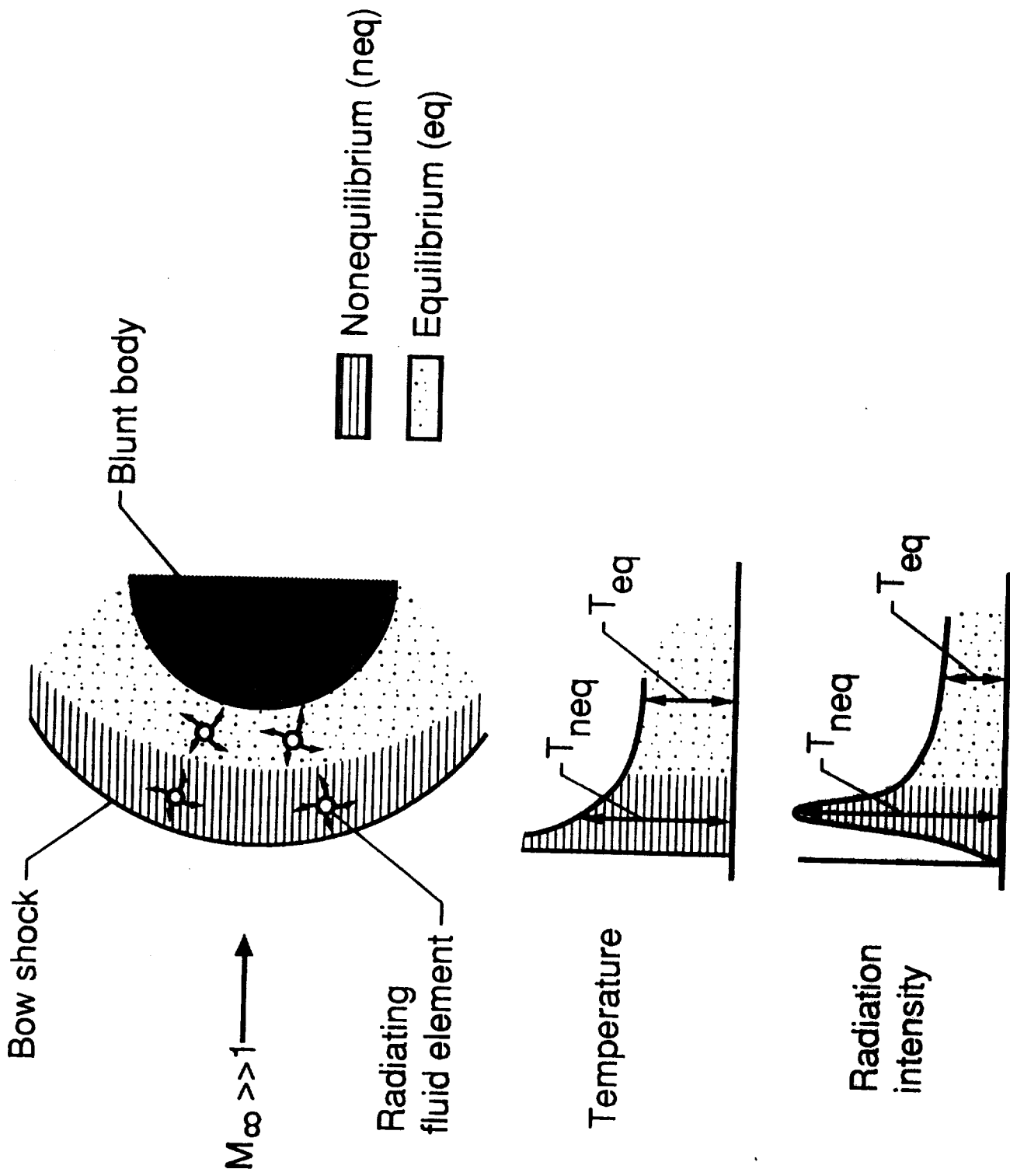
Fig. 15 Schematic of blunt body radiating flow
field.
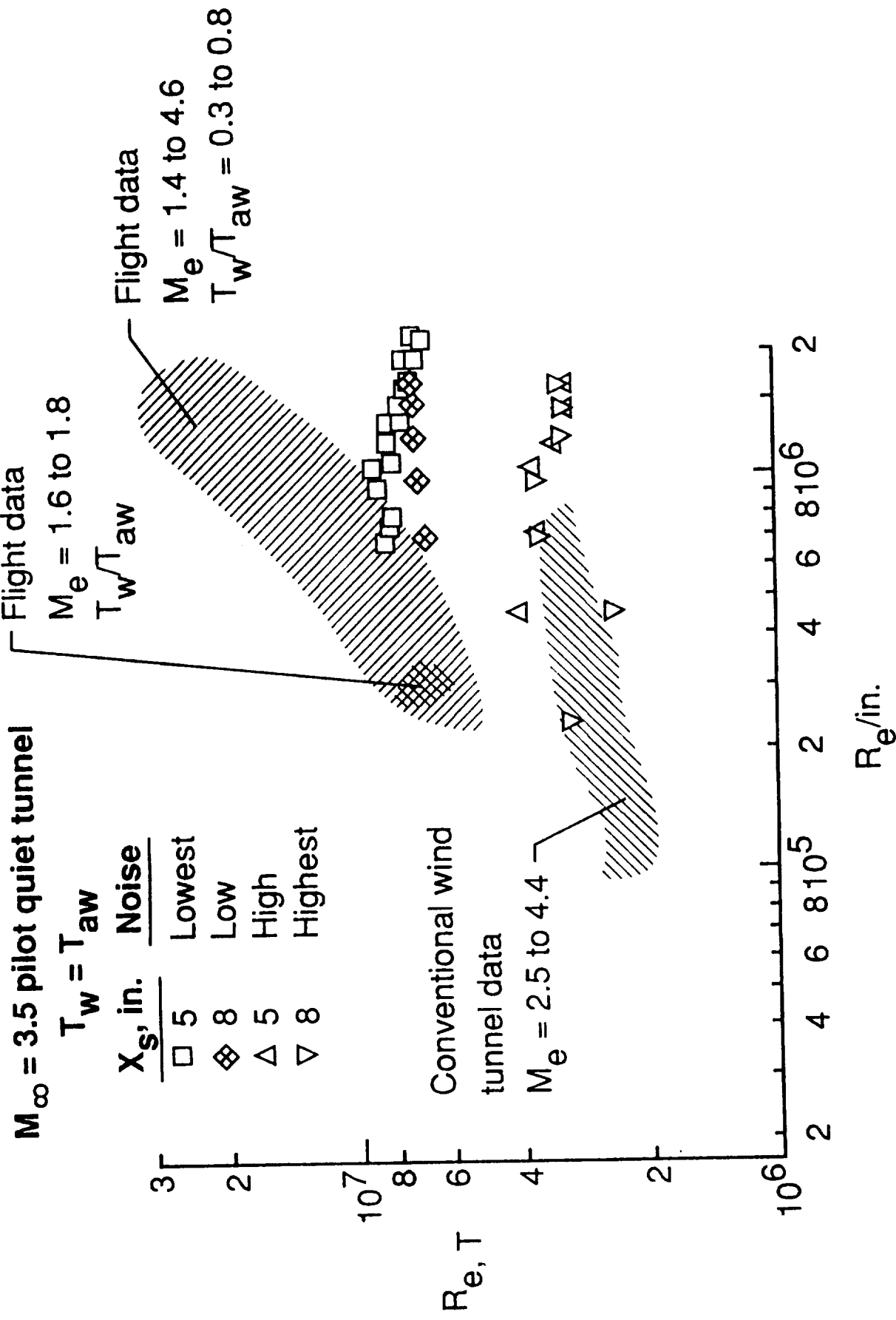
Fig. 16 Transition Reynolds numbers on sharp cones (from Beckwith and Miller, 1990).
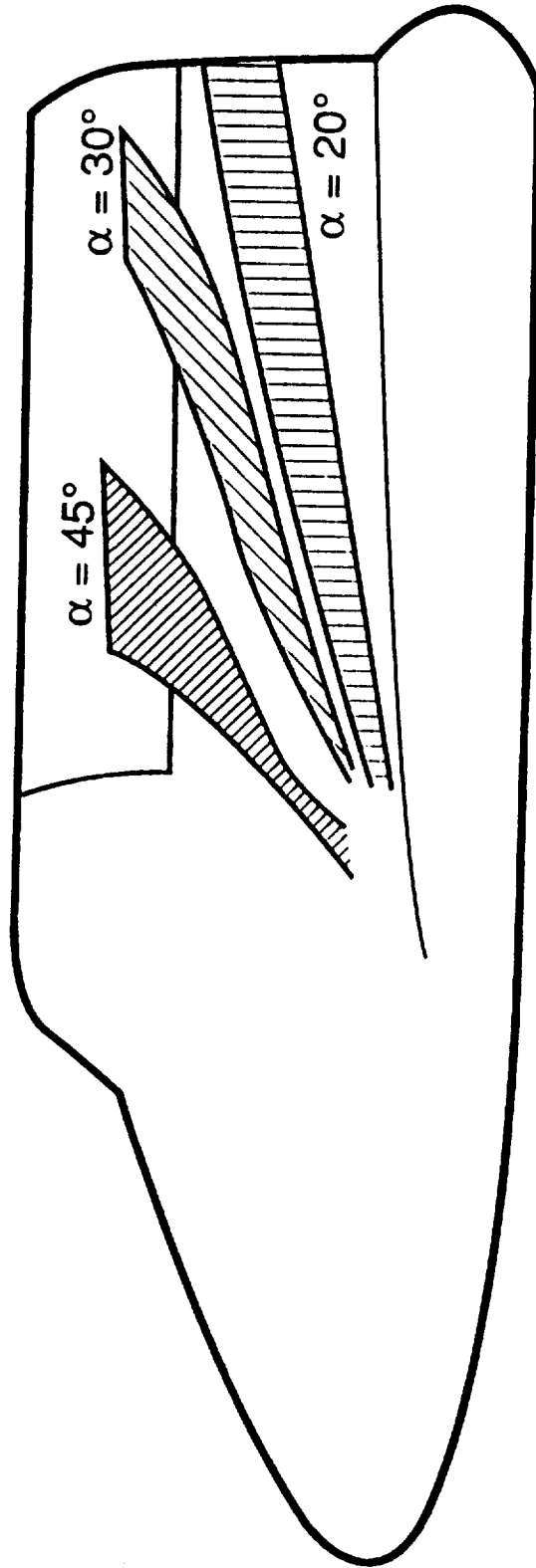
Fig. 17 Effect of angle of attack on side fuselage vortex movement for the shuttle (from Lee and Harthun, 1982).

The figure shows fuselage cross-sections labeled with angles: α = 45°, α = 30°, and α = 20°.
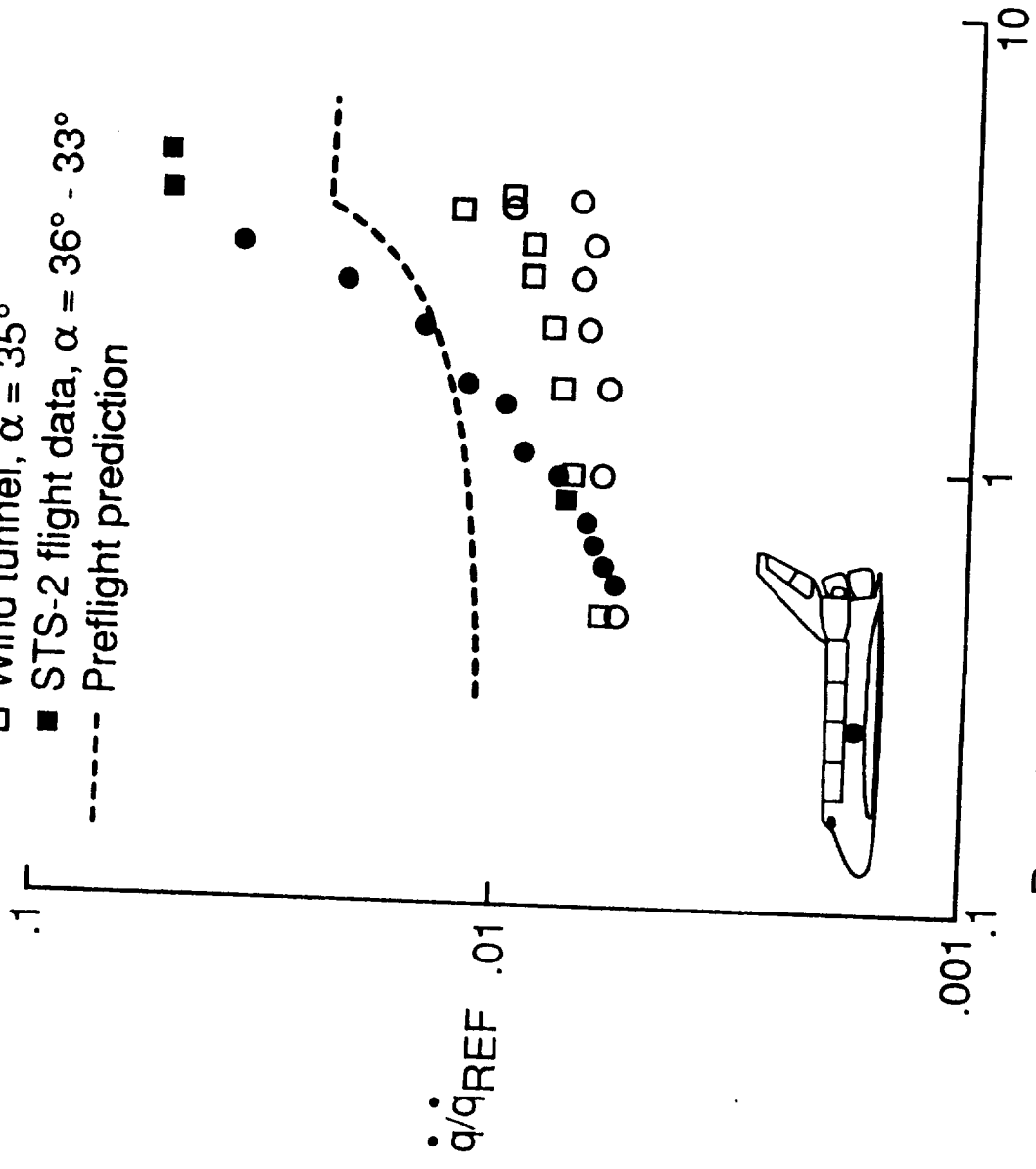
Fig. 18 Comparison of wind tunnel and flight heating to the shuttle mid fuselage side (from Lee and Harthun, 1982).
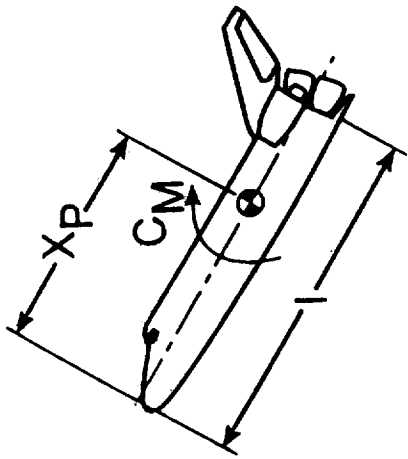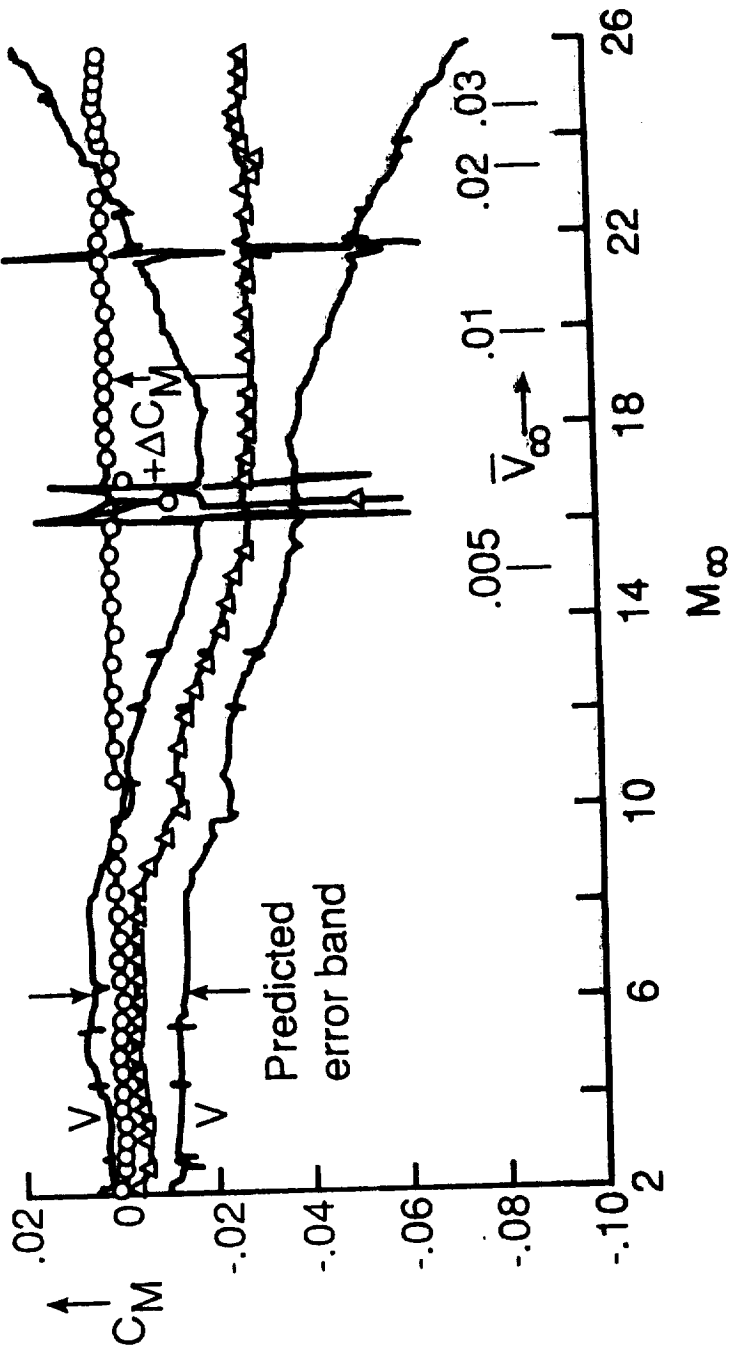
Fig. 19 Aerodynamic performance comparison
between prediction and flight for STS-5
(from Kappenwallner, 1987).

Notes on the Problem of Wind-Tunnel Model Scale Effects as they Relate to Systems Studies

James W. Fenbert, AVD/VIB
Christopher S. Domack, Lockheed

The primary objectives of aircraft system studies are to identify new high-payoff or high-leverage technologies and to quantify their effects by determining the sensitivities of the vehicle to those technologies. The necessity to accurately and efficiently characterize the inclusion of a new technology in the vehicle design and analysis is intrinsic to this process, and may profoundly influence the results of the system study. Thus, problems in obtaining, interpreting, or applying the data acquired in developing a new technology are often problems for the system studies examining that technology. For example, data on new aerodynamic technologies are often obtained by researchers using scaled wind-tunnel models and must be corrected for scale effects, the most important of which is Reynolds number. Some of the most significant wind-tunnel testing and Reynolds number scaling problems facing the High Speed Civil Transport (HSCT) are outlined below.

The fundamental problem associated with Reynolds number effects as they relate to system studies is the extrapolation of experimental data to full-scale conditions. Reynolds number effects on wind-tunnel test results requiring correction or extrapolation to full-scale introduce their own element of uncertainty into the system study results. When cycled through the aircraft

163

aerodynamic characteristics of these configurations has proven to be very difficult. One reason for this is that the structure and behavior of the flow over such wings can be very dependent upon Reynolds number. Experimental data are difficult to obtain at the high chord Reynolds numbers corresponding to any of the HSCT flight conditions from low-speed to cruise. Obtaining full-scale aerodynamic data is prohibitively expensive and practically never an option for system studies.

Lower-order computational methods do not comprehensively model the flow physics and may not accurately predict aerodynamic forces and moments throughout the entire flight envelope, although good agreement with test data has been obtained for limited flight regimes. These lower-order methods include linear aerodynamic theory (LT) and modified linear theory (MLT), which incorporates empirically-derived corrections to LT to improve correlation with test data. Higher-order computational fluid dynamics (CFD) analysis methods, although offering improved flow modeling fidelity, are quite expensive and time-consuming to run. The increased fidelity of the flow field analysis does not necessarily imply increased accuracy of force and moment results; the accurate prediction of drag is still lacking in many CFD codes. CFD modeling of complex multi-component configurations is often problematical, particularly for wings equipped with conventional high-lift devices such as leading-edge slats and

slotted trailing-edge flaps. These devices are typically very sensitive to Reynolds number effects in scale model testing, so the ability to analytically predict their full-scale performance would be a boon to the configuration aerodynamicist. Unfortunately, most CFD codes still lack the experimental verification that is a prerequisite for their widespread acceptance. Code-to-code verification is often conducted, but this exercise is of little meaning without physical data to calibrate the results. Also, most CFD methods lack the ability to be used in an inverse or "design" mode, currently the biggest advantage of the lower-order methods.

The low-speed aerodynamics of an HSCT configuration need to be well-defined as early as possible in the design process, because many of the design parameters which ultimately determine the shape and size of the vehicle depend on its low-speed performance. At low speeds and high lift (e.g., takeoff and landing conditions) the flow field around highly-swept, low aspect ratio wings tends to be highly three-dimensional, with large regions of detached, vortex-dominated flow. Wind-tunnel testing to provide high Reynolds number data at low speed is very expensive and difficult at best and often impossible. This is because of the large size of both the model and the wind-tunnel required for the test. Few wind tunnels exist which can reproduce the flight conditions of the HSCT in the takeoff or landing modes. These flow conditions do not lend themselves to reliable

analysis by linear methods, leaving the designer to rely instead on (scarce, expensive) wind-tunnel data of similar configurations at much lower Reynolds numbers, or empirically-derived handbook methods. Neither method is really satisfactory for detecting design sensitivities due to subtle configuration changes. The advent of truly fast, easy-to-use, experimentally verified CFD codes will probably be of most value in this application for system studies, but this situation still appears to be many years distant.

Reynolds number also has an effect on the cruise performance of the HSCT configuration. This effect is not limited to a simple zero-lift drag correction, but also affects the drag-due-to-lift of the configuration. Extrapolation of skin friction drag to full-scale conditions and accounting for the drag associated with transition strips is fundamental to scale model wind-tunnel testing. Reynolds number not only affects the laminar and turbulent skin friction drag levels but also the location and nature of the boundary-layer transition from laminar to turbulent. The drag-due-to-lift scaling problem with wind-tunnel test data is in the estimation of attainable leading-edge thrust, which is dependent on Reynolds number. Two different approaches may be taken to this problem, neither of which is fully satisfactory. The model wing design can be performed for the full-scale Reynolds number, producing a wing camber and twist which will not obtain the efficiency predicted when tested at lower Reynolds number. This approach

requires a correction for attainable leading-edge thrust in addition to the normal zero-lift drag corrections. The other option is to design the model wing camber and twist distribution for wind-tunnel Reynolds number, eliminating the need for the leading-edge thrust correction. However, this approach merely validates the computer code, not the full-scale wing design. Also, this approach sacrifices an important element of scale fidelity and does not necessarily indicate the full-scale vehicle performance.

Some differences in wind-tunnel model geometry and full-scale airplane geometry are almost always required, particularly for small scale models. Significant deviations from scale may be necessary in order to fabricate, instrument, or suspend the model in the wind tunnel. There may also be aerodynamic reasons for deviations from scale; for example, nacelle boundary layer diverter height on a model is proportionally greater than on the full-scale airplane in order to keep the wing/body boundary layer(s) out of the nacelle. This is a particularly severe limitation in HSCT model supersonic testing since efficient propulsion/airframe integration increases the lift on the vehicle and can essentially offset the wave drag of the nacelles. This "efficient integration" is highly dependent on precise positioning and shaping of the engine nacelles on the configuration. The increased distance between the wing and the nacelles necessary because of the proportionally thicker model boundary layer thus

167

introduces another error in the data. It is thus virtually impossible to correctly model all important physical characteristics at once. The full-scale predictions must be "built up" from several tests using a variety of models, corrections and approximations, each of which increase the uncertainty associated with the final results.

Other areas of uncertainty in wind-tunnel model testing have been documented in many previous works, and comprehensive treatments of some these areas may be found in the literature. These subjects include, but are not limited to: wind-tunnel wall corrections, buoyancy effects, sting deflection and interference, test section flow angularity and nonuniformity, full-scale propulsion system effects including jet plumes and propeller slipstreams, and estimation of full-scale airplane "miscellaneous" drag increments such as pressurization leakage, environmental control air intake and exhaust, and the drag of real-aircraft protuberances.

REPORT DOCUMENTATION PAGE

1. AGENCY USE ONLY (Leave blank)	2. REPORT DATE May 1993	3. REPORT TYPE AND DATES COVERED Technical Memorandum

4. TITLE AND SUBTITLE

Reynolds Number Influences in Aeronautics

5. FUNDING NUMBERS

WU 505-60-01-02

6. AUTHOR(S)

Dennis M. Bushnell, Long P. Yip, Chung-Sheng Yao, John C. Lin, Pierce L. Lawing,
John T. Batina, Jay C. Hardin, Thomas J. Horvath, James W. Fenbert,
and Christopher S. Domack

7. PERFORMING ORGANIZATION NAME(S) AND ADDRESS(ES)

National Aeronautics and Space Administration
Langley Research Center
Hampton, VA 23681-0001

8. PERFORMING ORGANIZATION REPORT NUMBER

9. SPONSORING / MONITORING AGENCY NAME(S) AND ADDRESS(ES)

National Aeronautics and Space Administration
Washington, DC 20546-0001

10. SPONSORING / MONITORING AGENCY REPORT NUMBER

NASA TM-107730

11. SUPPLEMENTARY NOTES

12a. DISTRIBUTION / AVAILABILITY STATEMENT

Unclassified-Unlimited
Subject Category 02

12b. DISTRIBUTION CODE

13. ABSTRACT (Maximum 200 words)

Reynolds number, a measure of the ratio of inertia to viscous forces, is a fundamental similarity parameter for fluid flows, and therefore, would be expected to have a major influence in Aerodynamics and Aeronautics. Reynolds number influences are generally large, but monatomic, for attached laminar (continuum) flow; however, laminar flows are easily separated, inducing even stronger, non-monatomic, Reynolds number sensitivities. Probably the strongest Reynolds number influences occur in connection with transitional flow behavior. Transition can take place over a tremendous Reynolds number range, from the order of 20×10^3 for 2-D free shear layers up to the order of 100×10^6 for hypersonic boundary layers. This variability in transition behavior is especially important for complex configurations where various vehicle and flow field elements can undergo transition at various Reynolds numbers, causing often surprising changes in Aerodynamics characteristics over wide ranges in Reynolds number. This is further compounded by the vast parameterization associated with transition, in tyhat any parameter which influences mean viscous flow development (e.g., pressure gradient, flow curvature, wall temperature, Mach number, sweep, roughness, flow chemistry, shock interactions, etc., and incident disturbance fields (acoustics, vorticity, particulates, temperature spottiness, even electro static discharges) can alter transition location to first order. The usual method of dealing with the transition problem is to trip the flow in the, generally lower Reynolds number, wind tunnel to simulate the flight turbulent behavior. However, this is not wholly satisfactory as it results in incorrectly scaled viscous region thicknesses and cannot be utilized at all for applications such as turbine blades, and helicopter rotors, nacelles, leading edge and nose regions and High Altitude Long Endurance and hypersonic airbreathers where the transitional flow behavior is an innately critical portion of the problem.

14. SUBJECT TERMS

Reynolds number; Scale effects; Transonic; High lift; Hypersonic

15. NUMBER OF PAGES

172

16. PRICE CODE

A08

17. SECURITY CLASSIFICATION OF REPORT Unclassified	18. SECURITY CLASSIFICATION OF THIS PAGE Unclassified	19. SECURITY CLASSIFICATION OF ABSTRACT Unclassified	20. LIMITATION OF ABSTRACT

NSN 7540-01-280-5500